MODELING VISCOELASTIC CELLULAR MATERIALS
FOR THE PRESSING OF WOOD COMPOSITES
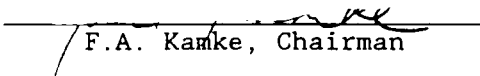
by

Michael P. Wolcott

Dissertation submitted to the Faculty of the
Virginia Polytechnic Institute and State University
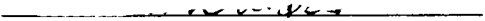in partial fulfillment of the requirements for the degree of
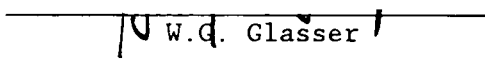
DOCTOR OF PHILOSOPHY

in

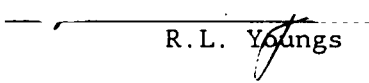Materials Engineering Science

APPROVED:

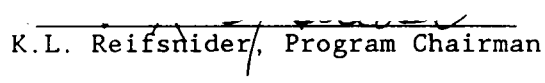F.A. Kamke, Chairman

D.A. Dillard   W.C. Glasser

T.E. McLain   R.L. Youngs

K.L. Reifsnider, Program Chairman

September, 1989

Blacksburg, Virginia

MODELING VISCOELASTIC CELLULAR MATERIALS
FOR THE PRESSING OF WOOD COMPOSITES

by

Michael P. Wolcott

Committee Chairman: Frederick A. Kamke
Wood Science and Forest Products

(ABSTRACT)

With the large number and diversity of materials available today, the ability of the manufacturer to control properties is critical for the success of a product in the market. Although we have little or no control over the engineering properties of solid wood, the potential for the design of material properties in composites is great. Large strides are presently being made in the design of non-veneer structural panels by using material science principles. However, a large gap in our knowledge of the composite system is in the understanding of how raw material properties and processing variables interact to influence the internal geometry and material properties of the components _in situ_. The ability to use production variables to control material properties of the composite is an extremely valuable tool.

The goal of this research is to provide an understanding of how the heat and mass transfer inside a flakeboard during pressing, interacts with the viscoelastic behavior of individual flakes to influence density gradient formation and _in situ_ flake properties. The specific objectives:

1. To use observed changes in the temperature and gas pressure of the internal environment of panels during the pressing cycle to describe the composition of the gas phase.

2. To use the calculated composition of the gas phase and measured temperature for the internal environment as boundary conditions for a fundamental heat and mass transfer model to access changes in the temperature and moisture content of the wood component during pressing.

3. To use the temperature and moisture content relations above to qualitatively relate press conditions to the formation of density gradients through changes in the glass transition temperature of the amorphous polymers in wood.

4. To utilize micromechanical models of cellular materials in conjunction with linear viscoelasticity of polymers to develop a nonlinear viscoelasticity model for wood in transverse compression.

The approach couples the viscoelastic behavior of the amorphous polymers in wood with the structure imposed by anatomy. These theories, if applicable to wood, can greatly simplify the study of many similar systems combining enviromental conditions and mechanical properties.

ACKNOWLEDGEMENTS

LIST OF TABLES

LIST OF FIGURES

CHAPTER 1

PROJECT DESCRIPTION

INTRODUCTION

One advantage of composites over traditional materials is the ability to tailor the material properties to meet design requirements. The basic properties of the composite will be a function of the in situ raw material properties and the geometry in which the components are arranged. Material engineers and scientists have been more successful in the design process for synthetic fiber reinforced composites than for wood based composites, mainly because of the microstructural complexity and variability of the latter. However, proficiency in design of wood based composites is necessary if these products are to compete with other materials in future markets. This research is aimed at improving our understanding of fundamental material behavior during the processing of wood-based composites.

Density Gradient Formation

Many non-veneer, wood based composites are produced in a highly automated process where the wood and adhesive components are flat pressed using extreme heat and pressure. Heat is conducted into the mat from platens that attain mechanical pressures and temperatures on the order of 5.5 MPa and 200°C. Initially, moisture contained in the wood near the heated platens vaporizes, vapor pressure increases, and the gaseous water is driven vertically to the center and horizontally to the edges of the mat. This simultaneous heat and mass transfer results in transient temperature and humidity gradients in the mat (Suchsland 1962, Humphrey and Bolton 1979, Kamke and Casey 1988a, 1988b).

When the pressure applied to the mat is coupled with the interior transient temperature and humidity conditions, density gradients form in

the processed board. Density gradients influence material properties of the composite in four ways:

> 1. Density is strongly correlated to the strength and engineering properties of the individual wood components (Price 1976, Geimer et al. 1985).
>
> 2. The stress under which the wood is compressed affects the strength and engineering properties of the wood component in situ by forming micro-failures in the cell walls (Geimer et al. 1985).
>
> 3. The quality of the adhesive/wood bond is related to the plasticization of the wood component; thereby, forming an intimate wood-adhesive-wood contact surface (Wilson and Krahmer 1976).
>
> 4. Density gradients change the geometry of the final structure in the composite (i.e. higher densities correspond with more wood components per unit volume of composites).

Several researchers have studied the effect of press closing time (PCT) on the range of density through the thickness of the board and the shape of the resulting profile (Strickler 1959, Plath and Schnitzler 1974, Smith 1982). These researchers determined that the distribution of densities through the thickness of the board are affected by PCT. Strickler (1959) also noted that mat moisture content and moisture content distribution influenced the resulting density gradients. PCT can influence deformation in the mat directly through a rate of loading effect. In addition, because physical properties of the mat (e.g. permeability, thermal conductivity) are a function of the void spaces, environmental conditions within the mat can be altered through different PCTs.

In recent studies, environmental conditions (temperature and gas pressure) have been monitored in face and core layers of a flakeboard during the pressing cycle (Kamke and Casey 1988a, 1988b). Density through the thickness of these boards was determined using gamma radiation densitometry. Analysis of the data showed that temperature differences between the face and core layers at the time of press closing are greater for boards produced with a 2 minute PCT ($39.7^{\circ}C$) than a 1 minute

PCT (14.6°C). Core temperature was noted to change slowly during the
PCT. This result is likely because of the large amount of air in the
uncompressed mat and, therefore, the low thermal conductivity. The
density difference between core and face layers of boards produced with
the 2 minute PCT was less than boards with a 1 minute PCT. Interpreta-
tion of these results suggests that the environmental factor controlling
the formation of density gradients is not merely a temperature differ-
ence. However, without a significant increase in temperature, moisture
is not likely to change rapidly in the panel. Therefore, after evaluat-
ing these observations, I conclude that the density gradient is formed
largely from differential relaxation through the thickness of the mat
during the remainder of the press cycle. The influence of PCT is,
therefore, in altering the simultaneous heat and mass transfer process
by changing the boundary conditions and physical properties of the mat
with respect to time.

Mathematical models have been developed to predict internal mat
temperature and moisture content in particleboard during hot-pressing
(Humphrey 1979, Kayihan and Johnson 1983, Harless et al 1987). Two
major problems exist with this approach: (1) the models assume thermody-
namic equilibrium to be maintained between the gas and wood components,
thereby, neglecting any resistance to heat and mass transfer at the
surface of the flake and (2) with the lack of an experimental method to
measure moisture content in situ during processing, any form of exper-
imental verification is lacking for the moisture component of the
models. However, the change in moisture content of the entire panel
during the pressing cycle suggests that moisture plays a large role in
the production process of wood-based composites.

Experimental methods do exist for measuring the internal tempera-
ture and gas pressure of a wood-based composite during processing
(Humphrey 1979, Kamke and Casey 1988a and 1988b). Because these parame-

ters are a direct consequence of the internal environment, they can be used as a method to determine the composition of the gas phase surrounding the wood component. With a knowledge of the internal gas phase, the exchange of heat and mass across the boundary of the flake surface can be determined using a fundamental heat and mass transfer model.

Moisture content has been observed to change the glass transition temperature (T_g) of the amorphous polymers of wood (Salmén 1984, Kelley et al. 1987). Below T_g, molecular motion is limited and mechanical properties are not greatly affected by temperature (Billmeyer 1984). However, when the temperature of the polymer approaches T_g, stiffness of the material decreases rapidly, corresponding to the marked increase in molecular motion.

Because moisture and temperature vary simultaneously in a panel during the pressing cycle, the process is extremely difficult to access qualitatively. The primary affect of these variables on the mechanical properties of wood are through the viscoelastic properties. Knowledge of how the glass transition temperature varies during the pressing cycle may provide valuable insight into mechanisms of panel consolidation.

Environmental Conditions and Viscoelastic Response

The mechanism that seems to play a large role in forming density gradients is viscoelastic properties of the wood component in compression perpendicular to the grain under non-steady state humidity and temperature environments. This mechanism is consistent with recent findings when steam injection pressing has been employed (Geimer 1985). A thorough understanding of this response is critical for the efficient use of steam injection pressing because the operator has a large amount of control over the internal environment of the mat. The following discussion describes some of the complex mechanisms, which may influence these viscoelastic processes.

An analogous behavior of the viscoelastic response of polymers with different time, temperature, and moisture content has been observed for many systems (Ferry 1980). The time-temperature-moisture superposition techniques utilize the relation of these variables. The underlying assumption of the superpositon technique is that the variables of temperature and moisture content merely accelerate the time dependent response. Therefore, viscoelastic material parameters can be determined at different temperatures and moisture contents and shifted horizontally along the log time scale to produce a master curve. Although the observation of this equivalence was originally empirical, a theoretical basis has been developed for amorphous polymers. Most of these theories can be based on concepts of free volume.

Free Volume Theories for Viscoelasticity

Free volume is defined as the difference between the occupied volume and specific volume of a polymer (Billmeyer 1984). Free volume remains relatively constant in the glassy stage of a polymer and increases linearly with temperature above T_g. Above T_g, segmental mobility of the polymer molecules increases. This increases the free volume. A diluent in a polymer will increase free volume in proportion to the concentration of diluent (Ferry 1980).

Salmén (1984) used free volume theories to study the viscoelastic properties of water swollen wood in relation to thermal mechanical pulping. Kelley et al. (1987) showed the theories could be applied to wood swollen with formamide. These researchers were able to predict the shift factors required for time-temperature superposition techniques using the WLF equation, which has been universally applied to many polymer systems (Williams et al. 1955). Kelley et al. (1987), also, used the Kwei model to predict T_g of water swollen wood as a function of moisture content. The Kwei model incorporates terms to describe the

effect of secondary interactions and free volume on the T_g of a polymer diluent system (Kwei 1984). The work by Kelley et al. and Salmén demonstrate the applicability of free volume theories to describe and predict the viscoelastic response of solid wood.

Knauss and Emri (1981) proposed a free volume theory that accounts for changes in temperature, diluent concentration, and hydrostatic stress to predict nonlinear viscoelastic properties. This theory assumes that free volume will be changed by a dilatation (volumetric strain), whether that dilatation occurs from a change in temperature, diluent concentration, or stress. Given the range of temperature and moisture content that occur during the pressing cycle, the amorphous polymers in wood will be frequently well below the glass transition temperatures of the amorphous polymers.

Nonlinear Mechanical Response in Transverse Compression

This work focuses on the mechanical response of wood in transverse compression under different temperature and moisture environments. The stress-strain relation of cellular materials (foams) in this loading mode is a function of the deformation of the prevailing material structure. Because of the pronounced effect of material structure on the mechanical response of cellular materials loaded in transverse compression, this area must be addressed in detail.

Foams may be modeled as a three dimensional hexagonal network (Gibson et al. 1982, Gibson and Ashby 1982, Ashby 1983, Maiti et al. 1984). Gibson et al. (1982) produced two dimensional hexagonal networks from elastomers and metals to test theories of deformation modes. The theories were then extended to three dimensional foams (Gibson and Ashby 1982). They concluded that all foams deform similarly on a macro-level. However, different mechanisms are responsible for collapse in the cells and, therefore, different absolute values of stress-strain regions are

obtained. The foams are grouped into brittle, rigid plastic, and elastic categories. All of the man made foams studied deform macroscopically as a function of deformation in the individual cells. The distinct regions of a typical stress-strain curve of cellular materials in compression are:

1. linear elastic
2. plateau of stress with increasing strain
3. densification approaching the solid material

These three regions of deformation are exhibited by both man made and natural cellular materials (Maiti et al. 1984).

Bodig (1963, 1965) studied the mechanical behavior of wood in transverse compression and determined that several structural mechanisms are responsible for the nonlinearity exhibited. Bodig concluded that specimen geometry and orientation (load applied in radial or tangential direction) strongly influenced how the material reacted structurally. Easterling et al. (1982) used micromechanical relations like those for foams to study the stress-stain behavior of balsa (Ochroma lagopus) in transverse compression under ambient environmental conditions. It is apparent that the macroscopic deformation of solid wood in this study can be described using micromechanical models of the cell deformation. Because many levels of material organization exists in solid wood, specimen geometry can influence which level will dominant the macroscopic mechanical behavior. The test specimens used by Easterling et al. (1982) were small (20mm X 20mm X 40mm); therefore, the dominant inhomogeneity in the system is probably cell structure. This hypothesis should also hold for the wood components in composites because they are generally small. The analysis by Easterling is not complete for these purposes because the properties of the polymers in wood are strongly dependent on temperature and moisture.

Moisture Movement

Numerous attempts have been made at developing a theoretical model for describing heat and mass transfer in porous solids. A well-posed model developed for wood by Stanish et al. (1985) includes the mechanisms of conduction and convection heat transfer, mass transfer by gaseous diffusion, bound water diffusion, capillary pressure, and hydrodynamic flow of gas and free water. Bound water diffusion is assumed to occur under a chemical potential gradient. Stanish et al. reported good agreement between model predictions and experimental data for temperature and moisture content, when the permeability constants and vapor diffusivity were allowed to vary.

TECHNICAL OBJECTIVES

While approaching the goal of a completely engineered wood composite, this research is aimed at providing a fundamental understanding the interactions of the raw material properties, production parameters, and the structural geometry of the final product. The cellular structure and polymer properties of wood are severely altered by the production process of wood-based composites. However, this change has not yet been thoroughly addressed. The four specific objectives of the project are:

> 1. To use observed changes in the temperature and gas pressure of the internal environment of panels during the pressing cycle to describe the composition of the gas phase.

> 2. To use the calculated composition of the gas phase and measured temperature for the internal environment as boundary conditions for a fundamental heat and mass transfer model to assess changes in the temperature and moisture content of the wood component during pressing.

> 3. To use the temperature and moisture content relations above to qualitatively relate press conditions to the formation of density gradients through changes in the glass transition temperature of the amorphous polymers in wood.

> 4. To utilize micromechanical models of cellular materials in conjunction with linear viscoelasticity of polymers to

develop a nonlinear viscoelasticity model for wood in transverse compression.

RATIONALE AND SIGNIFICANCE

The ability to engineer material properties for specific design requirements is a powerful tool for applying a material to a diversity of uses and improving utilization of that material. Presently, the material engineering of wood based composites is in a rudimentary stage principally because of the complexity of the system. The anisotropic nature of wood properties combined with natural variability, contribute greatly to this complexity. The interaction of wood with environmental conditions causes additional problems in fundamental research. Therefore, any material science principles that can address fundamental behavior of the wood polymers or strucuture is highly desirable.

Production techniques for wood based composites utilize temperature and moisture effects on wood to optimize processing variables such as power and time requirements. Also, these techniques greatly affect material structure and properties, although the mechanisms are not well understood. To a large extent, this lack of understanding prevents the optimal production and use of wood-based composites. Failure to advance this science will have a detrimental effect on the competitiveness of wood products.

There is a certain appeal to the polymer based model, presented here, which can unify the interactions of time, temperature, moisture, and mechanical behavior in wood. The polymers that dictate the response under these conditions are common to all species of wood. Therefore, the general trends in the response should be applicable to most species. In addition, demonstrating that wood properties can be studied as a function of the polymer behavior coupled with the structural geometry of wood anatomy, has implications far beyond the scope of this particular problem. For instance, Salmén (1984) has applied similar polymer

theories to optimizing conditions for thermo-mechanical pulping. The same polymer principles proposed here are directly applicable to wood drying.

The production of wood based composites, in particular non-veneer structural panels, has been increasing since 1975 (Anonymous 1986). The structural flakeboard industry alone is projected to total 2 billion dollars per year (1984 dollars) by the year 2000 (Fuller and Berg 1984). The information generated by the research proposed here will greatly aid the development of new products through improved design information. The value added to the raw material from the possibility of these new products penetrating into non-wood product markets will be particularly beneficial to the forest products industry. Finally, the use of new processing techniques, such as steam injection pressing and radio-frequency curing, will be made more attractive through a better understanding of how material properties can be controlled using production variables.

LITERATURE CITED

Anonymous. 1986. Panel output, capacity continues to increase. Forest Industries, April, pp. 16-17

Ashby, M.F. 1983. The mechanical properties of cellular solids. Met. Trans. 14A:1755-1769. 3. Back, E.L., L. Salmen, and G. Richardson. 1983. Transient effects of moisture sorption on the strength properties of paper and wood-based materials. Svensk Papperstidning.

Billmeyer, F.W. 1984. Textbook of polymer science 3rd ed. John Wiley and Sons, New York, NY. 578 pp.

Bodig, J. 1963. The peculiarity of compression of conifers in the radial direction. For. Prod. Jour. 10:438.

_____. 1965. The effect of anatomy on the initial stress-strain relationship in transverse compression. For. Prod. Jour. 15(5):197-202. 6. _____. 1966. Stress-strain relationship for wood in transverse compression. Jour. of Mat. 1(3):645-666.

Easterling, K.E., R. Harrysson, L.J. Gibson, and M.F. Ashby. 1982. On the mechanics of balsa and other woods. Proc. R. Soc. Lond. A383:261-280.

Ferry, J.D. 1980. Viscoelastic properties of polymers 3rd ed. John Wiley and Sons, New York, NY. 641pp.

Fuller, B. and R. Berg. 1984. North American structural panel markets: The outlook for plywood, waferboard, and oriented strandboard through 2000. DRI Special Study Series No.6, Data Resources, Inc., Lexington, Mass.

Geimer, R.L. 1985. Steam-injection pressing of isocyanate-bonded aspen flakeboards: Latitudes and limitations. FPL Res. Paper #456. US For. Prod. Lab., Madison, WI.

_____, R.J. Mahoney, S.P. Laihnertz, and R.W. Meyer. 1985. Influence of processing-induced damage on strength of flakes and flakeboards. FPL Res. Paper #463. US For. Prod. Lab., Madison, WI.

Gibson, L.J., M.F. Ashby, G.S. Schajer, and C.I. Robertson. 1982. The mechanics of two-dimensional cellular materials. Proc. R. Soc. Lond. A382:25-42.

_____, and M.F. Ashby. 1982. The mechanics of three-dimensional cellular materials. Proc. R. Soc. Lond. A382:43-59.

Harless, T., F.G. Wagner, P.H. Short, R.D. Seale, P.H. Mitchell, and D.S. Ladd. 1987. A model to predict the density profile of particleboard. Wood and Fiber Sci. 19(1):81-92.

Humphrey, P.E. 1979. Fundamental aspects of wood particleboard manufacture. Ph.D. Dissertation. Univ. of Wales, Bangor, Wales, U.K. 158pp.

Humphrey, P.E. and A.J. Bolton. 1979. Modelling unsteady-state processes that occur during the hot pressing of wood based composites.

In: <u>Numerical methods in thermal problems.</u> Eds. R.W. Lewis, J.A. Johnson, and R. Smith.

Kamke, F.A. and L.J. Casey. 1988a. Gas pressure and temperature in the mat during flakeboard manufacture. For. Prod. J. 38(3):41-43.

_____. and _____. 1988b. Fundamentals of flakeboard manufacture: internal mat conditions. For. Prod. J. 38(6):38-44

Kayihan, F. and J.A. Johnson. 1983. Heat and moisture movement in wood composite materials during the pressing operatuion - a simplified model. In: Numerical Methods in Heat Transfer, Vol. 2, R.W. Lewis, K. Morgan, and B.A. Schrefler (Eds.), New York, NY. John Wiley and Sons.

Kayihan, F., M.A. Stanish, and G.S. Schajer. 1984. A mathematical model of drying for hygroscopic porous media. Presented at annual AIChE Meeting. San Francisco, CA.

Kelley, S.S., T.G. Rials, and W.G. Glasser. 1987. Relaxation behavior of the amorphous components of wood. Jour. of Mat. Sci. In press.

Knauss, W.G., and I.J. Emri. 1981. Nonlinear viscoelasticity based on free volume consideration. Computers and Structures. 13:123-128.

Kwei, T.K. 1984. The effect of hydrogen bonding on the glass transition temperature of polymer mixtures. J. Polym. Sci.: Polym. Lett. 22:307-313.

Maiti, S.K., L.J. Gibson, and M.F. Ashby. 1984. Deformation and energy absorbtion diagrams for cellular solids. Acta Metal. 32(11):1963-1975.

Plath, L. and E. Schnitzler. 1974. The density profile, a criterion for evaluating particleboard. Holz Roh-Werkst. 32(11):443-449.

Price, E.W. 1976. Determining tensile properties of sweetgum veneer flakes. For. Prod. Jour. 26(10):50-53.

Salmén, L. 1984. Viscoelastic properties of <u>in situ</u> lignin under water-satuated conditions. Jour. of Mat. Sci. 19:3090-3096.

Smith, D. 1982. Waferboard press closing strategies. For. Prod. Jour. 32(3):40-45.

Strickler, M.D. 1959. Properties of Douglas-fir flakeboard. For. Prod. Jour. 7:203-215.

Suchsland, O. 1962. The density distribution in flakeboard. Quart. Bull., Michigan Agri. Exp. Sta., Michigan State University. 45(1):104-121.

Williams, M.L., J.D. Ferry, and R.F. Landel. 1955. The temperature dependence of relaxation mechanisms in amorphous polymers and other glass-forming liquids. Jour. of Amer. Chem. Soc. 77:3701.

Wilson, J. and Krahmer. 1976. Particleboard microscopic observations of resin distribution and board fracture. For. Prod. Jour. 26(11):42-45.

CHAPTER 2

FUNDAMENTALS OF FLAKEBOARD MANUFACTURE:

WOOD-MOISTURE RELATIONSHIPS

ABSTRACT

A procedure is presented to estimate the relative vapor pressure, equilibrium moisture content, average flake temperature, and average flake moisture content in a flakeboard mat during hot-pressing. This method is based on measurements of temperature and total gas pressure in the mat during hot-pressing. A heat and mass transfer model was adapted from the literature to predict the temperature and moisture content inside an individual flake. Significant moisture gradients are predicted to develop within flakes. Convective heat transfer appears to control the change of moisture content within a flake. Thermodynamic equilibrium between the gas phase and the wood component is not achieved during hot-pressing.

INTRODUCTION

The wood component in a flakeboard mat during hot-pressing is subjected to rapidly changing gas pressure, temperature, and humidity (Kamke, Casey 1988a, 1988b). Temperature and moisture gradients are developed within the mat, which influence mechanisms involved in the panel formation. Extremes in temperature and moisture content affect the adhesive cure and penetration (Brady, Kamke 1988; Chow, Mukai 1972), which in turn affect the bond quality. The interaction of temperature, moisture content, and compaction pressure is responsible for the forma-

13

tion of a vertical density gradient in the panel (Strickler 1959; Wolcott et al. 1989). The local density will influence the physical properties of the panel as a result of the bonding area between adjacent wood elements (Back 1988), flake damage (Geimer et al. 1985), and the amount of cell wall substance per unit volume of panel.

Mathematical models have been developed to predict internal mat temperature and moisture content in particleboard during hot-pressing (Humphrey 1979; Kayihan, Johnson 1983; Harless et al. 1987). These models treat the flakeboard mat as a continuum with a characteristic void volume. Local thermodynamic equilibrium is assumed, therefore, any resistance to heat and mass transfer between the gas phase and the adjacent wood component is neglected. This may produce predicted mat temperatures and moisture contents that differ from those inside a wood flake.

Methods have not yet been developed to experimentally measure the moisture content of the wood component in mats during hot-pressing. However, the in situ temperature and total gas pressure can be measured (Humphrey 1979; Kamke, Casey 1988a, 1988b). These parameters can then be used to describe the composition of the gas phase surrounding the wood component. An exchange of heat and mass will occur across the boundary of the wood component as the system moves toward thermodynamic equilibrium. Some resistance to temperature and moisture movement must exist at the surface of the wood elements. Previous models account for this resistance by incorporating this effect into experimentally derived heat and mass transfer coefficients for the mat continuum.

Convective heat and mass transfer coefficients have been calcu-

lated for fixed and fluidized beds of granular materials (Frantz 1961; Toei et al. 1967; Treybal 1980). These coefficients are used to describe the transfer of heat or mass from the gas phase to the solid phase in the granular bed. If the composition of the gas phase and the transport resistances surrounding a wood flake can be measured or predicted, then the necessary boundary conditions would be available as inputs for a heat and mass transfer model of an individual flake. A model for predicting heat and mass transfer in wood is available (Stanish et al. 1985). Therefore, it is possible to use generalized equations and models that were derived independently of wood-flake mats to predict the change of temperature and moisture content of individual wood flakes during hot-pressing. This approach, however, does require knowledge of the gas phase composition within the flakeboard mat.

The objectives of this work were:

1. To develop a method for estimating the gas phase composition in a flakeboard mat during hot-pressing.

2. To use a previously developed heat and mass transfer model for wood to estimate the flake temperature and moisture content during hot-pressing.

3. To assess the amount of resistance to heat and mass transfer at a surface of a flake during the hot-pressing operation.

METHODS

High temperature EMC

Sorption models have long been used to predict the equilibrium moisture content (EMC) of wood as a function of relative humidity and temperature (less than 100°C) (Simpson 1971, 1973). Simpson (1973)

evaluated several types of sorption equations for their ability to describe the EMC data listed in the Wood Handbook (U.S. Forest Products Laboratory 1987). When a non-linear regression technique was used to perform the curve-fitting, Simpson judged that the two-hydrate form of the Hailwood-Horobin equation provided the best fit. This equation has been used to describe the EMC in heat and mass transfer models for wood. The equation and coefficients determined by Simpson (1973) are:

$$EMC = \frac{1800}{W} \left[\frac{KH}{1-KH} + \frac{K_1KH + 2K_1K_2K^2H^2}{1 + K_1KH + K_1K_2K^2H^2} \right] \qquad [2.1]$$

where:
$W = 349 + 1.29\ T + 1.35 \times 10^{-2}T^2$
$K = 8.05 \times 10^{-1} + 7.36 \times 10^{-4}T - 2.73 \times 10^{-6}T^2$
$K_1 = 6.18 + 5.07 \times 10^{-3}T - 3.00 \times 10^{-4}T^2$
$K_2 = 2.39 + 2.56 \times 10^{-2}T - 3.03 \times 10^{-4}T^2$
$H = $ relative vapor pressure
$T = $ temperature (°C)

Whereas average sorption relationships are well documented for wood at low temperatures, data at elevated temperatures (higher than 100°C) are limited. Simpson and Rosen (1981) reviewed the literature for both experimental and extrapolated data on wood moisture contents at one atmosphere pressure and elevated temperatures. They concluded that the data for elevated temperatures could be adequately described using the one hydrate form of the Hailwood-Horobin equation, with the parameters presented for the low temperature sorption data by Simpson (1971). However, the two-hydrate form of the Hailwood-Horobin theory was not evaluated. In addition, Resch et al. (1988) published data on sorption characteristics of yellow poplar (Liriodendron tulipifera) at high tem-

peratures and pressures greater than one atmosphere. The elevated temperature data presented by Simpson and Rosen (1981) for one atmosphere of pressure, and the data by Resch et al. (1988) at pressures greater than one atmosphere, were evaluated in this study using both the one and two-hydrate forms of the Hailwood-Horobin equation. The coefficients used in the equations are the same as presented by Simpson (1971, 1973).

The experimental EMC values were compared to the results from the empirical equations using the root mean square error (Benjamin, Cornell 1970), which is a measure of the average deviation that can be expected over the range of experimental values. Table 2.1 displays the mean square error and the maximum deviation for both equations and data sets. Less error exists between the predicted and measured EMC for the data collected at one atmosphere of pressure than at the elevated pressures. The predictions are poorest for the pressurized conditions at 140°C. The data at this temperature is suspect because the desorption isotherm lacks the sigmoidal form exhibited at 120°C and 160°C (Resch et al. 1988).

An analysis of covariance was used to determine if a statistical difference existed between the individual regression lines of the experimental EMC values versus the predicted EMC (Snedecor, Cochran 1967). This analysis showed that no significant difference can be discerned among the regression lines for these four comparisons at the 0.05 alpha level.

It has been shown in Table 2.1, that the predicted EMC can vary substantially from the experimental EMC under certain conditions. However, considering the limited experimental data, we have chosen to use

the two-hydrate form of the Hailwood-Horobin equation presented by Simpson (1973).

Estimating the gas phase composition

When the flake mat is initially compressed some air and water vapor is trapped within the void network. Because the voids are small, the wood component controls the water vapor content. Subsequent heating of the outer surfaces of the mat rapidly generates water vapor, thus increasing the total gas pressure at the surface. The positive pressure differential between the surface and the core results in the hydrodynamic flow of heat-laden water vapor to the core of the mat. In the core, the incoming water vapor is mixed with the existing environment. Condensation in the core is possible. The addition of water vapor from the surface causes an increase of total pressure in the core. A positive pressure differential is established from the interior of the mat laterally to the edges. Thus, a mixture of water vapor and air will flow through the edges of the mat. The air in the gas phase will never be replenished during hot-pressing. Therefore, the mole fraction of the air in the voids will continually decline.

A series of plots of temperature and total gas pressure in the core of flake mats during hot-pressing were presented by Kamke and Casey (1988b). The total gas pressure rises until the rate of dissipation through the edges of the mat exceeds the rate of water vapor generation. This occurs when the bound water supply is nearly depleted or the lateral permeability of the mat increases as a result of venting.

The environmental variables measured inside a mat during hot-

pressing are temperature and total gas pressure. However, the bound
water content in wood responds to changes in temperature and water vapor
pressure. To describe the moisture content change of the wood compo-
nent, the relative water vapor pressure in the mat can be calculated
based on local temperature and total gas pressure data. At the begin-
ning of the press cycle the initial relative vapor pressure inside the
mat is determined from the initial mat moisture content and temperature
using an inverted form of Equation [2.1]. The initial partial pressure
of the water vapor (p_w) is calculated as:

$$p_w = H \ p_{sat} \hspace{3cm} [2.2]$$

where:
$\quad$ H $\quad$ = relative vapor pressure.
$\quad$ p_{sat} = saturated vapor pressure, atm.

The p_{sat} is calculated using the empirical equation derived by Stanish
et al. (1985):

$$p_{sat} = \frac{RT}{18} \ e^Q \hspace{3cm} [2.3]$$

where:
$\quad$ Q = $-46.49 + 0.26179T - 5.0104 \times 10^{-4}T^2 + 3.4712 \times 10^{-7}T^3$
$\quad$ R = gas constant = 0.08206 atm m^3/mole K
$\quad$ T = temperature, K.

The water vapor content is defined as:

$$C = \frac{p_w}{P} \hspace{3cm} [2.4]$$

where:
$\quad$ C = water vapor content, moles of water
$\quad\quad$ vapor/total moles of gas.
$\quad$ P = total gas pressure, atm.

The water vapor content at any other time during the press cycle is estimated based on the following assumptions:

1. At any location in the mat the change in total gas pressure results from the internal generation of water vapor, hydrodynamic flow from other regions in the mat, and a temperature effect as defined by the ideal gas law.

2. Gas continuously leaks through the edges of the mat. The rate of leakage is proportional to the pressure differential. The leakage coefficient is constant over time and location in the mat.

3. Air is not replenished in the mat. The water vapor content will not decrease during hot-pressing.

4. Only water vapor and air are present in the gas phase.

From Assumption 4, the vapor pressure of the formaldehyde resin is neglected. Whereas, this assumption is not strictly correct, it has been shown that the increase in the internal gas pressure from formaldehyde is insignificant (Kamke and Casey 1988b). Therefore, considering the total gas pressure is comprised only of the partial pressures of the water and air:

$$P = p_w + p_a = p_w + (1 - C) \, P \qquad [2.5]$$

Substituting the ideal gas law for the partial pressure terms yields:

$$P = (c_w + c_a) \, RT \qquad [2.6]$$

where:
c_w = molar concentration of water vapor, $mole/m^3$.
c_a = molar concentration of air, $mole/m^3$.

Differentiating Equation [2.6] with respect to time gives:

$$\frac{dP}{dt} = RT \left[\frac{dc_w}{dt} + \frac{dc_a}{dt} \right] + R(c_w + c_a) \frac{dT}{dt} \qquad [2.7]$$

The time derivative of the molar concentration of water vapor is dependent on internal generation of water vapor, flow inside the mat, and leakage out of the mat. This analysis is concerned with the conditions at a point in the mat. Therefore, the mechanisms that are responsible for the change in molar concentration of water vapor are not separated, and this term is treated as a dependent variable.

The molar concentration of the air is dependent on flow inside the mat and leakage out of the mat. The significance of the leakage is that it results in a continuous decrease in the partial pressure of air. Assumption 3 states that air is not replenished, therefore, the water vapor content, C, will increase in addition to the amount resulting from internal generation. The transport mechanisms affecting air flow cannot be separated using this analysis. To account for the change in water vapor content as a result of leakage, an effective mat permeability factor was defined to relate the relative change of the molar concentration of air to the total pressure differential between the interior of the mat and the ambient environment.

$$\frac{dc_a}{dt} = -(1 - C) K (P - P_{amb}) \qquad [2.8]$$

where:
   K = apparent mat permeability factor, $mole/m^3 \cdot atm \cdot sec$.
   P_{amb} = ambient total pressure, atm.

It must be emphasized that Equation [2.8] does not represent a strict

application of permeability. The geometrical considerations are combined in K. The effective mat permeability factor is treated as a constant, but the physical properties of the mat and particles will affect its value.

The molar concentration terms can be expressed as partial pressures by applying the ideal gas law, as shown by Equations [2.5] and [2.6]. The time derivative of the molar concentration of water vapor becomes:

$$\frac{dc_W}{dt} = \frac{1}{RT} \frac{dp_W}{dt} - \frac{p_W}{RT^2} \frac{dT}{dt} \qquad [2.9]$$

Substituting Equations [2.8] and [2.9] into [2.7], and solving for the time derivative of the partial water vapor pressure yields:

$$\frac{dp_W}{dt} = \frac{dP}{dt} + \frac{(p_W-P)}{T} \frac{dT}{dt} + (1-C)K(P-P_{amb})RT \qquad [2.10]$$

The known quantities in Equation [2.10] are P and T for $0 \leq t \leq t_{max}$, p_W and C for t - 0, and P_{amb} and R are constants. K can be calculated using experimental data when the value of p_W is known over a definite time period. The temperature and gas pressure data reported by Kamke and Casey (1988b) for the core of a mat pressed at 15 percent moisture content revealed a saturated environment. In this case, the change of the water vapor pressure is equal to the change of the saturated water vapor pressure, which is only a function of temperature. With this information, Equation [2.10] was solved numerically to obtain K equal to 8.9×10^{-4} mole/m^3·atm·sec. This value is used for all mats containing

the same flake geometry, average mat density and size.

Equation [2.10] is solved numerically using a backward differenc-
ing scheme to obtain the partial water vapor pressure as a function of
time. The relative vapor pressure is calculated using the relationship
in Equation [2.2]. The equilibrium moisture content is then estimated
from the sorption relationship given by Equation [2.1].

The environmental conditions surrounding a flake have been esti-
mated with the analysis presented above. These conditions consist of
measured temperature and total gas pressure data and estimated relative
vapor pressure over the entire press cycle. The next step is to model
the change of temperature and moisture content inside a wood flake as a
result of these internal mat conditions.

Heat and Mass Transfer Model

The model used to describe the heat and mass transfer inside of an
individual wood flake is one developed by Stanish et al. (1985) and
Schajer (1984). The heat and mass transfer process in wood is mathemat-
ically described by a set of one-dimensional transport equations (the
length and width directions are neglected) that are coupled using an
expression of thermodynamic phase equilibrium. The model considers heat
transfer via conduction and convection. Mass transfer occurs as a res-
ult of gaseous and bound water diffusion, and hydrodynamic flow of
gaseous and liquid water. Diffusion of bound water is considered to be
driven by a gradient in chemical potential. The bound water concentra-
tion is determined at the local temperature using an inverted form of
the one-hydrate Hailwood-Horobin model fit to low temperature sorption

data (Simpson 1971). The physical properties of the wood are allowed to vary with both space and time. Therefore, any transport equations that are dependent on these properties can vary similarly. The reader is referred to the literature for a more thorough discussion of the model. One factor that the model does not consider is the depression of the sorption isotherm with an applied compression stress. Ignoring this phenomenon will tend to make the predicted moisture contents higher than those if the factor was considered. The magnitude of this effect during the pressing cycle is not known.

Boundary conditions

The boundary conditions of temperature and relative vapor pressure surrounding a flake must be known to apply the heat and mass transfer model. The measured mat data presented by Kamke and Casey (1988b) was used for this information. Twelve yellow poplar flakeboard mats were pressed in a 610x610 mm laboratory hot-press to a nominal density of 750 kg/m^3. Two platen temperatures (154 and 190°C) and initial mat moisture contents (6 and 15 %) were used. The panels were bonded with 5% phenol-formaldehyde resin solids with a one-minute press closing time and twelve-minute total press time. Temperature and total gas pressure data were acquired by a computer at face and core locations in each mat. Relative vapor pressure was calculated from the temperature and total gas pressure data as described previously.

Other information required for solving the heat and mass transfer model are the convective heat and mass transfer coefficients that correspond to the surfaces of the flakes within the mat. An estimate of

these values is described in the following discussion.

RESULTS AND DISCUSSION

Transient EMC conditions

A plot of the measured temperature and calculated relative vapor pressure in the core and the face region of a flakeboard mat pressed at 190°C, with a 15 percent moisture content, is shown in Figure 2.1. Note the significant increase of the relative vapor pressure in both the face and the core beginning at 1.5 and 2.5 minutes into the press cycle, respectively. This corresponds to an increase of the total gas pressure, and does not begin until after the initial rise of temperature. When venting begins at 6 minutes, the relative vapor pressure in the face declines. However, the relative vapor pressure in the core remains at a high level. The temperature in the core declines during the venting period, indicating the presence of a significant amount of water in a condensed phase. As the total pressure of the core region is reduced, the latent heat of evaporation results in a net reduction of the temperature.

The transient EMC conditions that occurred at face and core locations in the mats considered are presented in Figure 2.2. Initially, the EMC conditions are equal to the initial mat moisture content as imposed by the procedure used to calculate relative vapor pressure. The EMC drops rapidly as the temperature increases in the mat. As the bound water in the wood evaporates and moves into the void spaces between flakes, the relative vapor pressure, and therefore, EMC conditions

increase. This is particularly evident in the core. When venting

begins (6 minutes into the press cycle), the water vapor rapidly dissi-

pates out of the panel, and the total gas pressure drops. The relative

vapor pressure and EMC may remain the same, increase, or decrease

depending on the amount of water remaining in the wood. It is interest-

ing to note that the EMC of the core in the 190°C and 15 percent mois-

ture content mat increases during the venting period. This occurs

because the latent heat of evaporation causes a reduction of the temper-

ature while the relative vapor pressure remains approximately constant.

Estimating parameters for the heat and mass transfer model

The use of a mechanistic model to describe the heat and mass

transfer in wood requires the knowledge of several physical parameters

and some transport coefficients. The physical parameters that must be

known include the flake thickness, density, permeability, bound water

diffusivity, water vapor diffusivity, and others. Due to the natural

variability of wood, these physical parameters will vary from flake to

flake. Stanish et al. (1985) presented most of the relationships neces-

sary for estimating these physical parameters. The flake density and

thickness can be measured, but these quantities change during the pro-

cess of hot-pressing. Describing the heat and mass transfer across the

boundary of the flake requires a knowledge of convective heat and mass

transfer coefficients. Empirical equations are available in the litera-

ture that can be used for calculating convective heat and mass transfer

coefficients for gas flow through granular beds of material. Using

results from the literature all of the physical parameters and transport

coefficients can be estimated independent of measurements made in a flakeboard mat during hot-pressing. However, a sensitivity analysis of these parameters and coefficients is required to better understand how they affect the overall solution.

A sensitivity analysis for the model was conducted using the experimental data collected from the twelve yellow poplar flakeboard mats. The initial flake thickness and density were used for the analysis. The dominant parameter was found to be the convective heat transfer coefficient. This result is consistent with the results from the literature on wood particle drying (Kamke, Wilson 1986). Because of the relatively short distance for heat and moisture movement inside of the wood flake, nearly all the resistance occurs at the surface. Therefore, the convective heat transfer coefficient is expected to be the controlling factor.

To demonstrate the influence of the convective heat transfer coefficient on the predicted average moisture content of flakes during hot-pressing, four simulations were run with the convective heat transfer coefficient differing by an order of magnitude (Figure 2.3). The average moisture content was predicted for both a face and core location in the mat (only the core is shown in Figure 2.3). As the convective heat transfer coefficient is decreased from a maximum value of 1000 W/m^2K, the predicted moisture content increases. The lowest convective heat transfer coefficient (1 W/m^2K) resulted in an unrealistic increase in the predicted moisture content in both the face and core locations. The convective heat transfer coefficients of 100 and 1000 W/m^2K show the expected rapid decrease in the predicted moisture content shortly after

the press closes. However, after approximately 3 to 4 minutes the moisture content in both the face and the core is predicted to increase. This result is also unrealistic because the total moisture content of the mat must decrease over time. Based on this reasoning, a value for the convective heat transfer coefficient on the order of 10 W/m^2K appears to exhibit the most reasonable results. In this case, the predicted moisture content in the face rapidly decreases at the end of the press closing time and begins a more gradual decline. The predicted moisture content in the core begins to decline at a later time and more gradually. This simulation is used merely for demonstration purposes. The convective heat transfer coefficient is calculated later using empirical equations developed for granular beds.

It is unreasonable to expect that the convective heat transfer coefficient would remain constant during the entire press cycle. The flow of heat due to convection is the result of gas movement through the mat, with this gas being primarily water vapor generated through evaporation. Because the evaporation rate of moisture from the wood particles changes during the press cycle, the rate of gas flow through the mat would also change. Therefore, the convective heat transfer coefficient would not be constant. Nevertheless, for the lack of more information, this analysis assumes a constant convective heat transfer coefficient.

Because the heat and mass transfer model is applied only to an individual flake, there is no balance of heat and mass that is mathematically satisfied over the entire flake mat. The environment data from the flake mats does not identify where water vapor is generated, but

only that it is present. As a result, the analysis of temperature and moisture content change in the face and core locations are performed independently.

Toei et al. (1967) developed methods for calculating the convective heat transfer coefficient (h) for super-heated steam drying of porous solids. Their experimental data was collected using a fixed-bed of clay and sawdust with a moving stream of steam passing through the bed. Their equation, with the terms regrouped, is:

$$h = 1.95 \left[\frac{GD_p}{\mu} \right]^{0.49} \left[\frac{c\mu}{k} \right]^{0.33} \left[\frac{k}{D_p} \right] \qquad [2.11]$$

where:
    G = mass gas flow rate (kg/m^2s)
    D_p= equivalent particle diameter (m)
    μ = viscosity of the gas (steam=1.3x10^{-7} Pa s)
    c = specific heat of gas (steam=2060 J/kg $^\circ$C)
    k = thermal conductivity of gas
        (steam=0.025 W/m$^\circ$C)

In estimating G for the hot-pressing operation, the focus is on the initial six minutes of the pressing cycle where nearly all of the temperature increase occurs. During this time, in the center of the mat, moisture is driven primarily from the face to the core region. It is assumed, for the moment, that the gas flow consists entirely of water vapor. For initial and final mat moisture contents of 15% and 6 %, respectively, and a cross-sectional area of 0.37 m^2, the average mass flow rate is estimated as 0.005 kg/m^2s. D_p was determined for an average flake (5 x 1 x 0.09 cm) using the method of equivalent surface area of a sphere (Perry, Chilton 1973). Using Equation [2.11] the value for

h is estimated to be 7 W/m^2K. This value corresponds well to the most reasonable moisture content profile generated using the sensitivity analysis shown in Figure 2.3 (h=10 W/m^2K). All subsequent analyses use h=10 W/m^2K.

The flake thickness and density also influence the predictions from the heat and mass transfer model. Because the flakes deform viscoelastically, and transient temperature and moisture gradients exist in the mat, the flakes are likely to continuously deform during much of the pressing cycle (Wolcott et al. 1989). However, fixed physical dimensions must be given for the wood element in the heat and mass transfer model. The results of simulations using the initial and final flake thickness and density are presented in Figure 2.4. As shown, there is little difference between the use of the initial or final flake thickness and density. The use of the final flake dimensions is more realistic because the flake must approach the final dimensions at the time the press is closed and much of the stress is relieved. Therefore, the remaining simulations use the final flake dimensions and density.

Flake moisture content predictions

The heat and mass transfer model predicts that a significant moisture content gradient develops in the flake (Figure 2.5). When the internal environment changes slowly, the gradients are small. However, during rapid changes the moisture gradient is significant. Interpretation of this result raises the question whether local thermodynamic equilibrium is an appropriate assumption when the mat is modeled as a continuum. In other words, the flake moisture content is not equivalent

to the EMC. The example in Figure 2.5 shows that the EMC and flake moisture content are close only at the beginning and end of the press cycle.

As shown in Figure 2.6, the flake temperature does not develop a significant gradient. The transport of heat in wood is much more rapid than the transport of moisture. In Figure 2.6, the measured temperature is that of the internal environment surrounding the flake being modeled. As expected it differs from the predicted flake temperature resulting from the significant convective heat transfer coefficient used in the analysis. If there was no resistance to convective heat transfer into the wood component, the measured environment and predicted flake temperatures would be coincident.

The predicted average moisture content for the four pressing schedules studied are presented in Figure 2.7. This method predicts an initial plateau of moisture content with a rapid decrease beginning after press closure in the face. The decrease of moisture content in the core is delayed up to one minute in these mats, and then begins a more graduate decline. Another plateau may be obtained in the core, followed by a final decrease of moisture content after venting begins at 6 minutes into the press cycle. It is interesting to note that condensation is predicted well into the press cycle in the low moisture content mats. This increase corresponds to the increase of total gas pressure in the core. A small peak in moisture content in the face of the high moisture content mats is predicted, beginning when the press is closed. This results from the entrapment of gas in the voids of the face region, and the corresponding increase of total gas pressure. This

is a pressure and volume phenomena.

SUMMARY AND CONCLUSIONS

A method has been presented to calculate the relative vapor pressure in the internal environment of a flakeboard mat during hot-pressing. This technique uses measured temperature and gas pressure data from the mat. A mathematical relation for EMC as a function of temperature and relative vapor pressure is used to determine the transient EMC conditions that exist in the mat.

Temperature and moisture content of the wood component are predicted using a fundamental heat and mass transfer model for wood. Use of this method shows that a significant resistance to convective heat transfer at the surface of a flake controls the heat and mass transfer between the wood flake and the internal environment. The temperature and moisture content of the wood component is not in equilibrium with the internal mat environment.

Several assumptions were required to solve the model presented here. While this may limit the quantitative use of the model, the predicted trends are reasonable and do not conflict with the limited experimental data that are available. These results have implications on the development of the vertical density gradient, adhesive bond formation, mat venting, springback, and other panel properties or behavior that depend on wood moisture content and temperature.

LITERATURE CITED

Back, E.L. 1987. The bonding mechanism in hardboard manufacture. Holz-forschung 41(4):247-258.

Benjamin, J. R. and C.A. Cornell. 1970. Probability, Statistics, and Decision for Civil Engineers. New York: McGraw Hill.

Brady, D.E. and F.A. Kamke. 1988. Effects of hot-pressing parameters on resin penetration. For. Prod. J. 38(11/12):63-68.

Chow, S.Z. and H.N. Mukai. 1972. Polymerization of phenolic resin at high vapor pressure. Wood Sci. 5(1):65-72.

Forest Products Laboratory. 1987. Wood handbook: Wood as an engineer-ing material. Agric. Handb. 72, p. 3-11. Washington, DC: U.S. Department of Agriculture.

Frantz, J.F. 1961. Fluid-to-particle heat transfer in fluidized beds. Chem. Engr. Prog. 57(7):35-42.

Geimer, R.L., R.J. Mahoney, S.P. Loehnertz, R.W. Meyer. 1985. Influ-ence of processing-induced damage on strength of flakes and flake-boards. FPL Res. Pap. No. 463. U.S. For. Prod. Lab., Madison, Wis.

Harless, T., F.G. Wagner, P.H. Short, R.D. Seale, P.H. Mitchell, D.S. Ladd. 1987. A model to predict the density profile of particle-board. Wood and Fiber Sci. 19(1):81-92.

Humphrey, P.E. 1979. Fundamental aspects of wood particleboard manufacture. Ph.D. Dissertation. Univ. of Wales, Bangor, Wales, U.K.; 158 p.

Kamke, F.A. and J.B. Wilson. 1986. Computer simulation of a rotary dryer: Part II: Heat and mass transfer. AIChE J. 32(2):269-275.

Kamke, F.A. and L.J. Casey. 1988a. Gas pressure and temperature in the mat during flakeboard manufacture. For. Prod. J. 38(3):41-43.

_____. and _____. 1988b. Fundamentals of flakeboard manufac-ture: internal mat conditions. For. Prod. J. 38(6):38-44.

Kayihan, F. and J.A. Johnson. 1983. Heat and moisture movement in wood composite materials during the pressing operation - a simplified model. In: Numerical Methods in Heat Transfer, Vol. 2, R.W. Lewis, K. Morgan, and B.A. Schrefler (Eds.); New York: John Wiley and Sons.

Perry, R.H and C.H. Chilton. 1973. Chemical Engineers' Handbook, 5 Ed. p. 5-62. New York: McGraw-Hill.

Resch, H., M.L. Hoag, and H.N. Rosen. 1988. Desorption of yellow poplar in superheated steam. For. Prod. J. 38(3):13-18.

Simpson, W.T. 1971. Equilibrium moisture content prediction for wood. For. Prod. J. 21(5):48-49.

_____. 1973. Predicting equilibrium moisture content of wood by mathematical models. Wood and Fiber 5(1):41-49.

_____. and H.N. Rosen. 1981. Equilibrium moisture content of wood at high temperatures. Wood and Fiber 13(3):150-158.

Schajer, G. S. 1984. DRYRUN, One dimensional wood drying computer program. Solid Wood Research and Development, Weyerhaeuser Company, Tacoma, WA.

Snedecor, G.W. and W.G. Cochran. 1967. Statistical Methods, 6 Ed., p. 432. Ames, Iowa: Iowa State University Press.

Stanish, M.A., G.S. Schajer, F. Kayihan. 1985. Mathematical models of wood drying from heat and mass transfer fundamentals. In: Drying '85, R. Toei; Mujumdar, A.S., pp. 360-367. New York, (Eds.) Hemisphere Publishing Corp.

Strickler, M.D. 1959. Properties of Douglas-fir flakeboard. For. Prod. J. 7:203-215.

Toei, R., M. Okazaki, M. Kimura, H. Ueda. 1967. Heat transfer coefficients on the super-heated steam drying of porous solids. Kagaku Kogaku 5(1):139-141.

Treybal, R.E. 1980. Mass-Transfer Operations. p. 202. New York: McGraw-Hill.

Wolcott, M.P., F.A. Kamke, and D.A. Dillard. 1989. Fundamentals of flakeboard manufacture: viscoelastic behavior of the wood component. Wood and Fiber Sci., in press.

Table 2.1: Statistical analysis for the one and two hydrate forms of
the Hailwood-Horobin sorption model fitted to EMC data for wood above
100°C. Data is from Simpson and Rosen (1981) and Resch et. al. (1988).

Model	Total Pressure (atm.)	Coefficient of Variation (% MC)	Root Mean Square Error (% MC)	Maximum Deviation (% MC)
1-Hydrate	1	12.8	0.90	2.1
	>1	29.5	1.23	4.4
2-Hydrate	1	11.6	0.86	3.7
	>1	27.6	1.19	4.7

.
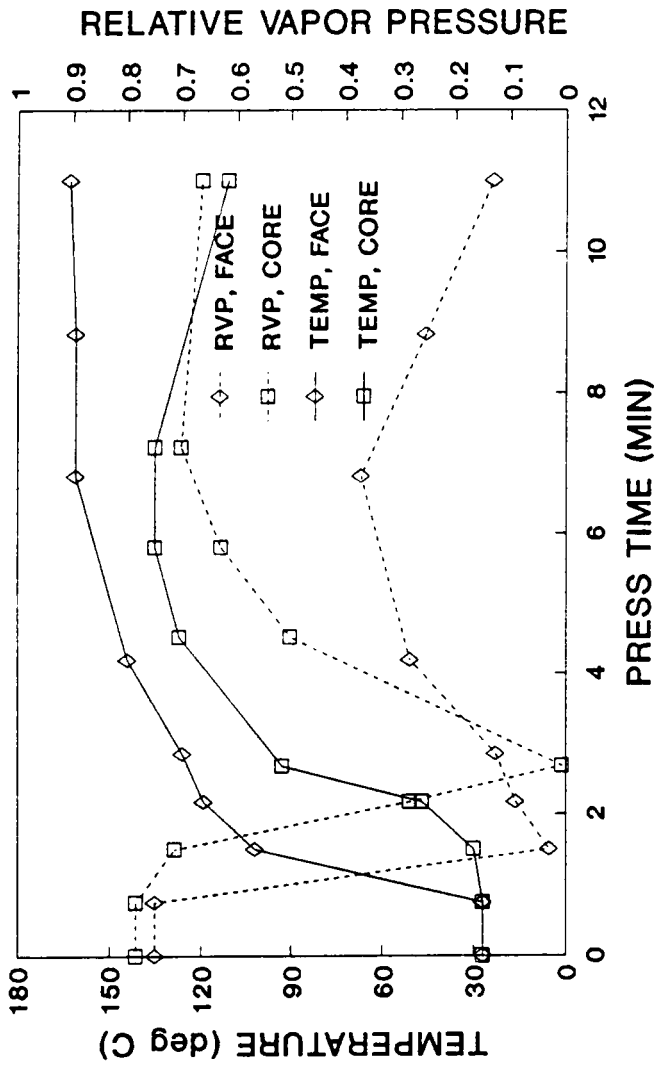
Figure 2.1: Measured temperature and predicted relative vapor pressure in the face and the core regions of a mat pressed at 190°C and 15% moisture content.
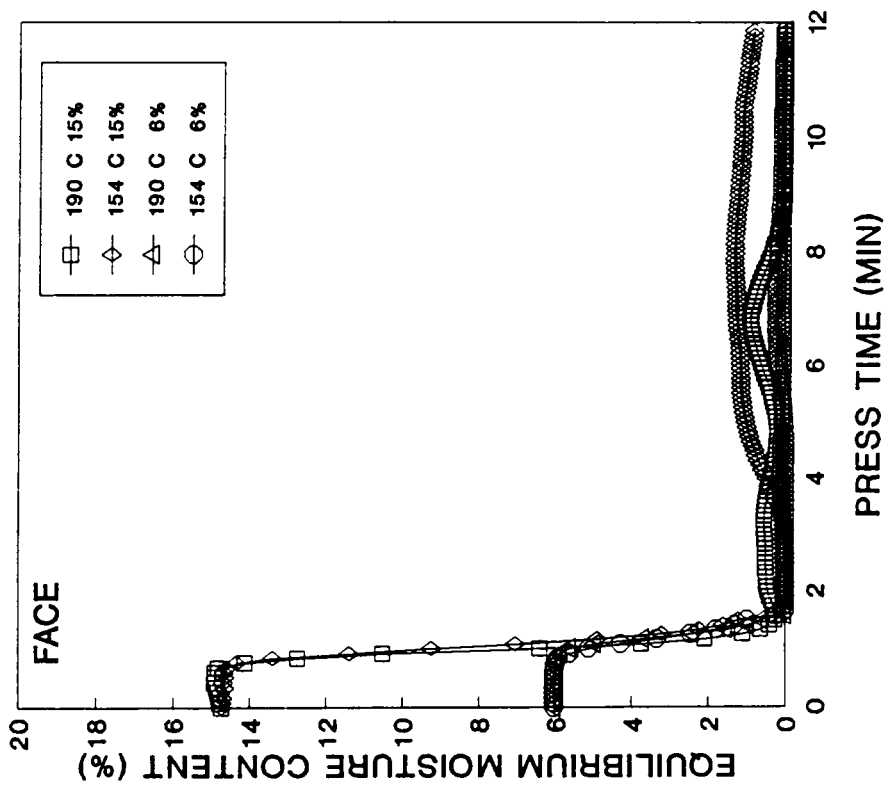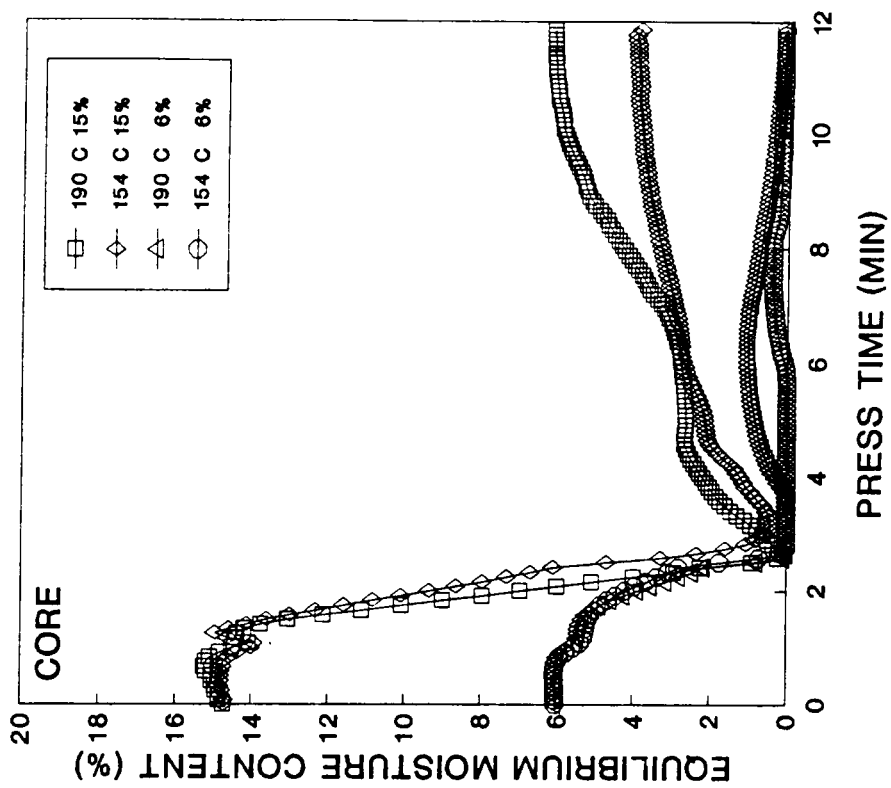
Figure 2.2: Predicted equilibrium moisture content based on measured temperature and total gas pressure in the face and core regions of mats pressed under the conditions indicated.
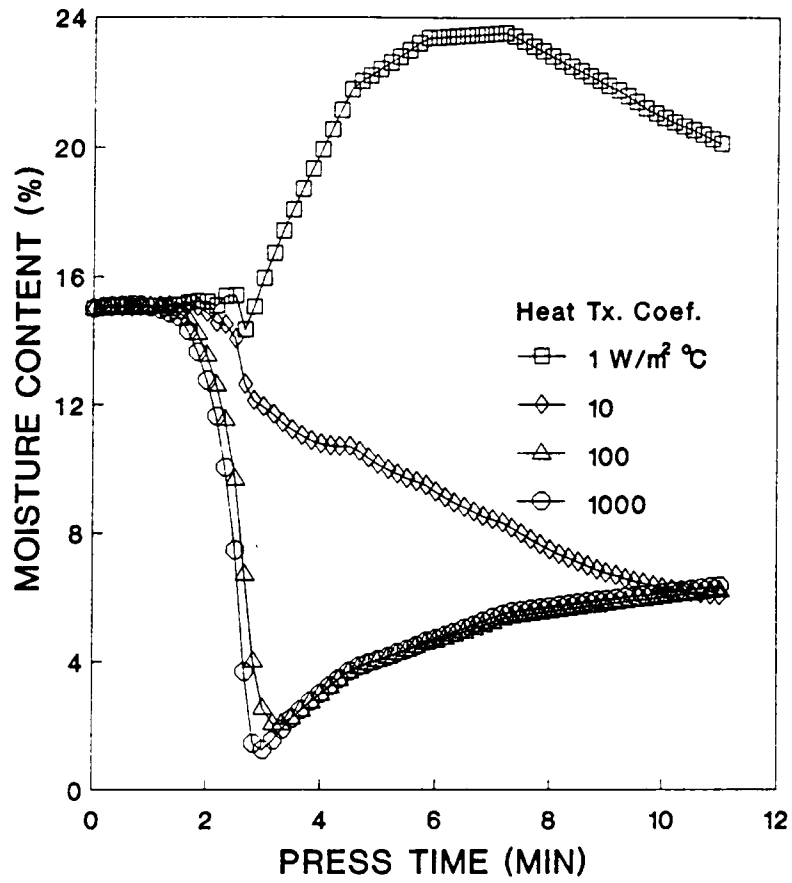
Figure 2.3: Predicted average moisture content of a flake in the core of a mat pressed at 190°C and 15% moisture content as a function of the convective heat transfer coefficient.
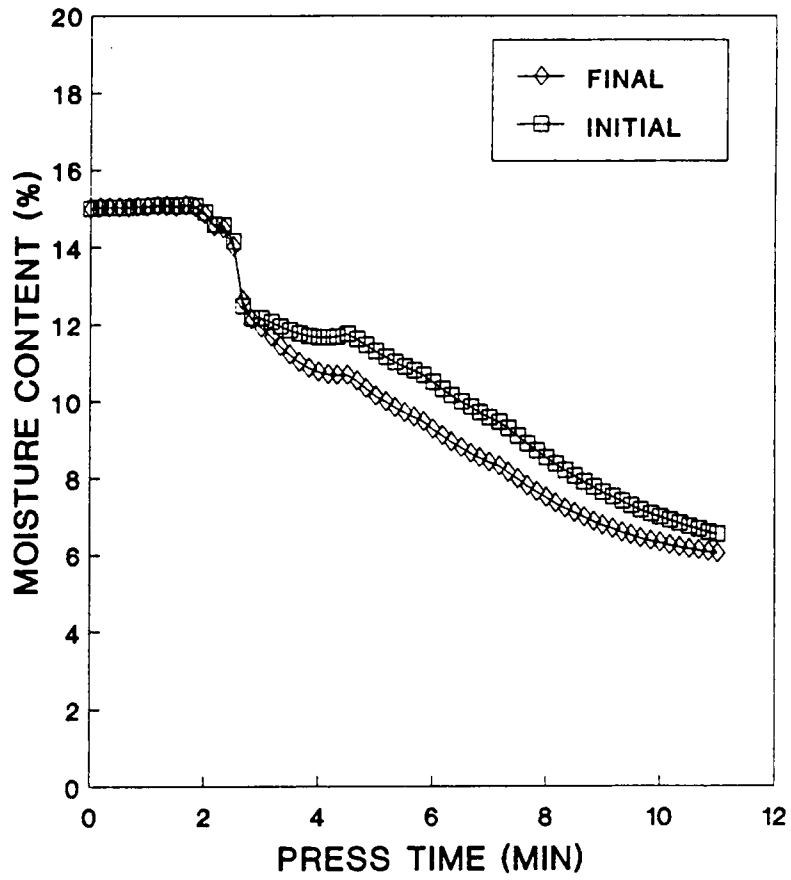
Figure 2.4: Predicted average moisture content of a flake in the core of a mat pressed at 190°C and 15% moisture content assuming initial and final flake thickness and density.
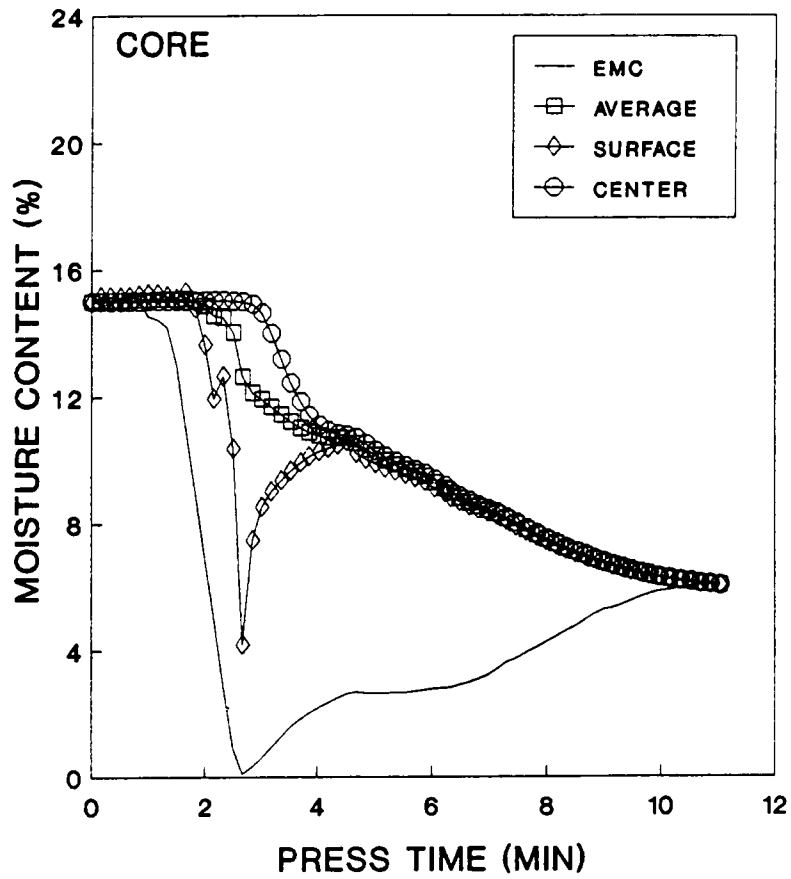
Figure 2.5: Predicted equilibrium moisture content and moisture gradient of a flake in the core of a mat pressed at 190°C and 15% moisture content.
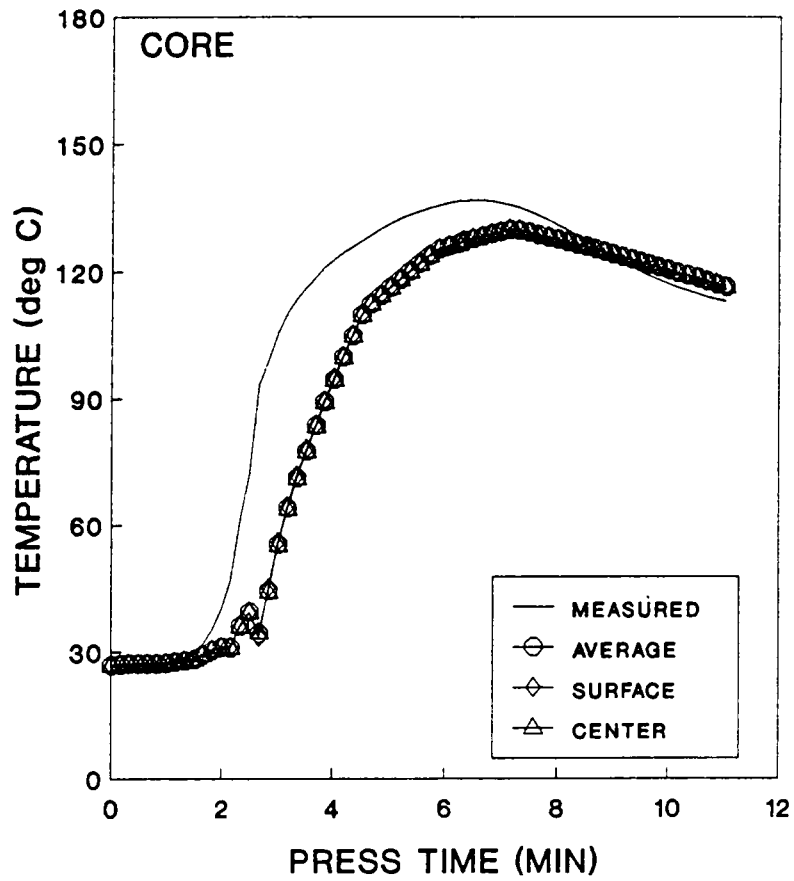
Figure 2.6: Measured temperature and predicted temperature gradient of a flake in the core of a mat pressed at 190°C and 15% moisture content.
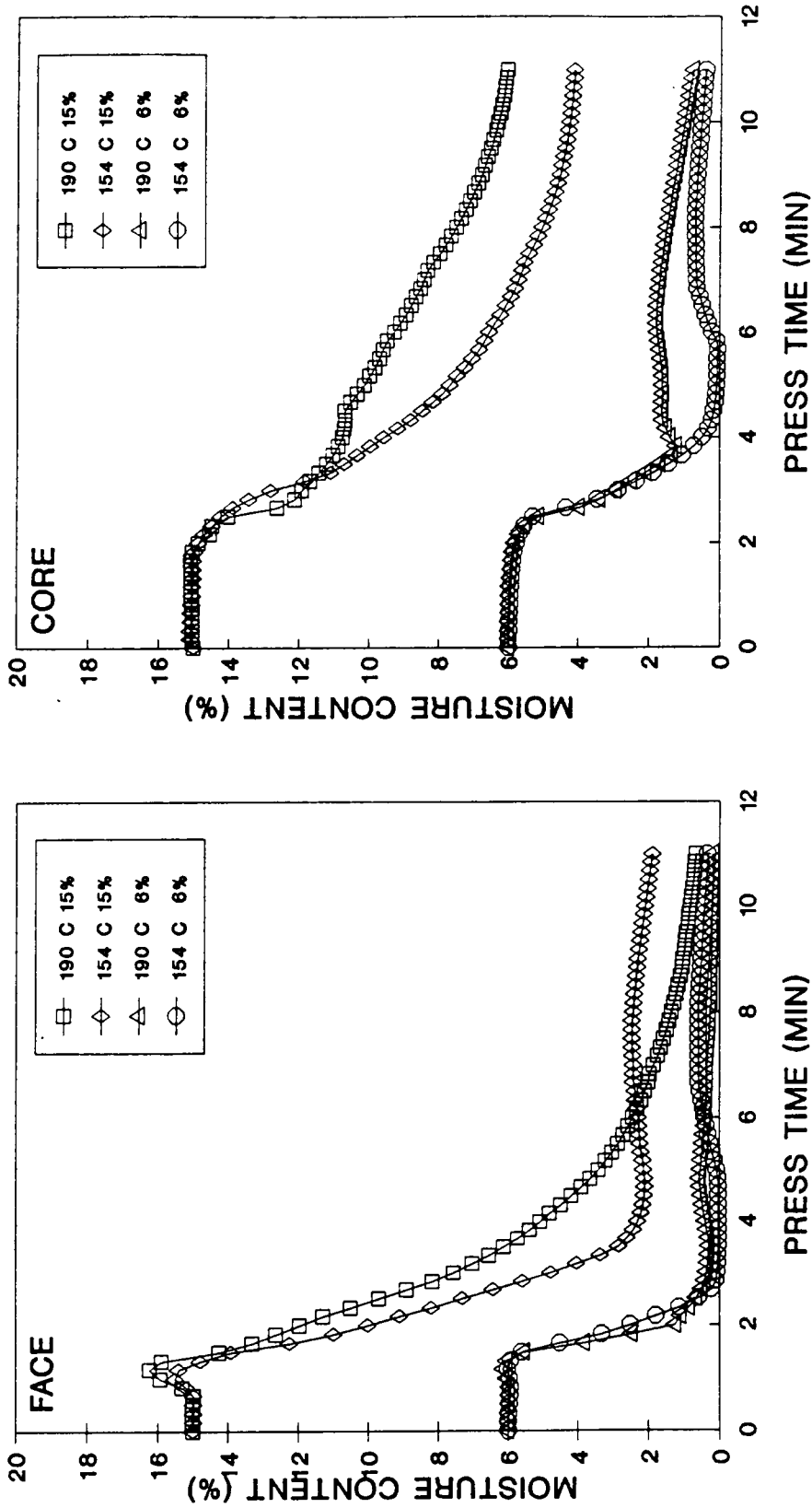
Figure 2.7: Predicted average flake moisture content in the face and core regions of mats pressed under the conditions indicated.

CHAPTER 3

FUNDAMENTALS OF FLAKEBOARD MANUFACTURE:

VISCOELASTIC BEHAVIOR OF THE WOOD COMPONENT

ABSTRACT

Theories of the viscoelastic behavior of amorphous polymers are
reviewed and used to describe the density gradient formation in flake-
board. This technique utilizes measured temperature and gas pressure at
discrete locations inside a flake mat during hot-pressing to predict the
glass transition temperature of wood as a function of press time. The
difference between the flake temperature and the predicted glass transi-
tion temperature is a relative indicator of the amount of flake deforma-
tion and stress relaxation at a location in the mat. A knowledge of the
stress history imposed in the mat is then used to relate flake deforma-
tion and stress relaxation to the formation of a density gradient. This
analysis allows for a significant portion of the density gradient to
develop after the hot press has closed. Experimental data for various
density gradients support the theories presented here.

INTRODUCTION

With the large number and diversity of materials available today,
the ability of the manufacturer to control properties is critical for
success of the product in the marketplace. Although we have little or
no control over the engineering properties of solid wood, the potential
for the design of material properties in wood composites is great. Large
strides are presently being made in the design of non-veneer structural

43

panels by using material engineering and science principles (Hunt and Suddarth 1974, Laufenburg 1983, 1984, Back 1987). However, a large gap in our fundamental knowledge of wood composite systems is in the understanding of how raw material properties and processing variables interact to influence the internal geometry and material properties of the components in situ.

The ability to use production variables to control material properties of wood composites is a valuable tool that has been studied on an empirical basis (Geimer 1980, Kelley 1977). For non-veneer wood composites, the focal point of the production process is the hot press. The pressing cycle incorporates simultaneous heat, mass, and momentum transfer to consolidate individual wood particles into a contiguous product. Because of the extreme physical conditions, the pressing cycle will have a profound influence on the in situ material properties and internal geometry of the wood components. This paper will discuss the interaction of the hot pressing process and the viscoelastic behavior of the wood component.

THE PRESSING CYCLE

During the hot pressing cycle, heat is conducted into the mat from platens that attain temperatures in the range of 150°C to 225°C. Both conductive and convective heat transfer occur inside the mat. Initially, moisture in the wood near the heated platens vaporizes, total gas pressure increases in the outer portion of the mat, and the heat-laden vapor is driven vertically to the center and horizontally to the

edges of the mat. This simultaneous heat and mass transfer results in transient temperature, gas pressure, and moisture content gradients in the panel during pressing (Maku et al. 1959, Suchsland 1962, Humphrey 1979, Kamke and Casey 1988a, 1988b).

During the press closing time a maximum compaction pressure of 4 to 8 MPa are imposed on the panel. After the targeted mat thickness is achieved, the compaction pressure required to hold position declines as a result of stress relaxation. Presumably, higher localized pressures result from the heterogenity of the mat. The stresses in the mat result in permanent deformation of the wood component because the average product density is usually greater than that of the original wood component.

The transient temperature and moisture gradients inside the mat result in non-uniform and changing compression properties of the wood component. When the compaction pressure applied to the mat is coupled with the changing compression properties, a density gradient develops. After the thermosetting adhesive has sufficiently cured, the venting process begins. The compaction pressure is slowly relieved, allowing the internal gas pressure to dissipate before opening the press.

When the pressure applied to the mat is coupled with the interior transient temperature and moisture conditions, density gradients form in the processed panel. Density gradients are important to pressed wood composites because they influence material properties of the composite in following ways:

> 1. Density is strongly correlated to the strength and engineering properties of the individual wood components (Price 1976, Geimer et al. 1985, Casey 1987).

2. The stress under which the wood is compressed affects the strength and engineering properties of the wood component in situ by forming micro-fractures in the cell walls (Geimer et al. 1985).

3. The bond strength is related to the plasticization of the wood component (Back 1987). Forming an intimate wood-adhesive-wood contact surface is necessary to increase the bonding area.

4. Density gradients determine the geometry of the final internal structure of the composite (i.e. higher densities correspond with more wood elements per unit volume).

VISCOELASTIC BEHAVIOR OF AMORPHOUS POLYMERS IN WOOD

Mechanical Behavior of Amorphous Polymers

For polymers, the dependence of mechanical properties on time, temperature, and diluent concentration (i.e. moisture content) is unified through the viscoelastic properties. From our present knowledge of the morphology and structure of the individual polymers in wood, certain information on their viscoelastic response can be inferred using polymer and composite theory. For the moisture contents usually encountered in the processing of wood composites, less than 15 percent, it is reasonable to assume that the semi-crystalline cellulose is not viscoelastic (Salmèn et al. 1985). Therefore, the influence of moisture and temperature is restricted to the amorphous polymers in wood, namely the hemicelluloses and lignin.

Amorphous polymers are termed viscoelastic because they can exhibit a range of properties from viscous fluids to linear elastic solids depending on the temperature, diluent concentration, or time scale of the test (Figure 3.1) (Ward 1983). The glassy state of a polymer corre-

sponds with low temperatures, low diluent concentrations, and high
frequencies (i.e. short times). It is characterized by a high modulus
and brittle fractures at small strains. At high temperatures, high
diluent concentrations, and low frequencies (i.e. long times), the
polymer is in the rubbery state that is characterized by large strains
at failure and a modulus that is approximately three orders of magnitude
lower than in the glassy state. At higher temperatures and longer time
scales, some polymers (i.e. thermoplastics) will exhibit viscous flow.
However, the unmodified polymers in wood probably undergo thermal degra-
dation before they exhibit a true viscous region. This should not be
confused with the viscous component of viscoelastic behavior, which does
occur in wood. Between conditions associated with the glassy and rub-
bery regions, a polymer is in the transition state. In this region,
large changes in polymer properties result from small changes in time,
temperature, or diluent concentration.

Time-Temperature-Diluent Concentration Equivalence

The analogous behavior of polymers with different time, tempera-
ture, and diluent concentrations is exhibited best in thermorheologi-
cally simple systems (Christensen 1982). In these polymer systems, the
time dependent mechanical response at different temperatures and diluent
concentrations are related by a change in the time scale only. Once the
time dependent response of a polymer is determined over a large range of
times (termed a master curve), the effect of a temperature change is
equivalent to a horizontal shift of the master curve via a time multi-
plier (the shift factor) (Figure 3.1). This equivalence is on a spe-

cific volume basis. Therefore, the magnitude of the response must be corrected for changes in density.

The time-temperature equivalence of viscoelastic properties has been used for accelerated testing techniques and is termed time-temperature superposition (Ferry 1980). This technique consists of short term creep or stress relaxation tests at different temperatures. The relaxation modulus or creep compliance curves are shifted along the log time axis to construct the master curve. The time multipliers are then recorded for each shift to determine the shift factor.

A time-temperature equivalence has been verified for wood saturated with water (Salmèn 1984) and formamide (Kelley et al. 1987). A time-moisture content equivalence have been verified by Pecht (1985) for paper.

The Glass Transition Temperature

A material property that results from the relation of temperature to the physical states of a polymer is the glass transition temperature (T_g). T_g is the temperature that corresponds to a change in slope when specific volume is measured against temperature (Ward 1983). One method used to determine T_g of a polymer is dynamic mechanical thermal analysis (DMTA). This technique requires determining the dynamic mechanical properties of a polymer over a range of temperatures. T_g is associated with the peak in the loss tangent (the ratio of the loss modulus, E", to the storage modulus, E'). This peak usually occurs near the center of the drop in storage modulus between the glassy and rubbery plateaus (Figure 3.2).

Free Volume Theories on Viscoelasticity

Free volume can be defined as the difference between the occupied volume and the specific volume of a polymer (Billmeyer 1984). Occupied volume is defined as the volume occupied by the actual mass of the molecule plus any volume it occupies because of thermal vibrations that exclude other molecules from its domain (Adamson 1980). Free volume remains relatively constant in the glassy stage of a polymer and increases linearly with temperature above T_g.

The association of a diluent with a polymer, such as water and wood, also affects free volume. Diluent molecules are relatively small in relation to polymer molecules. Therefore, a diluent in a polymer will increase free volume in proportion to its concentration (Ferry 1980).

Free volume theories are used to predict shift factors in the time-temperature superposition techniques, as well as the dependence of T_g on diluent concentrations. The Williams-Landel-Ferry (WLF) equation shows that for temperatures above T_g, the shift factor for time-temperature superposition is similar for all amorphous polymers (Ferry 1980). Although this observation was originally empirical, a fundamental basis for the equation has been provided using free volume concepts. The WLF equation has been shown to hold for temperatures in the range from T_g to $T_g+100^{\circ}C$ with most amorphous polymers (Ward 1983). Salmèn (1984) showed that the WLF equation was consistent with shift factors determined for water saturated wood for temperatures in the range of T_g to $T_g+55^{\circ}C$. Kelley et al. (1987) determined that the WLF equation was valid to $T_g+85^{\circ}C$ for wood plasticized with formamide. These agreements with the

WLF equation lend credibility to the concept that the viscoelastic response of solid wood is a direct function of the viscoelastic properties of the amorphous constituent polymers.

Diluent-Polymer Interactions

Many researchers have studied the effect of moisture content on the T_g of extracted hemicelluloses and lignin with varying results (Goring 1971, Back and Salmèn 1982, Irvine 1984). Only Kelley et al. (1987) and Irvine (1984) have studied this dependence for wood polymers in situ. Models to predict the variation of T_g with moisture content, that are based solely on free volume considerations, have been applied to semi-crystalline cellulose, hemicelluloses, and lignin (Goring 1971, Back and Salmèn 1982, Salmèn and Back 1977). These models adequately describe the variation in T_g for hemicelluloses and semi-crystalline cellulose over a range of moisture contents (Salmèn and Back 1977, Back and Salmèn 1982). However, they are only applicable to in situ lignin for moisture contents less than 10% because they fail to predict the plateau observed in T_g at higher moisture contents (Kelley et al. 1987). In polymer-diluent systems with a large degree of interaction via secondary bonding, T_g can vary with diluent concentration through a decrease in secondary interactions between polymer molecules. The secondary bonds between polymer molecules act as pseudo-crosslinks between polymer molecules. T_g is known to vary proportionally to the number of crosslinks when crosslink density is small (Kwei 1984). The Kwei model accounts for both changes in free volume and secondary interactions. The equation proposed by Kwei is (1984):

$$T_g = \frac{W_1 T_{g1} + kW_2 T_{g2}}{W_1 + kW_2} + qW_1W_2 \qquad [3.1]$$

where:
    W = weight fraction
    k = adjustable parameter for free volume
        effects
    q = adjustable parameter for secondary
        interactions
    1,2 denote polymer and diluent respectively

The first portion of the equation is an additive rule of the volume mixture. The term, qW_1W_2, is proportional to the number of secondary interactions between the polymer and diluent.

Characterization of the Amorphous Polymers in Wood

Although it is likely that some variation in polymer properties exists between and within species of wood, differences in the properties attributed to phase changes in the polymers are undoubtedly much larger. Therefore, it is reasonable to discuss material properties for the amorphous polymers in wood as if they were invariant within nature.

This discussion of moisture dependence is in terms of overall moisture content in the solid wood. In reality, the moisture content of the individual polymers will be different from each other and that of the solid wood. Using the moisture content of the solid wood is easier when T_g information is needed to infer solid wood behavior as is being done here; however, the moisture content of the individual polymers should be used when comparing the behavior of individual polymers. No information is available for the sorption characteristics of hemicelluloses and lignin in situ, however, limited work was performed on extracted polym-

ers (Cousins 1976, 1978). Solid wood moisture contents will be used in the remainder of this discussion unless otherwise stated.

Kelley et al. (1987) described the variation in T_g of hemicelluloses and lignin _in situ_ with solid wood moisture content using the Kwei model. Good agreement was found with the results presented by Irvine (1984). However, Salmèn (1984) observed a T_g of approximately 100°C for _in situ_ lignin under water saturated conditions using dynamic mechanical analysis at the same frequency used by Kelley et al. The results of Salmèn were consistent with those presented by other authors but differed from the 65°C determined by both Kelley et al. and Irvine. The difference between these results could stem from the non-equilibrium free volume states that may arise from transient moisture conditions. Salmèn maintained strict moisture control during the temperature changes. Kelley et al. and Irvine conditioned the samples to an initial moisture content and then provided no explicit control for moisture content during the tests. The results of Kelley et al. are used in the analysis presented here because the non-equilibrium moisture states of the pressing operation is similar to the transient moisture states of their T_g scans.

The variation of T_g with moisture content calculated with the Kwei equation is presented in Figure 3.3. At 0% moisture content, the T_g of both hemicelluloses and lignin was assumed to be approximately 200°C as given by Salmèn (1984). This value is difficult to validate because both polymers rapidly degrade near this temperature (Schaffer 1973, Back and Salmèn 1982). The T_g of lignin decreases with increasing moisture content and begins to plateau at 70°C with a moisture content of 10 to

15%. However, the T_g of hemicelluloses continues to decrease with increasing moisture content until it reaches a value of approximately -20°C near 30% moisture content. The T_g of hemicelluloses is 30°C at approximately 10% moisture content. Therefore, at higher moisture contents, phase changes in hemicelluloses are only important at subambient temperatures. Likewise, it can be inferred that for moisture contents between 10 and 15%, the moisture dependence of solid wood modulus at ambient temperatures is primarily a function of phase changes in the hemicelluloses.

The magnitude of the drop in mechanical properties associated with the phase change will be different for hemicelluloses and lignin. This can not be measured directly _in situ_. However, approximate figures can be determined through knowledge of the polymer morphology and studies of extracted polymers. Hemicelluloses are linear polymers and should show a change in modulus of approximately three orders of magnitude. Lignin is a moderately branched, three-dimensional polymer. Such a system usually exhibits a decrease in log modulus on the order of 1.5. Data from Cousins (1978) shows a drop in log modulus of 2.6 for extracted hemicelluloses. Salmèn (1982), in modelling the temperature and moisture dependence of wood fibers, estimated a drop in log modulus of 1.8 for lignin. Similar decreases in modulus are noted for crosslinked lignin co-polymers (Rials and Glasser 1986).

Because of the spiral winding and reinforcing nature of the cellulose microfibrils, the decrease in modulus of solid wood will be less than that in the individual polymer undergoing the phase change. Differences are seen parallel and perpendicular to the fiber direction

resulting from the preferential orientation of the microfibrils.
Greater drops will occur in modulus perpendicular to the grain than
parallel to the grain (Salmèn 1982). Because of the complexity of this
subject, a more complete treatment of this subject is beyond the scope
of this paper.

RELATING THE VISCOELASTICITY OF POLYMERS TO THE PRESSING CYCLE

I propose that the concepts of polymer viscoelasticity can be used
to optimize many facets of the pressing cycle. The primary application
deals with understanding and predicting how the vertical density gra-
dient is formed in non-veneer composite panels. However, as a
consequence of the viscoelastic response resulting in the density gra-
dient, many other panel properties and production parameters are
affected. These properties include but are not limited to adhesive bond
quality, springback, and dimensional stability. The following discus-
sion will concentrate on how the density gradient is formed using some
experimental data and theoretical calculations.

Wood is a heterogeneous material that is composed of anisotropic
cells. When flakes, veneers, or other particles are cut from solid
wood, the irregularity inherent to the resulting surface will yield
little contact area between adjacent wood elements. To produce a good
adhesive bond, the wood must deform sufficiently to produce an intimate
wood-adhesive-wood contact (Back 1987). The largest contact area will
result when the polymers of the wood are in a physical state to allow
maximum deformation under minimum pressure; i.e. the rubbery state. It
is also imperative that the resin flow and form a continuous layer

rather than individual droplets (Wilson and Krahmer 1976, Brady 1987). Because viscosity of a resin increases while curing, the temperature in the mat must be carefully controlled to allow maximum wood deformation prior to initiating the curing process. Moisture interacts with the wood polymers to affect T_g and consequently affect the deformation. However, to successfully control this process, an understanding of resin curing under different moisture regimes is necessary (Chow and Mukai 1972).

The out of plane tension strength of non-veneer composite panels is frequently used in industry as a measure of the internal bond strength. Low internal bond strengths are usually attributed to poor adhesive performance; however, the wood may also fail prematurely. Smith (1982) and Strickler (1959) studied the effect of production parameters on the mechanical properties of flakeboard. Both researchers concluded that the direct relationship between local density and internal bond strength did not hold for all pressing schedules. The cell walls of wood buckle when it is densified in compression perpendicular to the grain (Easterling et al. 1982). Fractures and plastic hinges have been noted in the buckled cell walls of some flakes; whereas, pure elastic buckling seems to occur in others (Figure 3.4) (Geimer et al. 1985). The conditions are most favorable for fractures to occur when the hemicelluloses and lignin are in the glassy state and the polymers are brittle. However, when the temperature of the wood is above the T_g of both amorphous polymers, then large strains can occur without fractures. Micro-fractures in wood can be detrimental to strength by providing places for larger fractures to originate. Annealing at high temperatures could possibly minimize the strength loss by blunting the crack tip, thereby, increasing the strain

energy needed to propagate the fracture.

Springback may also be related to how the cell walls buckle. If the cell walls do not fracture when they buckle, they will exert a certain restoring force when the amorphous polymers are in the rubbery state. This restoring force will result in a pressure needed to keep the press closed after initial relaxation has occurred. When the press is opened the cell walls will rebound and the springback results. The amount of springback in the panel will be dependent on how the cell walls collapse and the amount of stress relaxation that occurs during the pressing cycle.

The dimensional stability of the end product is merely an extension of the viscoelastic response resulting in springback. A force is exerted on the panel that is equal to the swelling pressure of adsorbed water. Like springback, the manner in which the cell walls collapse will strongly influence how they will respond to stresses. The stress relaxation that occurs in the press will also affect dimensional stability because the viscoelastic response of a material is a function of the entire stress history.

Formation of the density gradient

The formation of the density gradient is a complex phenomenon that involves the simultaneous processes of momentum, heat, and mass transfer. The momentum transfer is initiated by the mechanical pressure exerted by the press. These processes are interrelated through the sorption characteristics and the viscoelastic behavior of the mat. In particular, the viscoelastic theories of amorphous polymers can account

for the influence of temperature and moisture content on mat deformation by using a single variable, T_g. Because the most significant effect of temperature on the modulus of amorphous polymers occurs around T_g and the moisture influence is primarily in altering T_g, then comparing wood temperature during the pressing cycle to the T_g of lignin and hemicelluloses can provide valuable insight into how density gradients form.

Because densification will only occur from a mechanical force being applied, the compaction pressure applied to the mat during the pressing cycle must be examined. A typical compaction pressure curve is presented in Figure 3.5. The curve can be broken down into several distinct regions:

    A. press closure
    B. transient relaxation
    C. asymptotic relaxation
    D. venting

Press closure occurs during a predetermined amount of time known the press closing time (PCT). During the early portion of the PCT, the pressure is low while the flakes consolidate to eliminate large voids. As the mat densifies, the pressure increases rapidly in the latter portion of PCT. If the mat densifies in an elastic manner, the density gradient will form entirely during this portion of the press cycle. However, if the material properties of the wood elements are a function of time, temperature, and moisture content, then the density gradient must continue to develop during other portions of the press cycle.

The transient relaxation region begins when the stress on the mat decreases rapidly with time. Mechanically the mat is undergoing stress relaxation at a constant deflection. However, the individual wood ele-

ments in some regions of the mat can continue to densify with time while others recover stored elastic deflection. This process is possible because of differential stress relaxation within the mat caused by the transient environmental conditions. The additional densification results in plastic deformation from cell collapse.

The asymptotic relaxation region begins when the change of stress with time decreases to a relatively constant value. The separation between the two relaxation regions is not exact or important. The distinction between these regions is that changes in local mat density and therefore, plastic deformation can continue during the transient relaxation but are unlikely during asymptotic relaxation. This differentiation can be drawn because the pressure needed to maintain press position changes little with time during asymptotic relaxation. The role that the asymptotic relaxation region plays in density gradient formation is through the continued stress relaxation in different regions of the mat thereby affecting the amount of springback that occurs with individual wood elements. For example, suppose the temperature of the wood elements in the face of a panel is above T_g throughout the asymptotic relaxation region, but that in the core is not. The rate and amount of stress relaxation in the face is much greater than in the core. Upon opening the press, more elastic deflection will be recovered from the core than the face, thereby, contributing to the density gradient in the end product.

During venting, the press slowly opens and the pressure applied to the mat is lowered, thus to relieve the internal gas pressure. This is usually over a predetermined period of time depending on the platen

temperature and mat moisture content. Elastic recovery (springback) will occur during this portion of the press cycle. Additional viscous recovery will occur after the panel has been removed from the press. Both the elastic and viscous portions of recovery depend on the viscoelastic behavior of the wood polymers during the pressing cycle.

Procedures for Tracking T_g Through the Press Cycle

As discussed earlier, T_g of the wood polymers varies throughout the pressing cycle as a function of moisture content. Therefore, the moisture content variations in the wood component of the mat must be determined. To date, moisture content has not been continuously measured during processing of a composite panel. Maku et al. (1959) intermittently measured moisture content at different depths in the mat by stopping the press and weighing the wood particles. However, he did not use resin and the measurements were not continuous. Mathematical models have been developed that predict mat temperature and moisture content during the press cycle (Humphrey 1979, Wagner et al. 1987). However, the mat is treated as a continuum and local thermodynamic equilibrium is assumed. This is equivalent to allowing the wood particles to instantaneously equilibrate with the surrounding environment. The actual change of the particle moisture content is not known.

Without experimental data available on moisture content variations during the press cycle, measurements of temperature and gas pressure were used in conjunction with a one-dimensional heat and mass transfer computer program developed by Schajer (1984) to predict moisture content in the mat. The computer program is based on fundamental transport

theory and consists of a system of coupled partial-differential material and energy balance equations (Stanish et al. 1985). Assuming any increase in total gas pressure in the mat during pressing entirely attributed to increases in water vapor content, relative humidity changes in the mat can be calculated (Casey 1987). The measured temperature and predicted relative humidity profiles are then used as boundary conditions for a flake at a given location in the mat. The heat and mass transfer model is then solved to yield a predicted average flake moisture content and temperature.

Knowing the moisture content variations through the press cycle, the T_g of hemicelluloses and lignin in wood can be tracked through the press cycle and compared with the wood temperature at any given time. The variation of T_g for hemicelluloses and lignin with solid wood moisture content were described using the Kwei equation as described by Kelley et al (1987). Although Kelley's results are not entirely consistent with that of Salmèn (1982, 1984), the conditions of drying under which the experiments were conducted by Kelley et al. are more like the hot pressing process than are the equilibrium moisture conditions used by Salmèn.

Three replications of yellow poplar (<u>Liriodendron tulipifera</u>) flakeboard panels were produced with a 1 minute press closing time at two levels of initial mat moisture content (4% and 15%) and platen temperature (154°C and 190°C). Gas pressure and temperature were monitored at a face and core location within each panel during the pressing cycle (Kamke and Casey 1988a, 1988b). Six samples from each of the 12 panels were used to determine an average density profile through the thickness

of the panel (Brady 1987) using the gamma radiation method developed by Laufenburg (1986).

Results of T_g Tracking

The vertical density profiles for each of the four panel types are presented in Figure 3.6. Each line represents an average of the 18 density gradient samples. Because the thermocouples and gas pressure probes were placed at approximately the same depth while forming the mat (Kamke and Casey 1988a), the probe location in the final panel differed slightly depending on how the density gradient formed. The actual face and core probe locations are marked on each density profile.

Examples of the predicted change in flake moisture content and temperature during the press cycle are presented in Figure 3.7. The measured mat temperatures and gas pressures used as boundary conditions to predict the flake conditions are presented elsewhere (Kamke and Casey 1988b). For simplicity, the T_g for lignin, calculated using equation 3.1, is presented as the difference between T_g and the predicted flake temperature (T) (Figure 3.8). Only the data for T_g of lignin is presented because this transition dominates the behavior of these panel types. T_g is presented for the first 6 minutes of the press cycle; which corresponds to the end of the asymptotic relaxation period. The end of the transient relaxation period is denoted for each panel type. Horizontal lines drawn at 25°C and -25°C indicate the approximate transition zone for lignin. Values of T_g-T greater than 25°C indicate that the lignin is in the glassy state; whereas, values of T_g-T less than -25°C indicate that the lignin is in the rubbery state. Values between

25°C and -25°C will be referred to as the transition zone.

Transient Relaxation Period

I postulate that changes in localized density can occur during the transient relaxation period from differential stress relaxation through the thickness of the panel. Results presented here support this hypothesis.

The density at the face and core probe locations is similar for all panel types except for the 190°C and 15% panel (190°C-15%) (Figure 3.6). Despite the fact that all the panel types were pressed to the same thickness and target density, the entire density profile of the 190°C-15% panel is shifted upward with respect to the other panel types. The wood at the face location of this panel type was in the transition zone for much of the transient relaxation period and all of the asymptotic relaxation period (Figure 3.8). This is not true for any other panel type presented here. Although the face entered the transition zone near the end of press closing, the time that the core started a transition was well after the press was closed. Therefore, if densification ceased at the end of press closing, then no further densification should have occurred in the core.

Kamke and Casey (1988b) noted that a small plateau occurred in the gas pressure data for the face layer of the 190°C-15% panel. This plateau coincided with a slope change in the platen pressure curve and the initiation of gas pressure buildup in the core. They suggested that a possible explanation for this occurrence was a change in the void volume of the face location from differential relaxation through the thickness

of the mat. The gas pressure plateau occurs at approximately 2 minutes in the press cycle. Note that the core location of the 190°C-15% panel enters the transition zone at approximately this time. This plateau did not exist on any other panel type with a 1 minute press closing time. Likewise, none of the core locations for these panel types were in the transition zone during the transient relaxation period.

Given the theories presented here, a possible scenario for the behavior of the 190°C-15% panel during the transient relaxation period is as follows. When the core of this panel entered the transition region, the relaxation modulus of the wood began to change rapidly. These conditions allowed the core to densify while some elastic deformation recovered in the face. The increased void volume of the face caused the rate of gas pressure build up to slow, resulting in a plateau in the gas pressure data. The decreased void volume in the core resulted in an increased gas pressure at this location.

Asymptotic Relaxation Period

From both an intuitive and experimental standpoint it seems likely that the density gradient continues to actively form during the transient relaxation period. However, the role that stress relaxation during the asymptotic relaxation period plays has not yet been addressed. The higher density of the 190°C-15% panel may be attributed to either the transient or asymptotic relaxation periods because this panel was in the transition zone for a longer period of time during both relaxation periods than any other panel type studied here. Comparing the two panel types made with 15% initial mat moisture content may provide insight

into the role of the asymptotic relaxation period.

The wood in the face location of the $154^{\circ}C$-15% panel enters the transition zone for only very short periods of time during the transient and asymptotic relaxation periods. However, the core was in the transition zone for over half of the asymptotic period. The fact that the density of the core was not as great as in the $190^{\circ}C$-15% panel indicates that a significant amount of stress relaxation must occur during the asymptotic relaxation period to affect the density gradient. Without this stress relaxation or increased compressibility encountered by being in the transition zone during the transient relaxation period, little increase in density will result.

· The vertical density profiles of both panel types produced at 6% initial mat moisture content are extremely similar to that of the $154^{\circ}C$-15%. The wood in both the face and core probe locations of these panels were in the glassy region throughout the transient relaxation period. However, both the core of the $154^{\circ}C$-15% panel was in the transition zone for at least half of the asymptotic relaxation period, whereas, the 6% moisture content panel types were not. From this data, it is also apparent that stress relaxation during the asymptotic relaxation period must be substantial to affect the density gradient. A more thorough understanding of the viscoplastic nature of wood will be necessary to better differentiate between unrecoverable viscous and plastic deformation.

CONCLUSIONS

With prior knowledge of internal mat temperature and gas pressure it is possible to track T_g of _in situ_ lignin and hemicelluloses using a one-dimensional heat and mass transfer model to predict wood temperature and moisture content and the Kwei equation to describe the T_g dependence on moisture content. Using this method of T_g tracking, differences in the observed density gradients of panel types were generally consistent with the theories presented here except when the wood temperature did not exceed the T_g of lignin during periods when gross densification was postulated to occur. This discrepancy results from the lack of difference between T_g-T of face and core within a panel type when differences clearly exist in the panel density at these locations. Given these results, the values for T_g of lignin derived under non-equilibrium moisture conditions by Kelley et al. (1987) are adequate for describing T_g variations with moisture content during the pressing cycle of wood composites. However, further research on non-equilibrium effects is required.

Determining the simultaneous effects of moisture content and temperature on the viscoelastic response of wood during the pressing cycle can be accomplished by studying the difference between wood temperature and T_g when sufficient differences exist in the environmental conditions to produce different states of the polymers. However, T_g of lignin is not likely to be a useful variable to study when the environmental conditions are such that lignin is in the glassy state throughout the press closing and transient relaxation periods. Under these conditions, a full viscoplastic treatment of wood is necessary to understand the den-

sity gradient formation and how it may affect macroscopic panel proper-

ties.

.

LITERATURE CITED

Adamson, M.J. 1980. Thermal expansion and swelling of cured epoxy resin used in graphite/epoxy composite materials. J. Mater. Sci. 15:1736-1745.

Back, E.L. 1987. The bonding mechanism in hardboard manufacture. Holzforschung 41(4):247-258.

_____ and N.L. Salmèn. 1982. Glass transitions of wood components hold implications for molding and pulping processes. Tappi 65(7):107-110.

Billmeyer, F.W. 1984. Textbook of polymer science, 3rd ed. John Wiley and Sons, New York, NY. 578 pp.

Bodig, J. and B.A. Jayne. 1982. Mechanics of wood and wood composites. Van Norstrand Reinhold Co. Inc., New York, NY. 712 pp.

Brady, D.E. 1987. The effect of hot-pressing parameters on resin penetration and flakeboard layer properties. Master's Thesis. VPI&SU, Blacksburg, VA.

Casey, L.J. 1987. Changes in wood-flake properties in relation to heat, moisture, and pressure during flakeboard manufacture. Master's Thesis. VPI&SU, Blacksburg, VA.

Christensen, R.M. 1982. Theory of viscoelasticity: An introduction, 2nd ed. Academic Press Inc. New York, NY.

Chow, S.Z. and H.N. Mukai. 1972. Polymerization of phenolic resin at high vapor pressure. Wood Sci. 5(1):65-72.

Cousins, W.J. 1976. Elastic modulus of lignin as related to moisture content. Wood Sci. Tech. 10:9-17.

_____ 1978. Young's modulus of hemicellulose as related to moisture content. Wood Sci. Tech. 12:161-167.

Easterling, K.E., R. Harrysson, L.J. Gibson, and M.F. Ashby. 1982. On the mechanics of balsa and other woods. Proc. R. Soc. Lond. A383:31-41.

Ferry, J.D. 1980. Viscoelastic properties of polymers, 3rd ed. John Wiley and Sons, New York, NY. 641 pp.

Geimer, R.L. 1980. Data basic to the engineering design of reconstituted flakeboard. Proc. Wash. St. Univ. Particleboard Symp. (April 1980). WSU, Pullman, WA.

_____, R.J. Mahoney, S.P. Loehnertz, and R.W. Meyer. 1985.

Influence of processing-induced damage on strength of flakes and flakeboards. For. Prod. Lab. Res. Paper #463. U.S. For. Prod. Lab., Madison, WI.

Goring, D.A.I. 1971. Polymer properties of lignin and lignin derivatives. pp.695-768 In: K.V. Sarkanen and C.H. Ludwig, Eds. Lignins: Occurrence, formation, structure, and reactions. Wiley-Interscience, New York, NY.

Humphrey, P.E. 1979. Fundamental aspects of wood particleboard manufacture. Ph.D. Dissertation. Univ. of Wales, Bangor, Wales, U.K.

Hunt, M.O. and S.K. Suddarth. 1974. Prediction of elastic constants of particleboard. For. Prod. J. 24(5):52-57.

Irvine, G.M. 1984. The glass transitions of lignin and hemicellulose and measurement by differential thermal analysis. Tappi 67(5):118-121.

Kamke, F.A. and L.J. Casey. 1988a. Gas pressure and temperature in the mat during flakeboard manufacture. For. Prod. J. 38(3):41-43.

_____ and _____ 1988b. Fundamentals of flakeboard manufacture: internal-mat conditions. For. Prod. J. 38(6):38-44.

Kelley, M.W. 1977. Critical literature review of relationships between processing parameters and physical properties of particleboard. Gen. Tech. Report FPL-10. U.S. For. Prod. Lab., Madison, WI.

Kelley, S.S., T.G. Rials, and W.G. Glasser. 1987. Relaxation behaviour of the amorphous components of wood. J. Mater. Sci. 22:617-624.

Kwei, T.K. 1984. The effect of hydrogen bonding on the glass transition temperatures of polymer mixtures. J. Polym. Sci.: Polym. Lett. 22:307-313.

Laufenburg, T.L. 1983. Characterizing the nonlinear behavior of flakeboards. Wood and Fiber Sci. 15(1):47-58.

_____ 1984. Flakeboard fracture surface observations and correlations with orthotropic failure criteria. J. Inst. Wood Sci. 10(2):57-65.

_____ 1986. Using gamma radiation to measure density gradients in reconstituted wood products. For. Prod. J. 36(2):59-62.

Maku, T., R. Hamada, and H. Sasaki. 1959. Studies on the particleboard. Rept. 4. Temperature and moisture distribution in particleboard during hot-pressing. Wood Research, Kyoto Univ. 21:34-46.

Pecht, M. 1985. Creep of regain-rheologically simple hydrophillic

polymers. J. Strain Anal. 20(3):179-181.

Price, E.W. 1976. Determining tensile properties of sweetgum veneer flakes. For. Prod. J. 26(10):50-53.

Rials, T.G. and W.G. Glasser. 1986. Engineering plastics from lignin XIII. Effects of lignin structure on polyurethane network formation. Holzforschung 40(6):353-360.

Salmèn, N.L. 1982. Temperature and water induced softening behaviour of wood fiber based materials. Ph.D. Dissertation. Dept. of Paper Tech., The Royal Inst. of Tech., Stockholm, Sweden.

_____ 1984. Viscoelastic properties of in situ lignin under water-saturated conditions. J. Mater. Sci. 19:3090-3096.

_____ and E.L. Back. 1977. The influence of water on the glass transition temperature of cellulose. Tappi 60(12):137-140.

_____, P. Kolseth, and A. de Ruvo. 1985. Modeling the softening behaviour of wood fibres. J. Pulp and Paper Sci. 11(4):J102-J107.

Schaffer, E.L. 1973. Effect of pyrolytic temperatures on the longitudinal strength of dry Douglas-fir. J. Test. and Eval. 1(4):319-329.

Schajer, G.S. 1984. Dryrun: One dimensional wood drying computer program. Science and Process Control Unit, Solid Wood R&D, Weyerhaeuser Technology Center, Tacoma, WA. 45pp.

Smith, D. 1982. Waferboard press closing strategies. For. Prod. J. 32(3):40-45.

Stanish, M.A., G.S. Schajer, F. Kayihan. 1985. Mathematical models of wood drying from heat and mass transfer fundamentals pp.360-367. In: R. Toei and A.S. Mujumdar Eds. Drying '85. Hemisphere Publishing Corp., New York, NY.

Strickler, M.D. 1959. Properties of Douglas-fir flakeboard. For. Prod. J. 7:203-215.

Suchsland, O. 1962. The density distribution in flakeboard. Quart. Bull., Michigan Agri. Exp. Sta., Michigan State Univ. 45(1):104-121.

Wagner, F.G., T.E. Harless, D.S. Ladd, P.H. Short, R.D. Seale, and D.E. Lyons. 1987. MSU-PDP: A microcomputer model to predict the density profile of particleboard. User's manual. Vs. 2.0. Miss. St. Univ., Miss. St., MS.

Ward, I.M. 1983. Mechanical properties of solid polymers, 2nd ed.

Wiley-Interscience. New York, NY.

Wilson, J. and R.L. Krahmer. 1976. Particleboard microscopic observations of resin distribution and board fracture. For. Prod. J. 26(11):42-45.
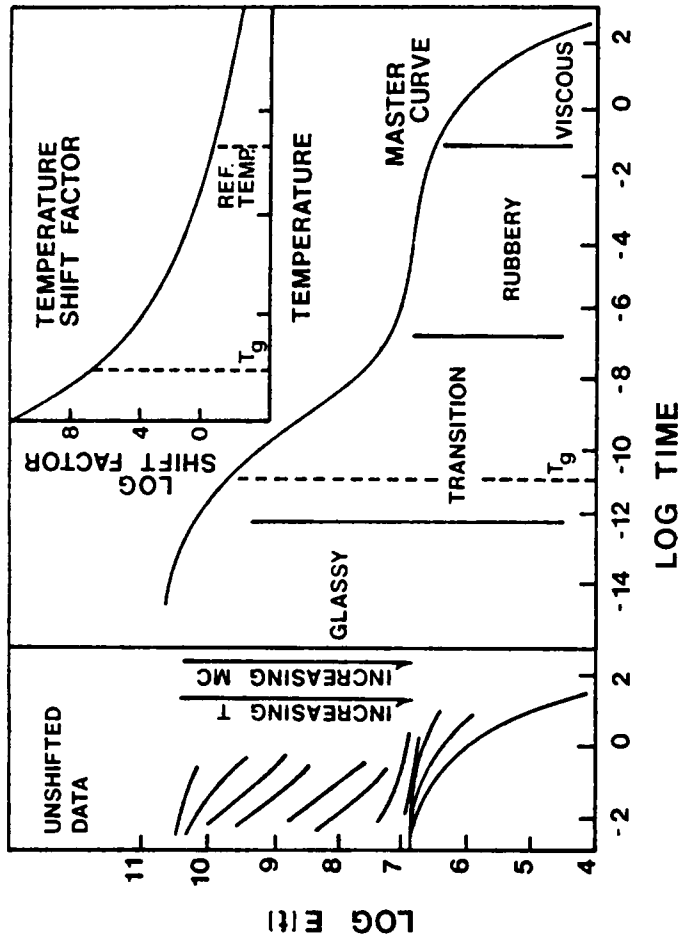
Figure 3.1: Typical variation of relaxation modulus [E(t)] for an amorphous polymer with time, temperature, and diluent concentration. The master curve denotes the specific viscoelastic regions of polymer behavior.
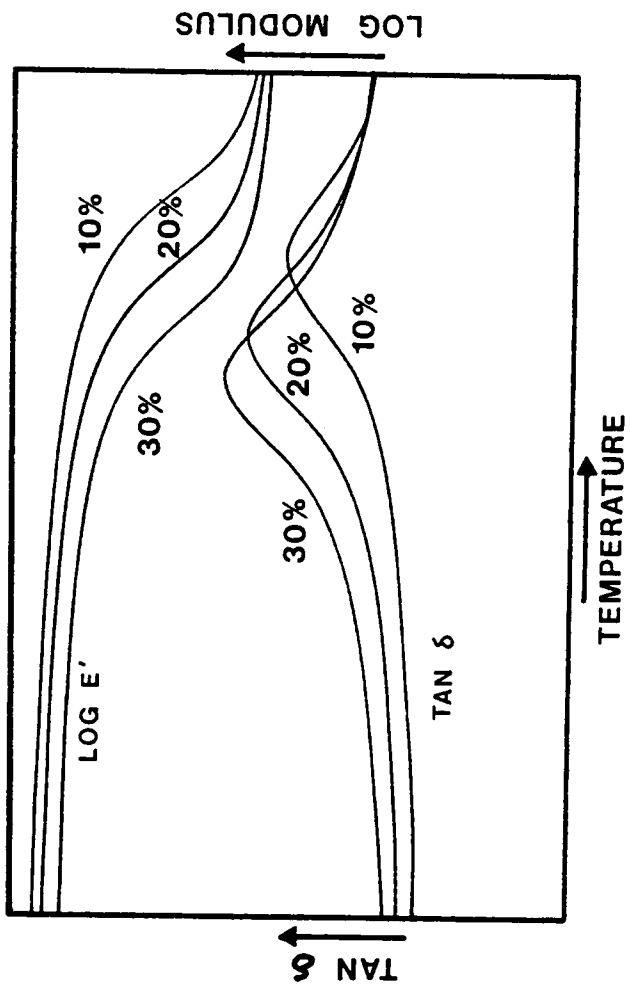
Figure 3.2: The temperature response of log E' and loss tangent for wood at different moisture contents (adapted from Kelley et al. 1987).
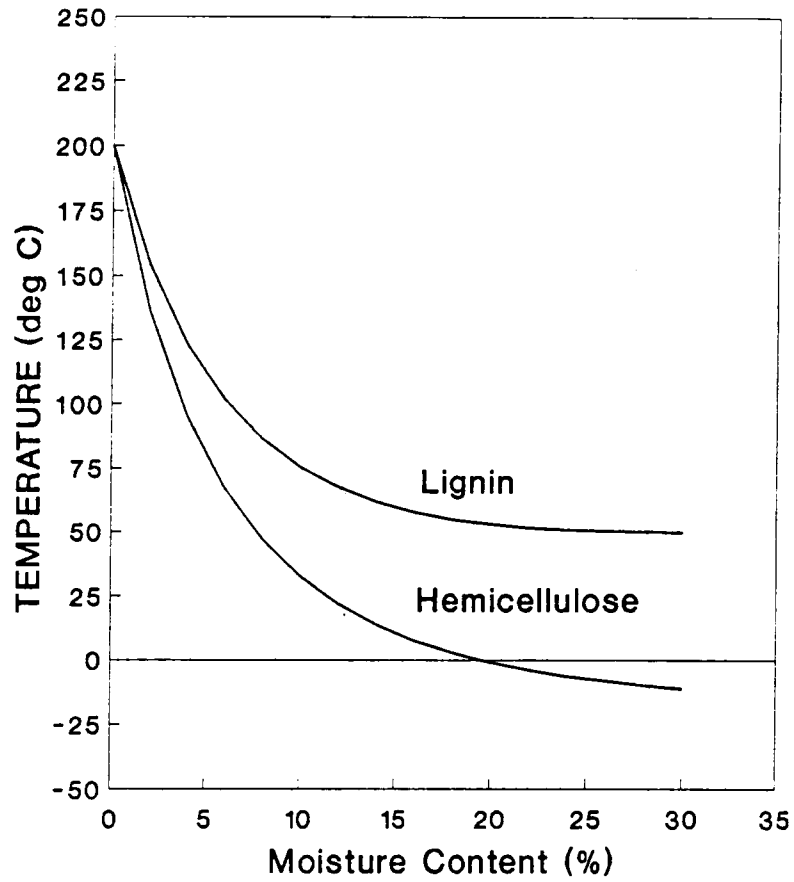
Figure 3.3: The moisture dependence of T_g for _in situ_ lignin and hemi-
cellulose as predicted by the Kwei model (Kelley et al. 1987).
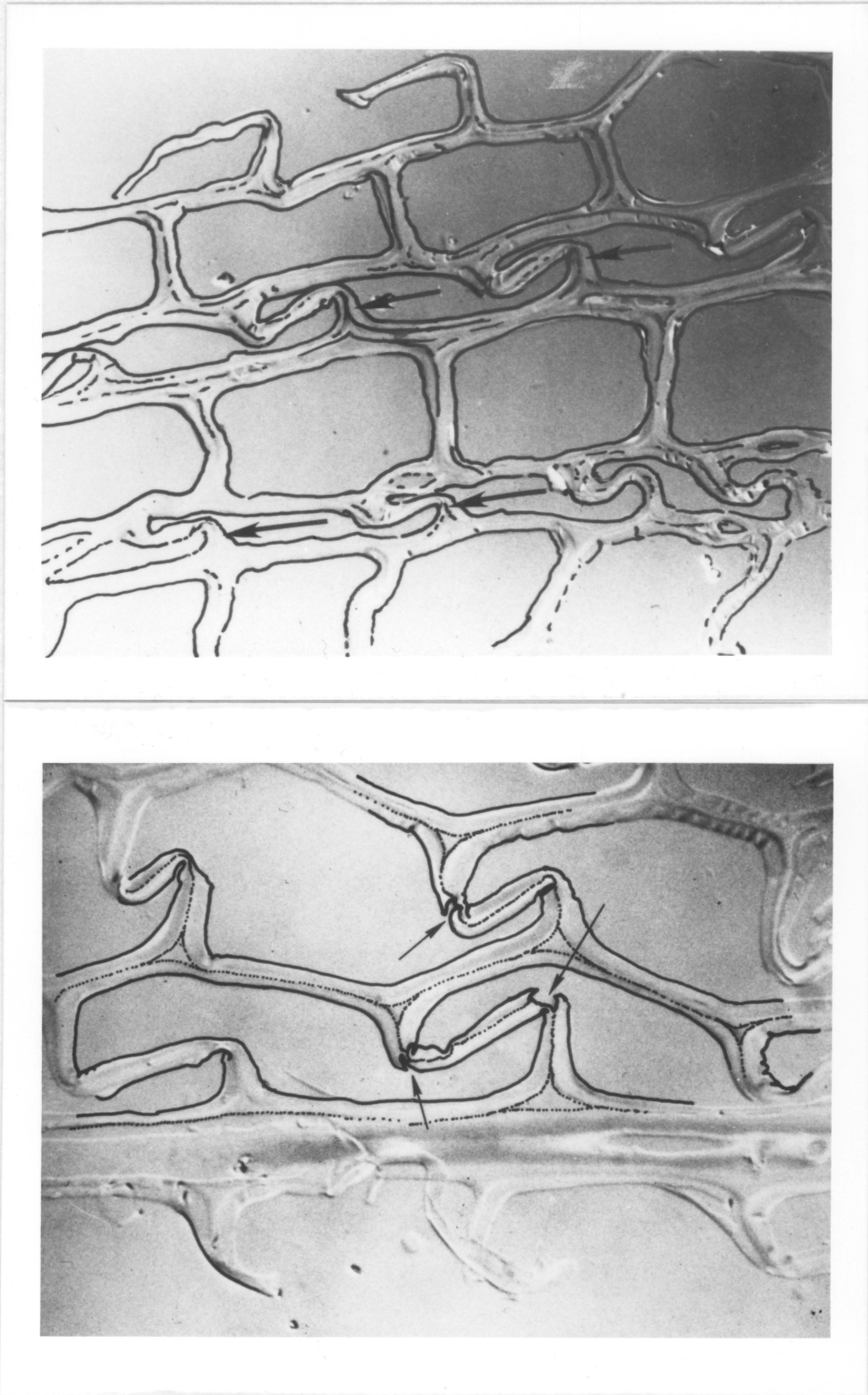
Figure 3.4: Cross-sectional views of Douglas-fir flakes recovered from a pressed panel showing (a) elastic collapse and (b) fractures in the cell walls (Geimer et al. 1985).
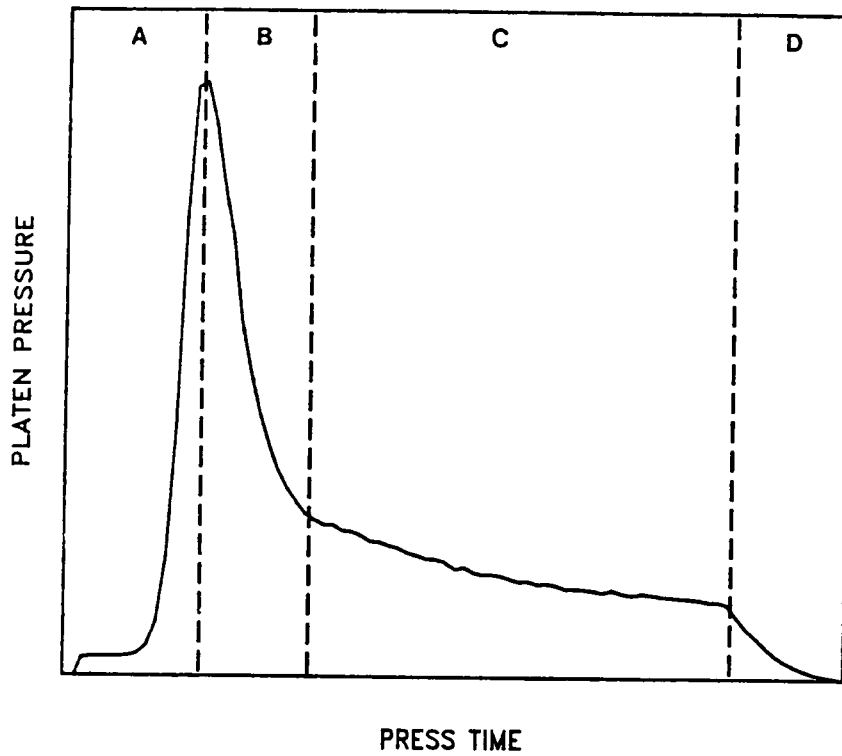
Figure 3.5: A typical platen pressure curve denoting specific regions. A: press closing; B: transient relaxation; C: Asymptotic relaxation; D: venting.
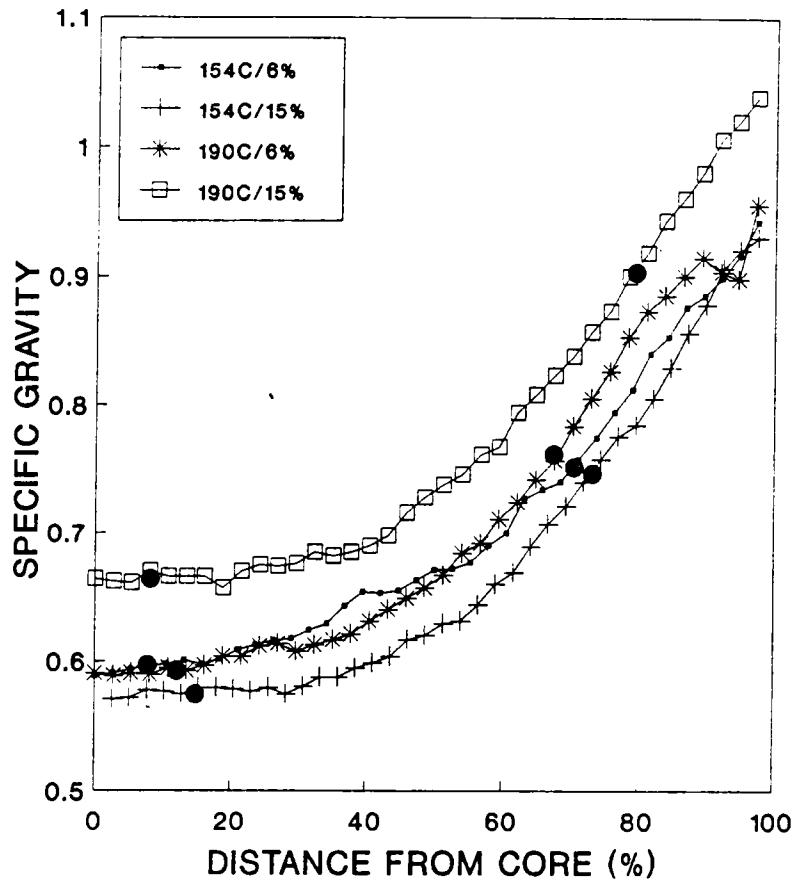
Figure 3.6: Average vertical density gradient profiles for panels. The actual probe locations are marked for the core and face.
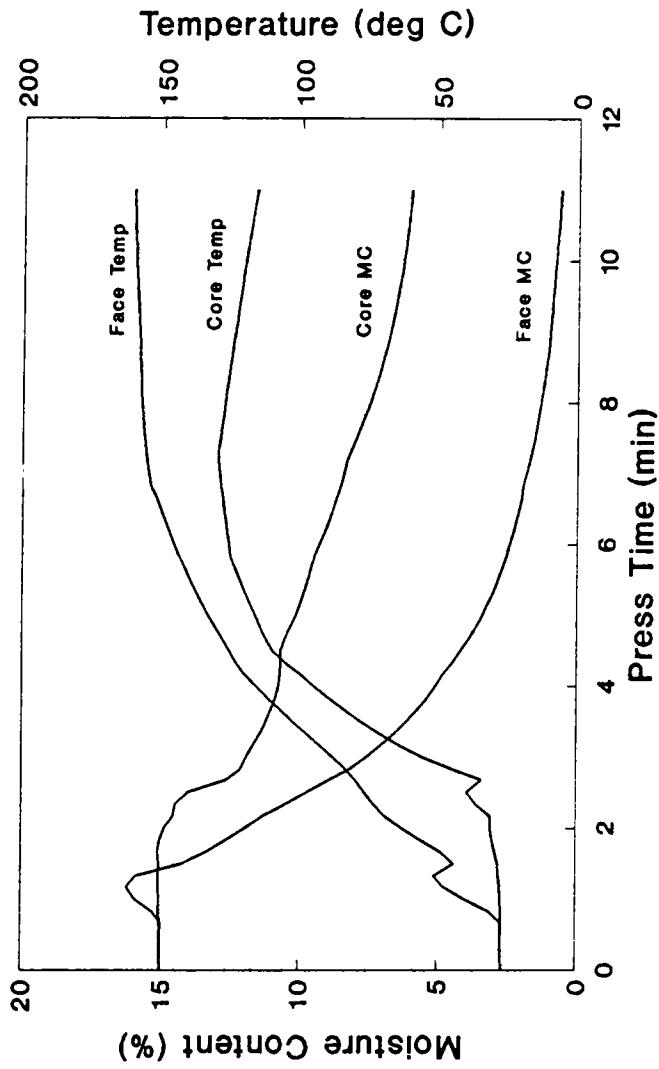
Figure 3.7: Average flake temperature and moisture content for the 190°C-15% panel type as predicted using a one-dimensional heat and mass transfer model.
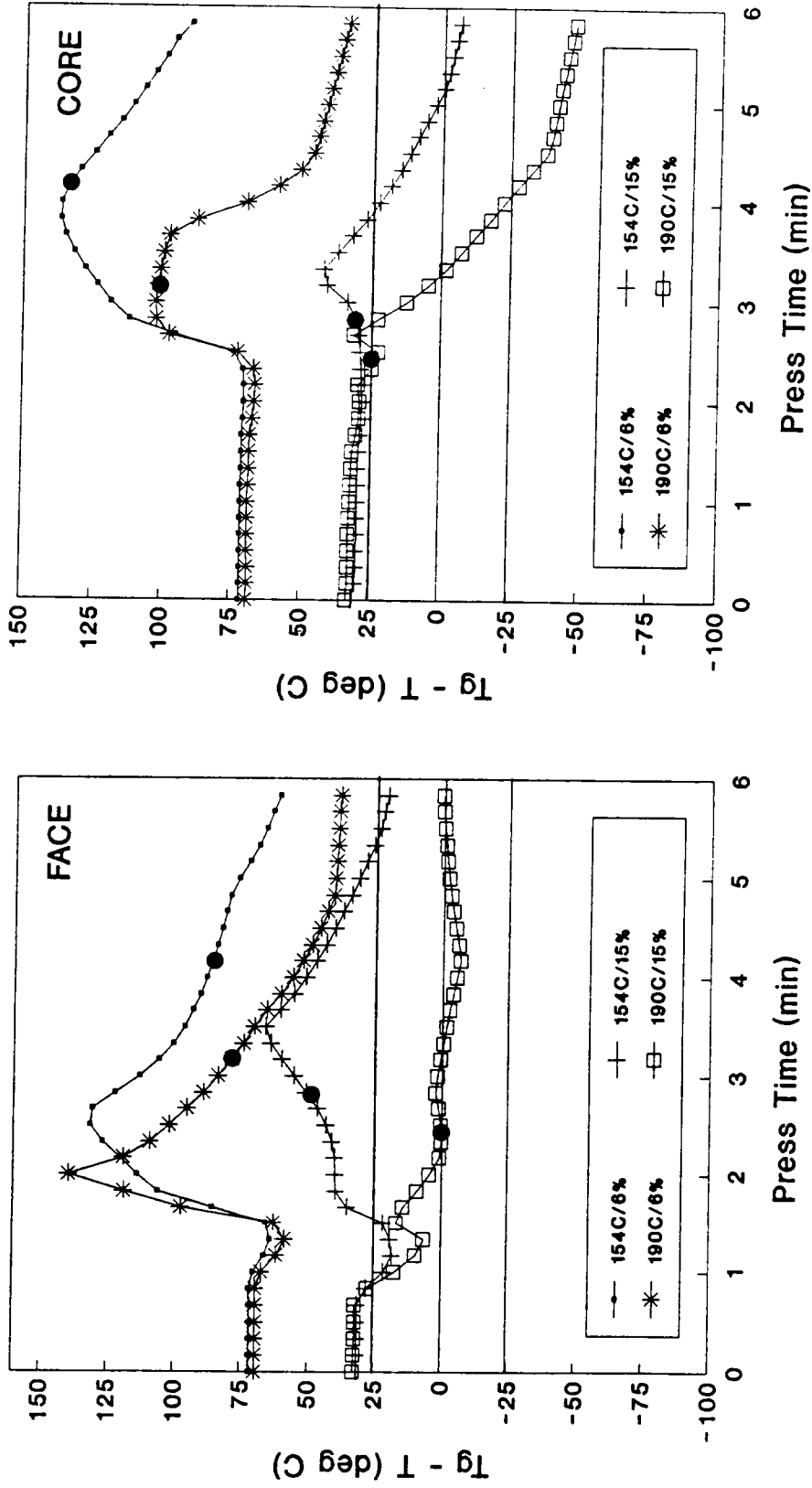
Figure 3.8: Predicted difference between T_g and average flake temperature for in situ lignin in the face and core probe locations for panels. The end of the transient relaxation period is marked for each panel type.

CHAPTER 4

MODELING THE COMPRESSION BEHAVIOR OF WOOD

USING THEORIES OF CELLULAR MATERIALS

ABSTRACT

The mechanical properties of cellular materials in compression are highly non-linear resulting from the collapse of the cellular structure. The amount and type of cellular collapse may be important in the resulting mechanical and physical properties of wood-based composites that are densified during hot-pressing. A strict analysis of the consolidation process during hot-pressing must examine the viscoelastic behavior of wood in transverse compression. This behavior is highly non-linear. The work presented here examines a model of structural collapse using theories of cellular materials. The study parameters include specimen geometry, moisture content, temperature, and orientation. The model uses wood density and cell modulus to predict macroscopic stress-strain relationships. Cell wall modulus is calculated from experimental results using the presented theories. A goal is to use this information as a form of non-linearizing function in a viscoelasticity analysis.

INTRODUCTION

Problem Statement

Cellular materials are widely used in structural applications. The stress-strain relationship of these materials in compression is highly non-linear, as a result of the cellular structure. The importance of this non-linearity is obvious for the performance of flexible foams

79

that are used for energy absorption. Another important area for model-ing non-linear compression properties is in the processing of wood-based composites.

· Virtually all wood-based composite materials utilize a hot-pressing process that consolidates the individual wood elements and adhesive into a contiguous product. When relatively large wood elements are used (i.e. flakes, strands, veneers), the wood is deformed in trans-verse compression. The mechanical response of the elements may be par-ticularly important in processes that significantly densify the wood elements. During densification, the cellular structure is permanently changed. The performance of the resulting material structure is influ-enced by the deformation process.

Mechanical Models for Cellular Materials

A characteristic mechanical response of cellular materials in compression is shown in Figure 4.1. The material begins deforming in a linear elastic manner. A yield point is exhibited at the onset of cellu-lar collapse. Then, the material continues to deform at nearly a con-stant stress level. At some limit strain, densification begins when a majority of cells have collapsed. During this stage, the stress increases rapidly as the collapsed cell walls consolidate.

Several micromechanics models have been developed to predict linear elastic properties of the cellular material from the cell geom-etry and mechanical properties of the cell wall (Gibson et al. 1982, Gibson and Ashby 1982, Meinecke and Clark 1973, Gent and Thomas 1959, Leaderman 1971, Ko 1965, Warren and Kraynik 1987). In addition, others

have been formulated to predict yielding (Gibson et al. 1982, Gibson and Ashby 1982, Whittaker 1971, Chan and Nakamura 1969). The primary shortcoming to applying these models to wood is that most theories model the unit cell as a cubic lattice structure of beams or struts (Meinecke and Clark 1973, Gent and Thomas 1959, Leaderman 1971, Ko 1965, Whittaker 1971), which is descriptive of open cell foams. The approach is also satisfactory for man-made closed cell foams because thick plate edges in the unit cell result from the surface tension of the polymer during processing (Ashby 1983). However, the walls of the unit cell in wood are distinctly plate-like. Therefore, resulting properties will be related to the deformation of plates rather than beams.

Gibson and Ashby have produced a comprehensive set of theories that address linear, non-linear, and failure properties for elastic, plastic, and brittle cellular materials (Gibson et al. 1982, Gibson and Ashby 1982, Ashby 1983, Gibson and Ashby 1988, Maiti et al. 1984). Because cellular materials are so common in nature, these theories have been applied to a number of natural materials including wood (Easterling et al. 1982, Maiti et al. 1984, Ashby et al. 1985), cork (Gibson et al. 1981), bone (Gibson and Ashby 1988), and the iris leaf (Gibson et al. 1988).

It was shown that the structural theories developed for honeycomb and closed cell foams (Gibson and Ashby 1982) can be applied to wood (Easterling 1982). These theories relate the Young's modulus (E) and yield stress (σ_y) of the wood to the Young's modulus and yield stress of the cell wall through experimentally derived constants and relative density (a ratio of the foam density to the cell wall density,

$\rho_r = \rho/\rho_w$). In addition, Maiti et al. (1984) developed deformation mode maps for the compression of elastomeric and rigid cellular materials. The collapse and densification regions of the stress-strain relationship were described approximately using a relation developed from an empirical distribution of cell wall lengths.

Objective

The hot-pressing process used to produce wood-based composites utilizes time, temperature, moisture, and mechanical pressure simultaneously to consolidate the individual wood elements into a contiguous material. Therefore, a thorough analysis of the deformation process must incorporate the viscoelastic response of the wood. In transverse compression, the viscoelastic properties of cellular materials are highly stress non-linear. This results largely from the collapse of the cellular structure. Therefore, the theories developed by Gibson and Ashby may be particularly useful in separating the geometrical non-linear response of the wood cells from the linear viscoelastic response of the cell wall polymers. The objective of this specific work is to model the non-linear mechanical response of wood in transverse compression; particularly as it pertains to cellular collapse. The modeling may give insight into the phenomenon of cellular collapse that can then be used to develop a non-linear term in a fundamental viscoelasticity model.

EXPERIMENTAL METHOD

Specimen Preparation

Wood specimens were planed to heights of 3, 5, 10, 20, 30, and 40 mm and a square cross-section of 20 mm on a side. In addition, wood flakes were produced on a laboratory scale disk flaker. The flakes were approximately 0.9 mm thick and a square cross-section of 20mm on a side. In general, yellow poplar (<u>Liriodendron tulipifera</u>) was used for all the tests; exceptions are specifically noted. All specimens were cut from mature wood and oriented with the principal material directions. Specimens were conditioned to the required moisture content and temperature prior to testing.

Test Methods

Specimens were compressed at 6% strain per minute on a universal hydraulic testing machine equipped with heated platens rigidly attached to the crosshead and base (Figure 4.2). Both aluminum loading blocks were machined flat and parallel to 0.25 mm. Each block was heated with four cartridge heaters that were inserted in the block near the surface remote to the specimen. A thermocouple was placed near each loading surface to monitor temperature as feedback for a temperature controller. A steel block separated the loading block from the cooling manifold. Water was passed through the cooling manifold to maintain an acceptable temperature at the load cell and base. Deflection was measured with a linear variable displacement transformer attached to the crosshead with a stiff aluminum arm. The load-deflection relationship of the testing apparatus was determined and compensated for in the test data. Both load and deflection were acquired in real time by computer and immediately converted into stress and strain.

The 3, 5, and 20 mm high specimens were conditioned at 30°C and 12% moisture content and compressed in the radial direction. Using a specially designed clip gage, the lateral expansion of test specimens in the non-linear region of the stress-strain relation was measured. The gage consisted of two steel arms (0.8 mm thick) soldered at right angles to opposite ends of an elastic bronze ribbon. A strain gage was bonded to the tension and compression sides of the ribbon. Sharp tips on the steel arms prevented the gage from slipping on the specimen during testing.

Most combinations of moisture content and temperature could be maintained during the test by sealing the specimen in poly(vinylidene chloride) (SARAN Wrap 560, 0.15 mm thick) envelopes. Flakes were sealed in three layers of aluminum foil (0.05 mm thick) because the deformation of the polymer film was significant compared to the deformation of the wood specimen. Pressures exceeding one atmosphere were needed to maintain saturated conditions at 120°C and 140°C. For these conditions, the compression apparatus was fitted with cylindrical loading blocks. A bellows-style reinforced rubber boot was clamped around the loading blocks with the test flake inside. A channel machined near the perimeter of the lower platen was filled with water to insure saturated conditions. The temperature of the blocks was then increased to the test temperature, thereby producing a saturated environment. Once the force on the load cell produced from the elevated pressure in the test chamber stabilized, the specimens were allowed to equilibrate for ten minutes. After equilibration, the compression test was conducted.

RESULTS AND DISCUSSION

Model Development

The Young's modulus of a closed cellular solid can be written as (Gibson and Ashby 1982):

$$E = C_2 \, E_w \, \rho_r^3 \qquad\qquad [4.1]$$

where:
  C_2 = constant
  E_w = cell wall modulus
  $\rho_r = \rho/\rho_w$ = relative density

This equation is derived from classical plate theory and applies for elastomeric and rigid cellular materials.

The σ_y of cellular materials is influenced by the deformation mode of the cell walls. Yielding in elastomeric foams results from elastic buckling of the cell walls. The yield point can be calculated by:

$$\sigma_y = C_3 \, E_w \, \rho_r^3 \qquad\qquad [4.2]$$

where: C_3 = constant

For rigid plastic cell wall materials that exhibit a yield point, yielding in the cellular solid results from the formation of plastic hinges. The yield stress, therefore, can be determined from the fully plastic moment of the cell wall (Gibson and Ashby 1982):

$$\sigma_y = C_4 \, \sigma_{y_w} \, \rho_r^2 \qquad\qquad [4.3]$$

where:
  C_4 = constant
  σ_{y_w} = cell wall yield stress

Note that C_3 in Equation [4.2] is the yield strain (ϵ_y), which is independent of density for elastic buckling. However, it can be shown from Equations [4.1] and [4.3] that the ϵ_y of rigid plastic foams is

theoretically dependent on density. Easterling et al. (1982) applied the plastic collapse equations to their analysis of wood, however, this requires prior knowledge or calculation of the σ_y of the cell wall material. Given that σ_y is likely to change with temperature and moisture content and wood is found to yield at a constant strain independent of density, temperature, and moisture content; elastic collapse will be assumed in developing the model further. This assumption will be discussed in greater detail in the following section.

In deriving an equation for the plateau and densification stress, Maiti et al. (1984) assumed that the longest cell walls buckle first, resulting in the yield point. They then postulated that the length of the cell walls that will buckle with increasing compression strain (ϵ) could be described as a function of the longest cell wall and the increasing relative density with strain ($\rho_r(\epsilon)$). The resulting equation rewritten for elastic collapse of a closed cell foam is:

$$\sigma = C_3 \, E_w \, \rho_r^3 \left[\frac{1 - \rho_r^{1/3}}{1 - \rho_r(\epsilon)^{1/3}} \right]^3 \qquad [4.4]$$

Combining Equations [4.1] and [4.4] it follows that:

$$\sigma = \frac{C_3}{C_2} \, E \left[\frac{1 - \rho_r^{1/3}}{1 - \rho_r(\epsilon)^{1/3}} \right]^3 \qquad [4.5]$$

Equation [4.5] can then be rewritten in the form:

$$\sigma = E \epsilon \psi(\epsilon) \qquad\qquad [4.6]$$

where: for $\epsilon < \epsilon_y$ $\quad \psi(\epsilon) = 1$

for $\epsilon > \epsilon_y$ $\quad \psi(\epsilon) = \dfrac{C_3/C_2}{\epsilon} \left[\dfrac{1 - \rho_r^{1/3}}{1 - \rho_r(\epsilon)^{1/3}} \right]^3$

If $\rho_r(\epsilon)$ is calculated using the plastic strain, then $\psi(\epsilon)$ is equal to unity when $\epsilon = C_3/C_2$. For large test specimens C_2 will equal unity, therefore, Equation [4.6] reverts to Hooke's Law when ϵ is equal to the yield strain (C_3). For ϵ less than ϵ_y, the discontinuous function is needed to force $\psi(\epsilon)$ equal to unity and maintain Hooke's Law.

Elastic Buckling vs. Plastic Collapse

Without doubt, the cell walls of wood either fracture or plasti-cally yield after or when they collapse because permanent deformation remains after the load is removed. However, the question arises whether the non-linear mechanical properties can be adequately modeled assuming elastic buckling.

Both our experimental tests (Kasal 1989) and data presented by Maiti et al. (1984) show that the ϵ_y for wood is relatively independent of density. One explanation for this phenomenon is that at low relative densities, the elastic buckling strain is reached prior to reaching the fully plastic moment. At higher relative densities, when plastic hinges develop, the ϵ_y changes slowly with density. This concept is proposed by Gibson and Ashby (1988) when explaining the effect of multiaxial loading on the σ_y.

To illustrate the argument presented above, the ϵ_y (Figure 4.3)

and stress (Figure 4.4) of wood is calculated and plotted as a function of relative density for elastic and plastic collapse. Because E_w and σ_{y_w} are unknown, they were calculated from the measured modulus and σ_y using Equations [4.1] and [4.3] respectively. For 20 mm cubes conditioned to 8% moisture content and 30°C, E_w=12 GPa and σ_{y_w}=49 MPa. We have found that C_3 is approximately equal to 0.015 for specimen heights greater than 10 mm. This agrees closely with the value of 0.014 determined by Maiti et al. (1984).

For low relative densities, the difference between the predicted values of σ_y is small. However, large differences exist between the predicted values of ϵ_y. For higher relative densities when plastic collapse is likely, the error introduced to the predicted yield stress by assuming elastic collapse is not serious for relative densities less than 0.35. The yield strain predicted using both methods are similar for high relative densities. Our tests with balsa (<u>Ochroma lagopus</u>) show that the yield strain is approximately 0.015, which is equal to that for higher density species such as yellow poplar and maple. A ϵ_y of approximately 0.012 was calculated for several densities of balsa from data presented by Easterling et al. (1982). Therefore, it seems likely that the cell walls collapse from elastic buckling for low relative densities. This does not exclude the possibility that the cell walls yield or fracture after collapse has occurred.

Expansion Ratio

We define the expansion ratio (μ) for cellular materials as the ratio of lateral strain to compressive strain in the non-linear stress-

strain region. Maiti et al. (1984) state that both rigid and elastomeric foams undergo no lateral expansion with compression strain in the non-linear stress-strain region. For wood, no expansion results in the longitudinal direction, however, the specimen will expand in the radial or tangential directions. The expansion ratio will affect the plateau and densification strains by influencing how fast density increases with compression strain. Therefore, for wood (Kasal 1989):

$$\rho_r(\epsilon) \;=\; \rho_r \, [1 - \epsilon_p + \mu\epsilon_p - \mu\epsilon_p^2]^{-1} \qquad [4.7]$$

$$\text{where: } \epsilon_p = \epsilon - \epsilon_y \quad \text{for } \epsilon > \epsilon_y$$

The surface of specimens with finite height are restrained by frictional forces. Lateral expansion at the loading surfaces will be limited by the frictional forces while the center expands resulting in a barrelling effect (Figure 5). Because of the extreme anisotropy in wood, expansion only occurs in the transverse direction. Assuming the barrelling occurs in the shape of a parabola, $\rho_r(\epsilon)$ can be calculated from the change in volume using:

$$\rho_r(\epsilon) = \rho_r \, [1 - \epsilon_p + 2/3\mu\epsilon_p - \mu\epsilon_p^2]^{-1} \qquad [4.8]$$

The influence of μ on the predicted non-linear response is shown in Figure 4.6. Densification strain decreases with lower values of μ. Experimentally, μ was found to decrease with specimen height. This is presumably a result of surface restraint. Characteristic values of μ for yellow poplar, at 30°C and 12% moisture content were between 0.1 and 0.15 for 20 mm cubes and decreased to approximately 0.05 for 0.09 mm flakes. An estimation for μ based on measurements before and after compression was found to over-estimate the true expansion ratio as

measured with the device described earlier.

Effect of Specimen Height

The linear elastic constant, C_2, is found to equal unity for man-made cellular materials (Gibson and Ashby 1982) and wood (Easterling et al. 1982). This is correct in terms of a true material response. However, the measured E is highly dependent on specimen height for both man-made foams (Menges and Knipschild 1982) and wood (Wolcott et al. 1989). It has been found that the apparent E increases non-linearly with specimen height. Whereas, σ_y remains invariant with specimen height and ϵ_y decreases with the reciprocal of E. A conclusive explanation for the behavior is lacking. However, the phenomenon has been related experimentally (Menges and Knipschild 1982) and theoretically (Wolcott et al. 1989) to the excessive deformation of the loaded surfaces, possibly from the influence of surface asperities as small as 0.25 mm.

The relationship described above can be modeled through C_2. For C_2 equal to unity, C_3 is equal to the yield strain. However, for other values of C_2, it can be shown that $\epsilon_y = C_3/C_2$ by substituting Equation [4.1] into Equation [4.2]. The effect of specimen height on C_2 is shown in Figure 4.7. C_2 is calculated from ϵ_y using a value of 0.015 for C_3. Because Equation [4.2] remains unchanged, σ_y is not affected by specimen height, as was observed.

Calculated Values of Cell Wall Modulus

For wood and other natural cellular materials, E_w is unknown.

This may also be true for man-made polymeric foams in which the polymerization process is influenced by the blowing agents. Equation [4.2] was used to calculate a value for E_w because σ_y remains invariant with specimen geometry. In calculating E_w for individual specimens, C_3-0.015 was used and the density of each specimen was determined. Values of E_w calculated as a function of temperature and moisture content are presented for 20 mm cubes and 0.9 mm flakes in Figures 4.8 and 4.9 respectively.

As expected, E_w was found to decrease with increasing temperature and moisture content. The only temperature and moisture content combination above the glass transition temperatures of lignin and hemicelluloses is 225°C for 0% moisture content. This condition also corresponds with the lowest cell wall modulus for both 20 mm cubes and 0.9 mm flakes. Elevated pressures in the previously described testing chamber were needed to achieve 120°C and 140°C temperatures while maintaining a moisture content of 16%. A lower E_w than observed was expected for these conditions. More testing at pressurized conditions will be needed to clarify these results.

The values for E_w determined from 20 mm cubes and 0.9 mm flakes were similar, however, those calculated from the flakes tended to be slightly higher. The effective E_w calculated for tangential flakes was found to be approximately half that of flakes tested in the radial direction. This can be attributed to the reinforcing nature of the rays and was accurately predicted by Easterling et al. (1982).

Non-Linear Strain Function

The non-linear strain function, $\psi(\epsilon)$, is a non-linear multiplier of E. Because it is solely a function of strain and density, this function essentially monitors the cellular collapse in the material. Calculated values of $\psi(\epsilon)$ as a function of ϵ and relative density are presented in log-log form in Figure 4.10. The following values were used for these calculations: C_3=0.015, C_2=1, μ=0.05, and Equation [4.8].

As was unconditionally imposed in Equation [4.6], $\psi(\epsilon)$ equals unity for values of ϵ less than ϵ_y. Then, $\psi(\epsilon)$ decreases until a minimum is reached with the onset of densification. We term the strain at which this minimum occurs the "densification strain" (ϵ_{den}). $\psi(\epsilon)$ then increases during the densification stage approaching infinity. Another value that can be consistently determined is the strain at which $\psi(\epsilon)$ equals unity (ϵ_u) after reaching ϵ_{den}.

Notice that the value of $\psi(\epsilon)$ at ϵ_{den} increases with density. Whereas, ϵ_{den} and ϵ_u both decrease as density increases. This means that as density increases the slope of the cellular collapse region will increase and strain at the onset of densification will decrease. These results are consistent with experimental results. Meinecke and Clark (1973) calculate the non-linear strain function from initial stress in stress relaxation experiments performed at different levels of constant stress. The behavior of $\psi(\epsilon)$, calculated using this method, is similar to our theoretical plots.

Experimental and predicted values for stress and strain at ϵ_{den} and ϵ_u were used to quantitatively determine how well $\psi(\epsilon)$ can predict the collapse and densification regions of the stress-strain relation for flakes. E and σ_y were determined for the compression stress-strain

data of individual flakes at different moisture contents and temperatures. Typical predicted and experimental curves are presented in Figure 4.11. On the average, predicted values of ϵ_{den} and ϵ_u are less than those measured experimentally. The mean error in predicting ϵ_{den} are 11.1% for stress and 8.2% for strain. For predicting ϵ_u the mean error was 9.5% for stress and 9.9% for strain. This error can result from damage associated with large strains and not accounting for the viscoelastic response during the test.

CONCLUSIONS

Theories for the mechanical properties of cellular materials developed by Gibson and Ashby can be used to accurately model wood in transverse compression. Unlike elastomeric foams, wood exhibits significant expansion after cellular collapse has begun. The effect of lateral expansion on the compression stress-strain relationship can be accounted for in a non-linear strain function. Whereas the assumption of elastic collapse may not be physically valid at high relative densities, it can be used to accurately model the non-linear material behavior of wood. However, elastic buckling may actually be the preferred mode of cellular collapse for low relative densities. The similarities between $\psi(\epsilon)$ and the non-linear strain function determined experimentally for stress relaxation tests by Meinecke and Clark (1973) is encouraging for extension of this analysis for modeling viscoelastic behavior.

LITERATURE CITED

Ashby, M.F. 1983. The mechanical properties of cellular solids. Mettal. Trans. A. 14A:1755-1769.

_____., K.E. Easterling, R. Harrysson, and S.K. Maiti. 1985. The fracture and toughness of woods. Proc. R. Soc. Lond. A398:261-280.

Chan, R. and M. Nakamura. 1969. Mechanical properties of plastic foams: The dependence of yield stress and modulus on the structural variables of closed-cell and open-celled foams. J. Cell. Plast. 5:112-118.

Easterling, K.E., R. Harrysson, L.J. Gibson, and M.F. Ashby. 1982. On the mechanics of balsa and other woods. Proc. R. Lond. A383:31-41.

Gent, A.N. and A.G. Thomas. 1959. The deformation of foamed elastic materials. J. Appl. Polym. Sci. 1(1):107-113.

Gibson, L.J. and M.F. Ashby. 1988. Cellular Solids: Structure and Properties. Pergammon Press, New York, NY. 357pp.

_____. and _____. 1982. The mechanics of three-dimensional cellular materials. Proc. R. Soc. Lond. A382:43-59.

_____., _____., and K.E. Easterling. 1988. Structure and mechanics of the iris leaf. J. Mater. Sci. 23:3041-3048.

_____., _____., G.S. Schajer, and C. Robertson. 1982. The mechanics of two-dimensional cellular materials. Proc. R. Soc. Lond. A382:25-42.

_____., K.E. Easterling, and M.F. Ashby. 1981. The structure and mechanics of cork. Proc. R. Soc. Lond. 377:99-117.

Kasal, B. 1989. Behavior of wood under transverse compression. Master's Thesis, Viriginia Polytechnic Institute and State University, Blacksburg, VA. 120pp.

Ko, W.L. 1965. Deformations of foamed elastomers. J. Cell. Plast. 1:45-50.

Leaderman, J.M. 1971. The prediction of the tensile properties of flexible foams. J. Appl. Polym. Sci. 15(3):693-703.

Maiti, S.K., L.J. Gibson, and M.F. Ashby. 1984. Deformation and energy absorption diagrams for cellular solids. Acta Metal. 32(11):1963-1975.

Meinecke, E.A. and R.C. Clark. 1973. Mechanical Properties of Poly-
    meric Foams. Technomic, Westport, CT. pp.30-47.

Menges, G. and F. Knipschild. 1982. Stiffness and strength: rigid
    plastic foams. pp. 27-72 in: Hilyard, N.C. (Ed.). Mechanics of
    Cellular Plastics. MacMillian Press, New York, NY.

Warren, W.E. and A.M. Kraynik. 1987. Foam mechanics: the linear elas-
    tic response of two-dimensional spatially periodic cellular mate-
    rials. Mech. Mater. 6:27-37.

Whittaker, R.E. 1971. The mechanical behavior of microporous poly-
    urethane foams. J. Appl. Polym. Sci. 15(5):1205-1218.

Wolcott, M.P., B. Kasal, F.A. Kamke, and D.A. Dillard. 1989. Testing
    small wood specimens in transverse compression. Wood and Fiber
    Sci. In Press.
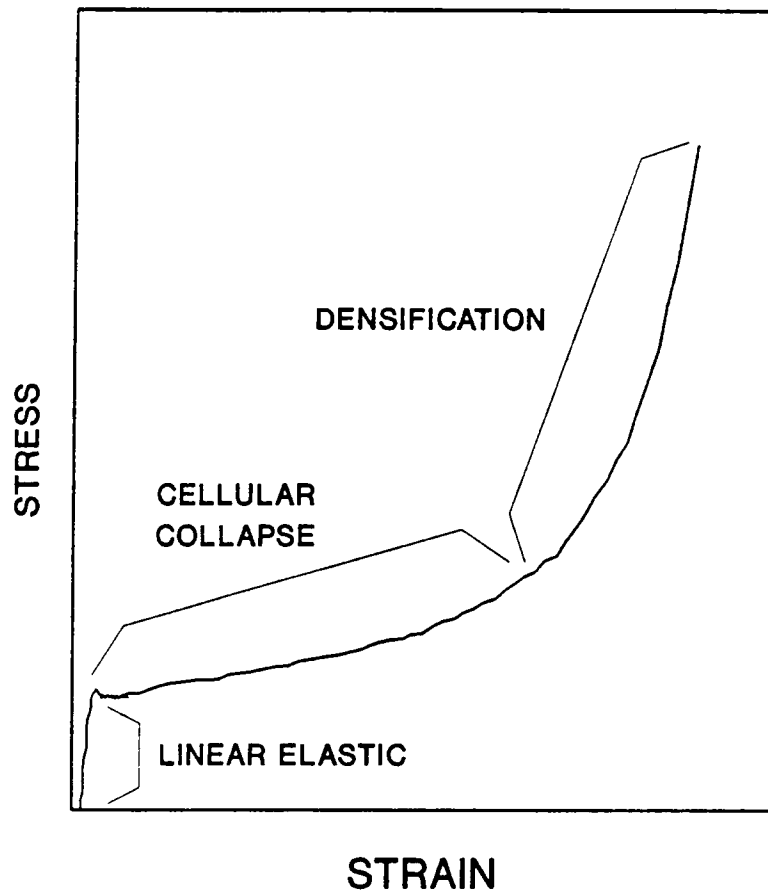
Figure 4.1: A characteristic stress-strain diagram for a cellular material.
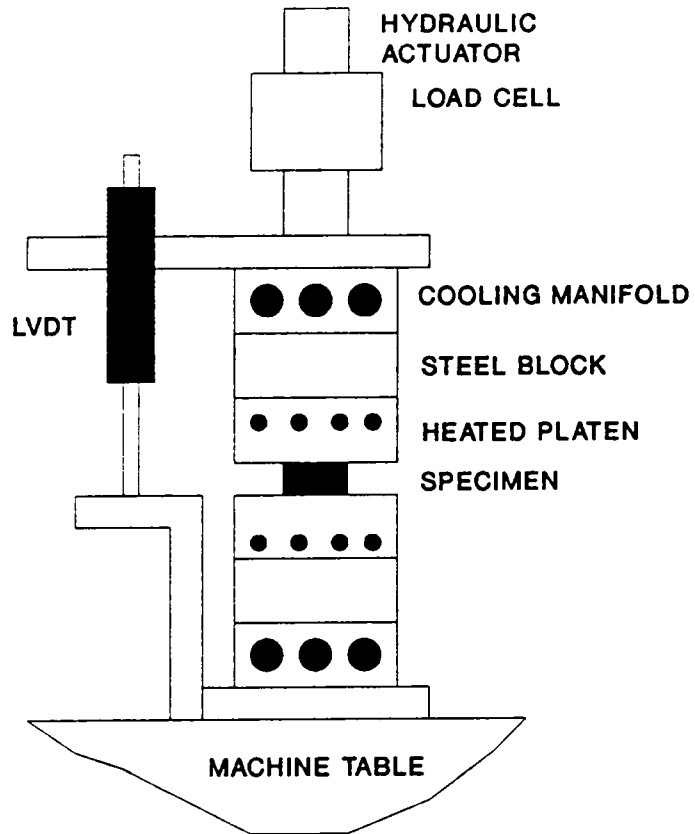
Figure 4.2: Schematic drawing of the test apparatus used for compression tests.
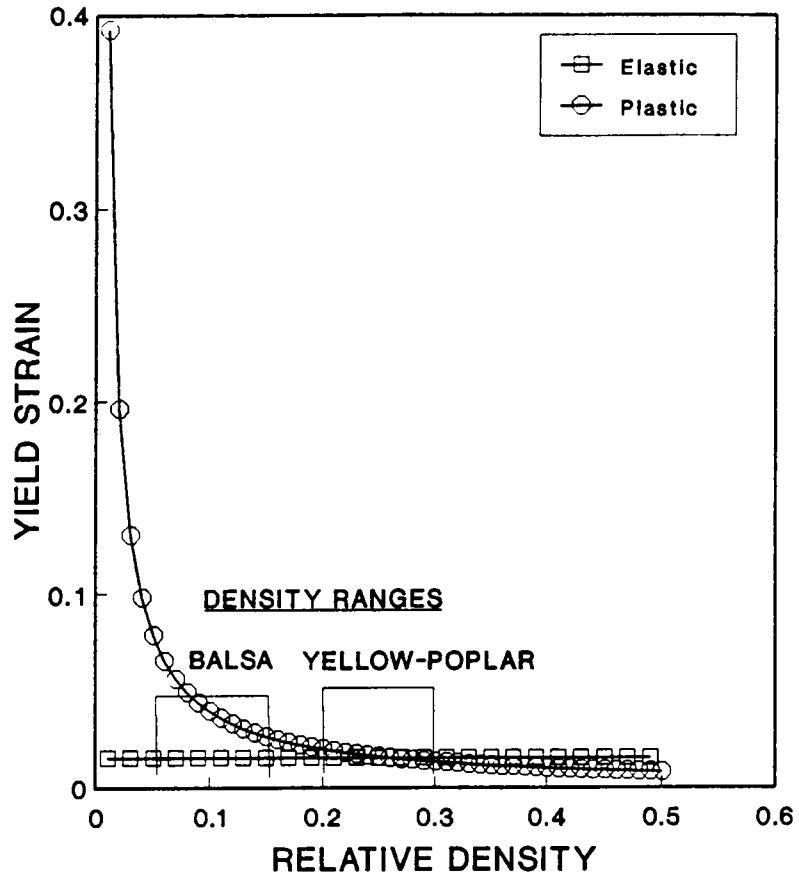
Figure 4.3: Yield strain as a function of relative density calculated assuming elastic and plastic collapse mechanisms.
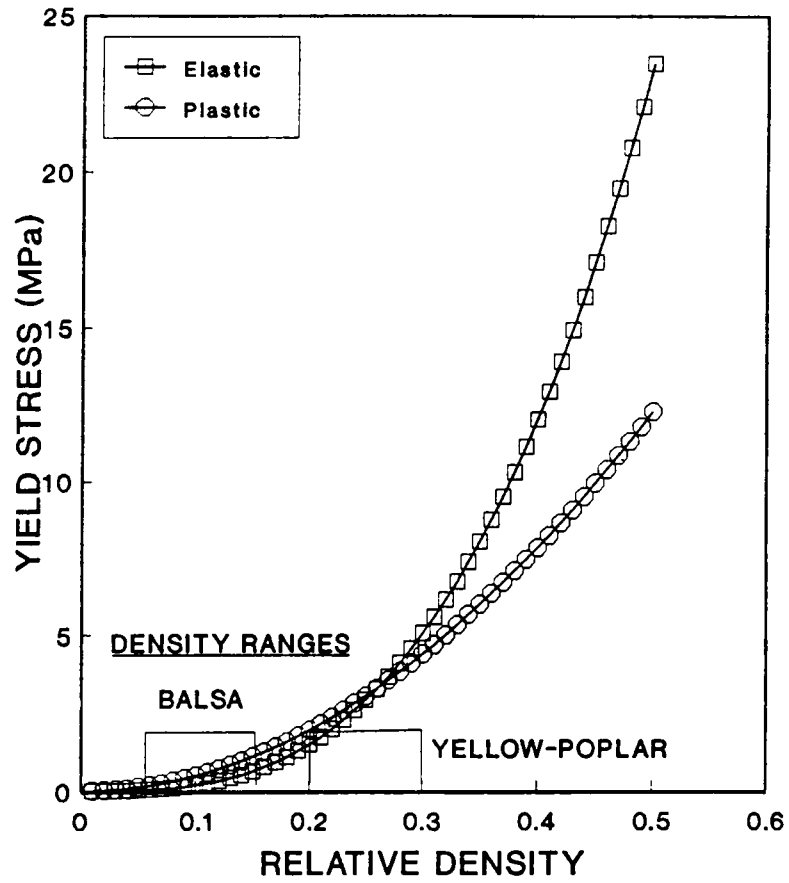
Figure 4.4: Yield stress as a function of relative density calculated
assuming elastic and plastic collapse mechanisms.
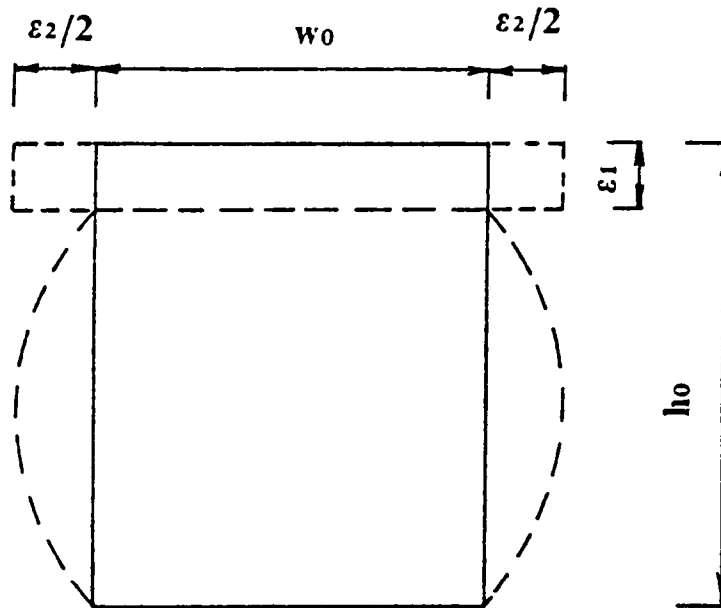
Figure 4.5: An illustration of the barrelling effect exhibited by cellular materials with a non-zero expansion ratio.
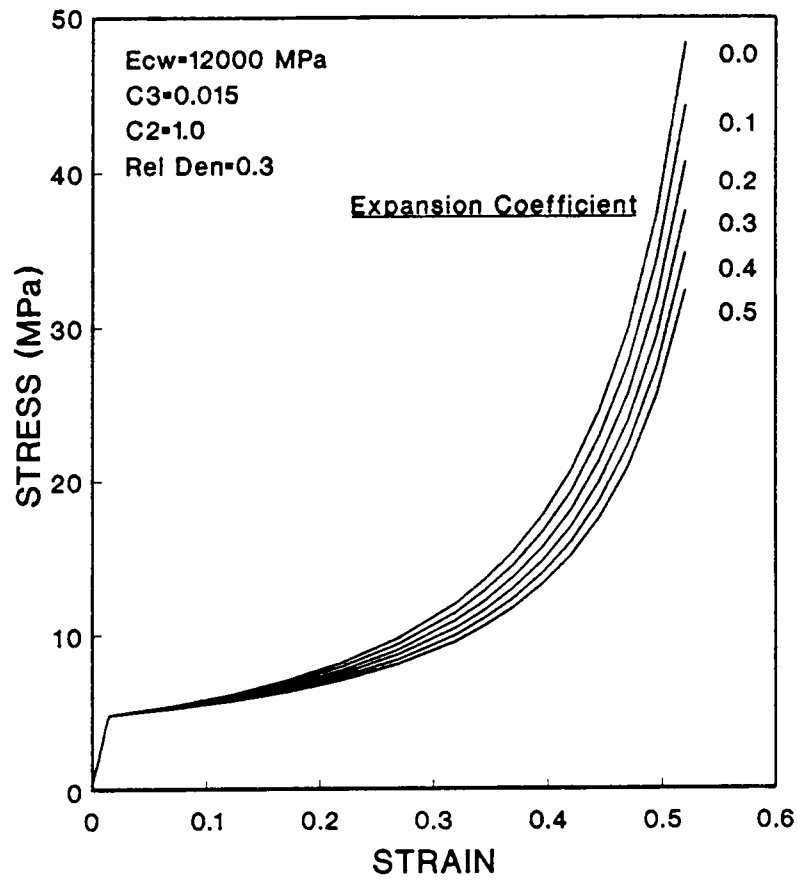
Figure 4.6: Predicted stress-strain diagrams as a function of relative density.
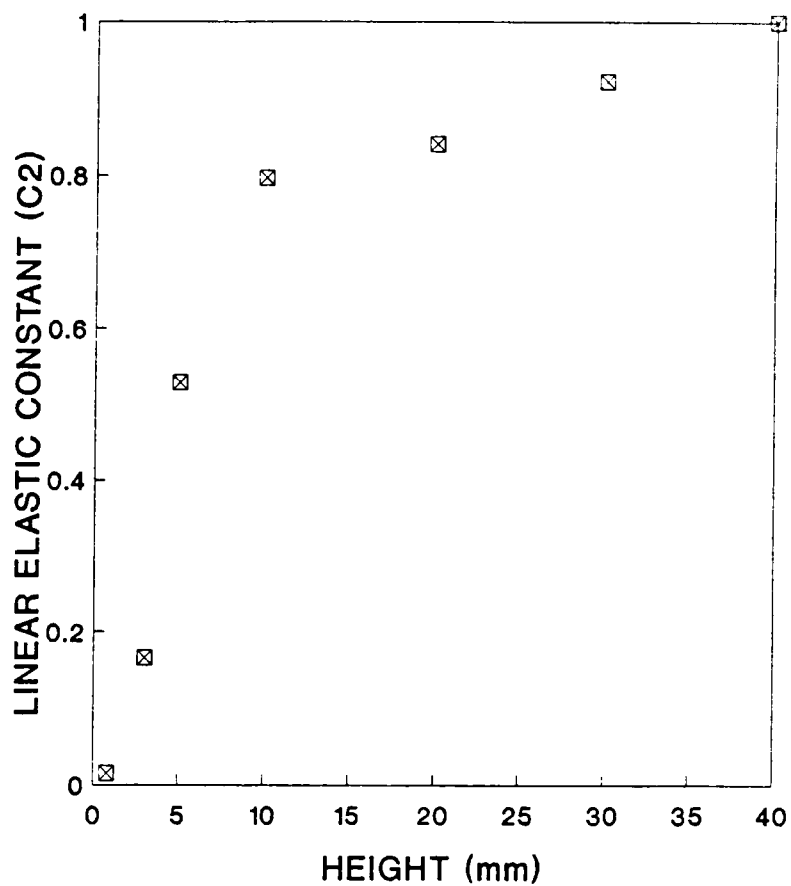
Figure 4.7: Experimentally determined linear elastic constant (C_2) as a function of specimen height.
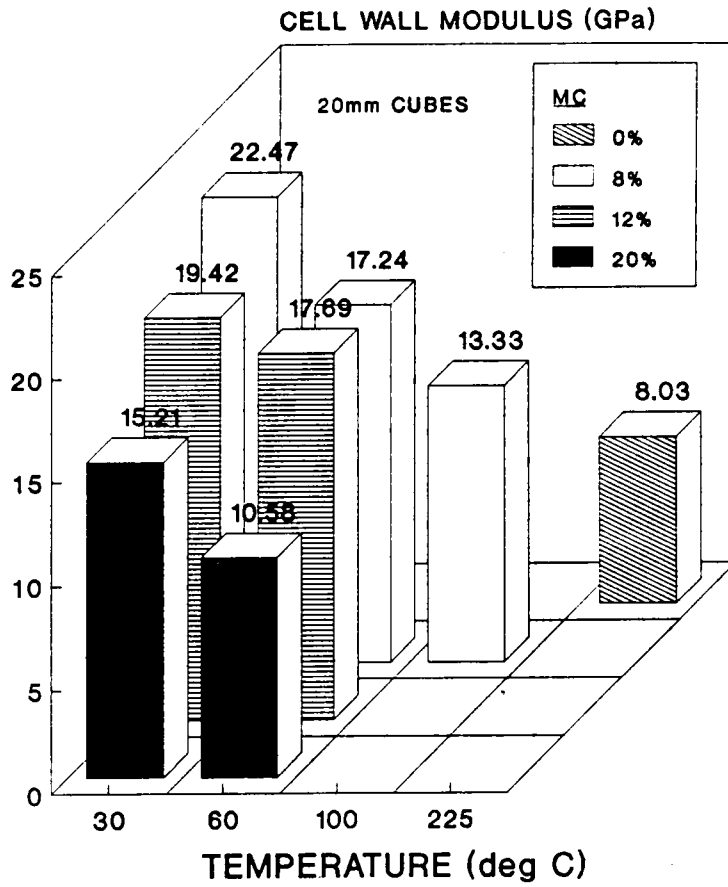
Figure 4.8: Calculated Young's modulus for the cell wall material as a function of temperature and moisture content for 20 mm cubes.
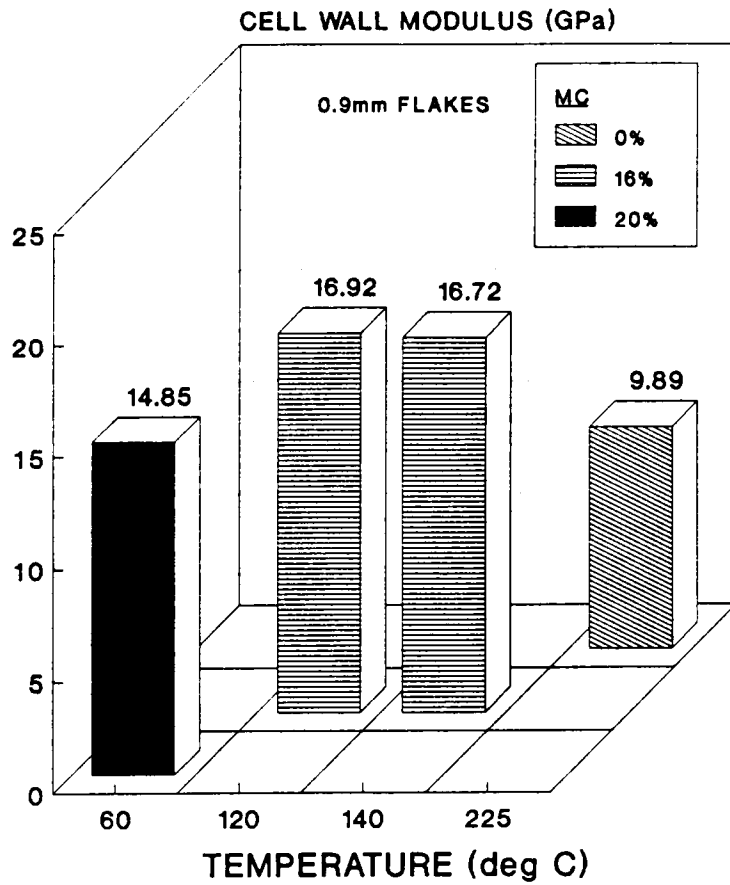
Figure 4.9: Calculated Young's modulus for the cell wall material as a function of temperature and moisture content for 0.9 mm flakes.
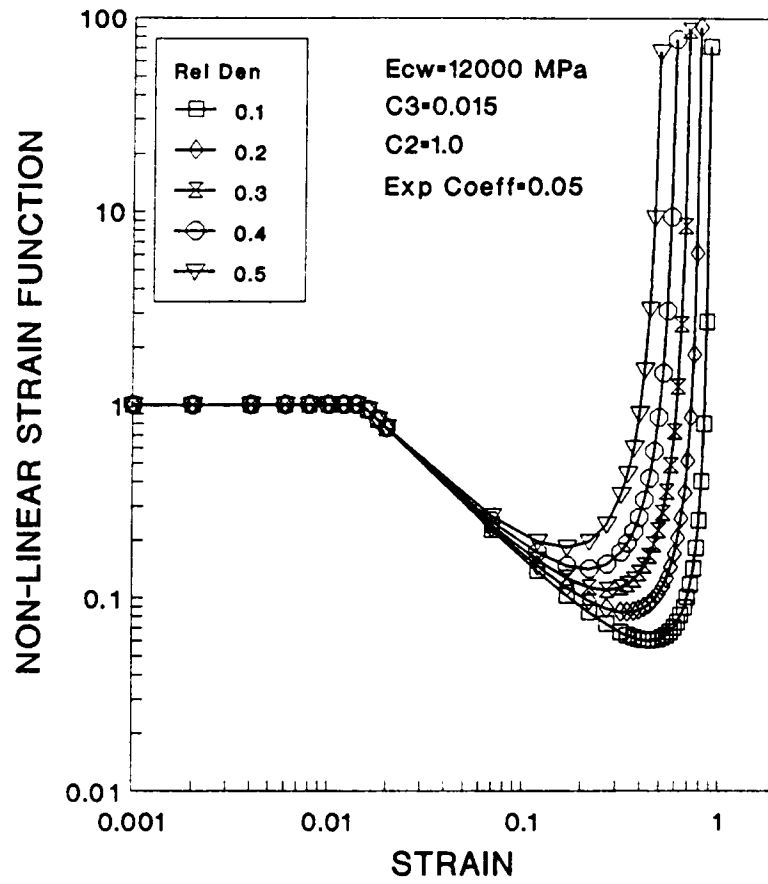
Figure 4.10: Predicted non-linear strain function ($\psi(\epsilon)$) as a function of strain and relative density.
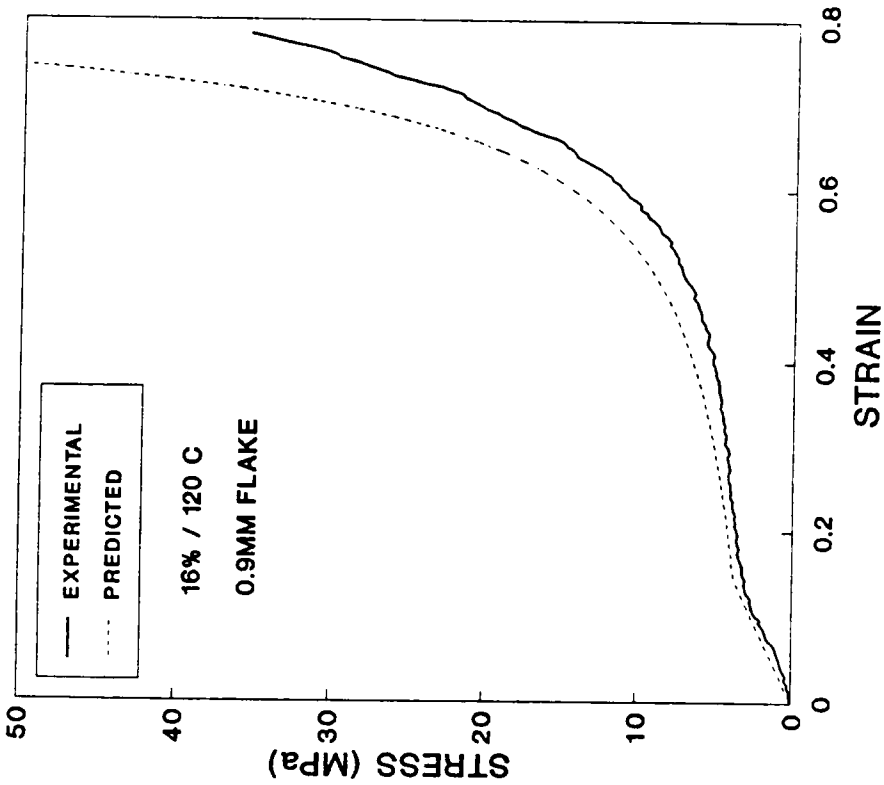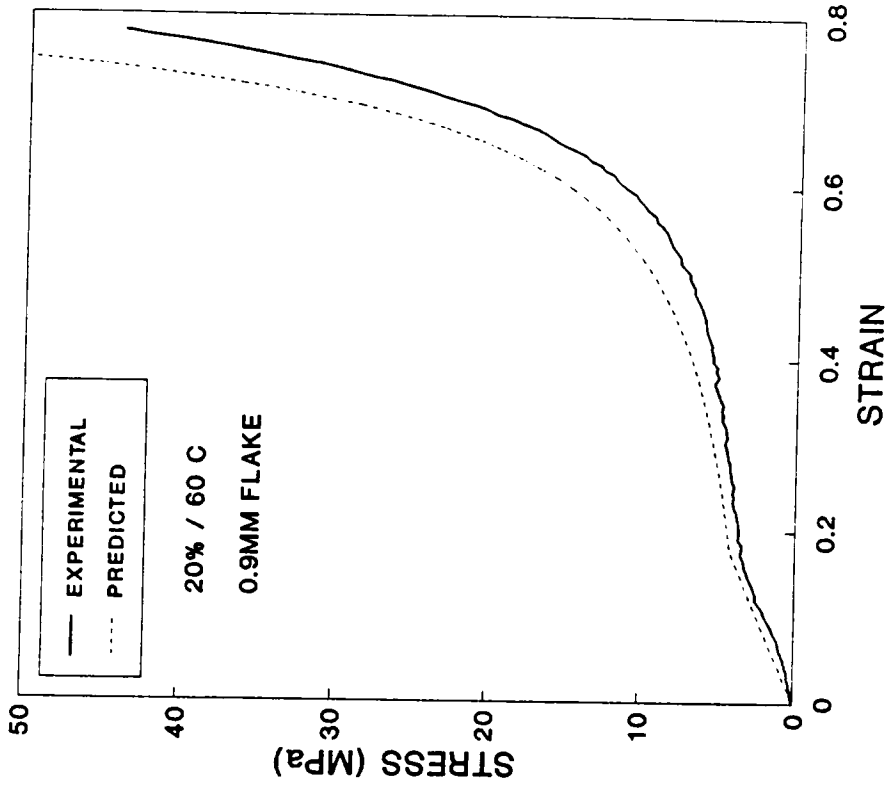
Figure 4.11: Experimental and predicted stress-strain diagram for 0.9 mm flakes.

CHAPTER 5

A NONLINEAR VISCOELASTICITY MODEL FOR

CELLULAR MATERIALS IN COMPRESSION

INTRODUCTION

Cellular materials are frequently used in structural applications where their viscoelastic properties are critical to performance. Flexible foams are typically used in dynamic loading situations for energy dissipation; rigid foams are often used in structural applications under long term static loading. The uniqueness of the mechanical behavior for both natural and synthetic cellular materials can be attributed to the interaction between the solid material properties and the cellular geometry. This interaction is particularly evident in compression when cellular collapse occurs. The action of the cellular structure is responsible for both the excellent energy absorption properties of polymeric foams and the extreme creep deformations and compression set that are possible. However, cellular geometry only accentuates the characteristic properties of the cell wall material.

Wood is a widely used natural cellular material. One application where nonlinear viscoelastic behavior in compression is important is the manufacturing process of wood-based composites. During production, wood elements are coated with a thermosetting adhesive and consolidated into a contiguous product in a hot-press. For many composites, the wood is compressed at high enough pressures that permanent densification results. The densification process influences the response of the end product to stress and moisture. The objective of this work is to develop a

107

nonlinear viscoelasticity model for cellular materials in compression to further understand how the production process influences material design in wood-based composites. For application to the production of wood-based composites, the model should incorporate the influence of environment on the linear viscoelastic response of the cell wall polymers and the collapse associated with the cellular geometry.

Viscoelastic Behavior of Cellular Materials

Several excellent reviews of the structure-property relationship of cellular materials exist (Gibson and Ashby 1988, Hilyard 1982, Meinecke and Clark 1973). Meinecke and Clark (1973) discuss stress relaxation and dynamic behavior in detail, however, little is mentioned of creep. Gibson and Ashby (1988) derive relationships for the creep rate of honeycombs and foams. Whereas, these relations do separate the reaction of the cell wall material and the cellular geometry, they do not explicitly address large deformations from cellular collapse.

Rosa and Fortes (1988) studied the nonlinear creep and stress relaxation of cork. When the cork was compressed to different levels of initial strain (ϵ_0), they observed that log-log plots of stress relaxation curves were straight parallel lines beginning at different stress levels. The relaxation data were fit to a simple power law of the form:

$$\frac{\sigma}{\epsilon_0} = mt^{-n} \qquad [5.1]$$

Whereas the values of m increased with decreasing levels of ϵ_0, the slope (n) was relatively constant. This behavior is indicative of most

synthetic polymer foams (Meinecke and Clark 1973) and has been observed in wood (Kunesh 1961, Youngs 1957). The constant rate of stress relaxation appears to be dependent on the cell wall polymers. Meinecke and Clark performed a vertical shift of these curves to derive a nonlinear strain function that is indicative of the structural nonlinearities.

The creep behavior of cellular materials is quite different from stress relaxation. Interpretation of data presented by Rosa and Fortes (1988) shows that relative creep strain, defined as the ratio of creep strain ($\epsilon(t) - \epsilon_o$) to ϵ_o, increases with applied stress (σ_o). However, above a characteristic stress level, the relative creep strain begins to decrease with higher levels of σ_o until it is lower than the linear creep levels. In traditional nonlinear viscoelastic materials, relative creep strain increases for all levels of σ_o outside the linear region. The creep behavior for cellular materials has a logical interpretation in cellular collapse. At low levels of strain, the cell walls undergo bending deformations. The creep strain will be entirely dependent on the relaxation of the cell wall material. However, with the onset of cell wall buckling, the cells collapse, adding greatly to the creep deformation. At stress levels indicative of large amounts of cellular collapse, little additional creep strain is observed. Finally, at extremely high stress levels, the cell walls consolidate and behave similar to the solid material.

These observations lend credibility to the hypothesis that the nonlinear creep deformation can be separated into linear material and structural nonlinear components. Equations derived for the linear viscoelastic behavior of honeycombs by Gibson and Ashby (1988) indicate

this behavior. At high rates of loading, the unrelaxed modulus dom-
inates the behavior and the equations reduce to that of the linear elas-
tic behavior. However at longer times the modulus is decreased.

ANALYTICAL METHODS

Structural Nonlinearities

The structural effects on the mechanical behavior of cellular mate-
rials can be best understood by examining a typical stress-strain dia-
gram (Figure 5.1). At small strains, a cellular material behaves in a
linear elastic manner. The properties of the cell wall material and
cellular geometry can be related to the Young's modulus of the cellular
material through the simple relation derived by Gibson and Ashby (1982):

$$E = C_2 \ E_w \ \rho_r^3 \qquad\qquad [5.2]$$

> where:
> C_2 = constant
> E_w = Young's modulus of cell wall
> ρ_r = relative density = $\rho \ / \ \rho_w$

The cellular geometry is represented by the relative density which is
the ratio of the density of the cellular material to the density of the
cell wall material.

A yield point in the cellular material is exhibited from the onset
of cellular collapse. This collapse can be initiated from elastic buck-
ling, plastic yielding, or brittle fracture of the cell wall. The
yielding in wood can be adequately modeled by assuming elastic collapse
(Wolcott et al. 1989). A plateau in the stress-strain diagram results
from continued cellular collapse. At some strain, a majority of the
cells have collapsed. Additional strain results in a rapid increase in

stress. This upturn of the stress-strain diagram marks the onset of the densification region (Gibson and Ashby 1988).

Clearly, the characteristic shape of the stress-strain diagram is a direct result of the geometric nonlinearity resulting from the response of the cellular structure. Rusch (1969) first proposed the separation of the structural and cell wall material response through a modification of Hooke's Law:

$$\sigma = E \epsilon \psi(\epsilon) \tag{5.3}$$

The nonlinear strain function, $\psi(\epsilon)$, is a function of the applied strain that governs the geometric non-linearities. It can be derived experimentally through the vertical shift of stress relaxation curves that acts as a multiplier of the modulus (Meinecke and Clark 1973) or from the observed plastic strain in a stress-stain diagram (Rusch 1969). A modification of equations derived for the plateau stress by Maiti et al. (1984) allows $\psi(\epsilon)$ to be described as follows (Wolcott et al. 1989):

$$\psi(\epsilon) = \frac{\epsilon_y}{\epsilon} \left[\frac{1-\rho_r^{1/3}}{1-\rho_r(\epsilon)^{1/3}} \right]^3 \tag{5.4}$$

where: $\rho_r(\epsilon)$ = relative density as a function of strain

Dilatation results from cellular collapse even in uniaxial loading. Therefore , $\rho_r(\epsilon)$ is a monitor of the cellular collapse. For elastomeric foams, little or no lateral expansion occurs in the specimen within the nonlinear region of the stress-strain relationship. For this case, $\rho_r(\epsilon) = \rho_r/(1-\epsilon)$. However, lateral expansion has been noted for wood.

When the loaded surfaces are restrained from frictional forces, the specimen exhibits barelling and $\rho_r(\epsilon)$ can be determined by (Wolcott et al. 1989):

$$\rho_r(\epsilon) = \rho_r \left[1 - \epsilon_p + 2/3 \; \mu\epsilon_p - \mu\epsilon_p^2 \right]^{-1} \qquad [5.5]$$

where:
ϵ_p = plastic strain = $\epsilon - \epsilon_y$
μ = expansion coefficient

Linear Viscoelasticity

Boltzmann Superposition Integral

For linear viscoelastic materials, the time dependent response for an arbitrary loading history may be expressed in the form of a convolution integral commonly referred to as the Boltzmann Superposition Principle (Ferry 1980). For creep the time dependent strain ($\epsilon(t)$) is related to stress (σ) by :

$$\epsilon(t) = D(t) \; \sigma(0) + \int_0^t D(t-\varsigma) \; \frac{d\sigma}{d\varsigma} \; d\varsigma \qquad [5.6]$$

Likewise, in stress relaxation, the stress as a function of time ($\sigma(t)$) can be represented by:

$$\sigma(t) = E(t) \; \epsilon(0) + \int_0^t E(t-\varsigma) \; \frac{d\epsilon}{d\varsigma} \; d\varsigma \qquad [5.7]$$

It can be shown that the linear creep compliance ($D(t)$) is related to the linear relaxation modulus ($E(t)$) through the integral:

$$\int_0^t D(\varsigma) \; E(t-\varsigma) \; d\varsigma = t \qquad [5.8]$$

Cellular materials often have a small linear range for viscoelastic properties. Because this range is often strain dependent, creep tests are difficult to conduct properly because they will creep out of the linear range. For this work, stress relaxation data was collected within the linear region in accordance with a technique to be outlined later. The creep compliance was then calculated from the relaxation modulus through a numerical solution of equation [5.8].

Method of Reduced Variables

It was first noted empirically that for many materials, the viscoelastic response at different temperatures was equivalent through a horizontal shift in the log of time. Therefore, time dependent material properties could be determined using short term tests at different temperatures and shifted on the time axis to derive the long term response of the material at a characteristic temperature. After the individual curves are shifted on the time axis it is termed a master curve. The new time scale can be represented by reduced time which is given by the relation:

$$t' = \int_0^t \frac{d\zeta}{a(T)} \qquad [5.9]$$

At a constant temperature, equation [5.9] will reduce to: $t' = t/a(T)$.

An equivalent approach to time-temperature superposition has been used with moisture (Maksimov et al. 1976, Maksimov el al. 1975). In the case of both moisture and temperature influence, t' becomes:

$$t' = \int_0^t \frac{d\zeta}{a(T)\ a(M)} \qquad\qquad [5.10]$$

To determine a given viscoelastic response, t' is merely substituted for t in the Boltzmann integral.

Although the methods of reduced variables was initially empirical, a theoretical basis has resulted. The behavior of $a(T)$ for temperatures above the glass transition temperature of amorphous polymers is described by the WLF (Williams-Landel-Ferry) equation (Williams et al. 1955). The WLF equation relates the change in free volume in a polymer above T_g to $a(T)$. Likewise, Knauss and Emri (1981) have developed a relationship for the shift factor as a function of temperature, moisture, and stress through the additive change in free volume resulting from the dilation caused by each of these variables. For temperature below T_g, $a(T)$ is found to typically follow an Arrhenius equation.

Resulting from the highly hygroscopic nature of wood, the viscoelastic properties during the pressing cycle must account for moisture and temperature effects. Therefore, a time-temperature-moisture superposition was utilized to construct a master curve. For the work presented here, both $a(T)$ and $a(M)$ were determined experimentally.

Mechanical Analogies

$E(t)$ and $D(t)$ can be mathematically represented in different ways. A convenient method is mechanical analogies. Creep is typically represented by Kelvin elements (a spring and dashpot in parallel) and stress relaxation by Maxwell elements (a spring and dashpot in series). The

response of a single Kelvin and Maxwell element are respectively:

$$\epsilon(t) = \frac{\sigma_o}{E}\left[1 - e^{-t/\lambda}\right]$$

[5.11]

$$\sigma(t) = \epsilon_o E e^{-t/\lambda}$$

[5.12]

where:
E = modulus of the spring
λ = retardation time

To produce a more realistic behavior, Kelvin elements are combined in series and Maxwell elements in parallel. The behavior of the generalized form of these models are :

$$\epsilon(t) = \sigma_o \sum_{i=1}^{n} \frac{1}{E_i}\left[1 - e^{-t/\lambda_i}\right]$$

[5.13]

$$\sigma(t) = \epsilon_o \sum_{i=1}^{n} E_i e^{-t/\lambda_i}$$

[5.14]

The experimentally determined relaxation modulus was fit to a series of Maxwell elements arranged in parallel. The retardation times (λ_i) were spaced at one per decade of time and the spring modulii (E_i) were determined from the data using a nonlinear regression method. Likewise, the calculated creep compliance was fit to a series of Kelvin elements in the same manner.

Extension of Boltzmann Integral for Nonlinear Response

An empirical extension of the Boltzmann integral to nonlinear materials has been used by Halpin (1965) to study elastomers. For one-dimensional stresses and strains, the convolution integral becomes:

$$\epsilon(t) = \int_0^t E(t-\zeta) \frac{d\epsilon}{d\zeta} \mathcal{F}(\epsilon) \, d\zeta \qquad [5.15]$$

A simplification of this integral was used by Meinecke and Clark (1973) for studying rate effects in the stress-strain response:

$$\epsilon(t) = \mathcal{F}(\epsilon) \int_0^t E(t-\zeta) \frac{d\epsilon}{d\zeta} \, d\zeta \qquad [5.16]$$

This simplification was found to be accurate at slow relaxation rates. Although not mathematically rigorous, this simplification appears reasonable from our knowledge of the nonlinear strain function. Given that $\psi(\epsilon)$ has been found to be independent of environmental and time effects (Rusch 1969), the structural collapse mechanisms will effectively decrease the modulus independent of the manner in which the material arrived at that collapse state. This is consistent with the formulation for $\psi(\epsilon)$ in equation [5.4] because it includes only structural dependent terms.

Numerical Methods

Many problems exist with the direct numerical evaluation of the Boltzmann integral; the largest of which are the long solution times required and stability of the solution at large time steps. A considerably easier method is the direct solution of the governing differential equations for a finite series of Kelvin or Maxwell elements. The governing differential equations for a Kelvin and Maxwell element derived from equations 5.11 and 5.12 respectively are:

$$\epsilon' = \frac{D}{\lambda}\,\sigma - \frac{1}{\lambda}\,\epsilon \qquad\qquad [5.17]$$

$$\sigma' = E\,\epsilon' - \frac{1}{\lambda}\,\sigma \qquad\qquad [5.18]$$

where:
$$D = 1/E$$

In this work, the stress or strain in each element was solved using a forward Euler method and the stresses or strain summed to reach the total solution.

EXPERIMENTAL PROCEDURES

Specimen Preparation

Green yellow poplar (_Liriodendron tulipifera_) blocks were split into large sections to obtain optimum orientation with the three principal material directions. The sections were planed and then, conditioned to a nominal 8% moisture content. Prismatic tension specimens with a cross-section of 20mm x 8mm and a length of 155mm were machined from the large sections with the radial direction oriented with the long axis of the specimens.

Stress Relaxation Tests

Relaxation modulus was determined using a single specimen tested at a series of different temperatures and moisture contents using a universal servohydraulic testing machine equipped with an environmental chamber. The test specimen was held at each end between two serrated steel plates that were bolted together. The length of the specimen held bet-

ween the plates at each end was 40 mm. The total gage length between the fastening plates at the two ends was 75 mm. The plates were fastened to the test machine by steel pins. This gripping arrangement allowed the specimen to be unfastened from the test machine at the completion of the daily tests while not actually removing it from the grips.

The stress relaxation tests were conducted by imposing a step increase in strain of 0.005 and maintaining this strain for approximately 600 seconds. The specimen was then returned to zero strain for an equal recovery period. Strain was measured using an extensometer (25.4 mm gage length) attached to the specimen with metallic coil springs. The load and strain data were acquired in real time by a computer.

Environmental Conditions

Two tension specimens were weighed and oven-dried to determine the original moisture content. This moisture content was then used to calculate the oven-dried weight of two additional specimens that were weighed at the beginning and end of each days tests to monitor moisture changes.

Prior to testing the specimen at each moisture content, it was conditioned for 12 hours at 39°C in the environmental chamber mounted on the testing machine. The temperature and relative humidity was incremented at the beginning of each recovery period to speed recovery and allow time for the environment to stabilize. In general, a stress relaxation test was conducted at temperatures between 39°C and 99°C at

3°C intervals. The actual moisture contents and temperature ranges tested are listed in Table 5.1.

The temperature and relative humidity conditions were calculated using the one-hydrate form of the Hailwood-Horrobin equation with parameters determined by Simpson (1971). Whereas the actual moisture content was found to be as much as 2% lower than that calculated, the deviation was found to be consistent at the low and high ends of the temperature range tested.

RESULTS AND DISCUSSION

Time-Temperature-Moisture Superposition

The relaxation modulus (E(t)) determined for different temperatures at a common moisture content was shifted along the log time axis to a reference temperature of 60°C. The individual master curves for each moisture content were then shifted on the log time scale to construct an overall master curve for both time and moisture content (Figure 5.2). Creep compliance (D(t)) was calculated from a numerical evaluation of equation [5.8] for each temperature E(t) master curve. The same shift factors determined from the construction of the overall E(t) master curve were used to construct the overall D(t) master curve (Figure 5.3).

The relationship between the log of the temperature shift factor (a(T)) to temperature was found to be linear for each moisture content except 3%. At 3% moisture content, the a(T) changes rapidly at low temperatures and slowly at high temperatures. Interpretation of this result suggests that at 3% moisture content, the amorphous polymers in wood are extremely glassy and the lower temperatures are approaching the

Vogel temperature where the shift factor approaches infinity (Ferry 1980).

An example plot of log a(T) versus temperature is shown in Figure 5.4. Linear regression equations were fit for each moisture content to be used in the mathematical model. Parameters calculated for these equations are listed in Table 5.2. The negative slope of log a(T) versus temperature is found to increase with increasing moisture content. This would correspond with lower activation energy for higher moisture contents in an Arrhenius type equation to describe a(T). Because water acts as a plasticizer in hydrophilic polymers, it lowers the energy required for a viscoelastic process to occur. This is consistent with the findings from a(T) presented above.

The log of the moisture shift factor (a(M)) was found to vary linearly with moisture content for moisture contents from 6% to 16%. The change in log a(M) with moisture content was greater between 3% and 6% moisture contents than at high moisture contents (Figure 5.5). The Knauss and Emri (1981) model relates the change in the shift factor to the change in free volume which results from a dilatation. This dilatation results from a change in moisture content, temperature, or stress. This indicates that a(M) should be related to the swelling in the cell wall polymers. For hydrophilic polymers, swelling is often less at low moisture contents than high (Adamson 1980). Swelling is related to the water molecules that hydrogen bond to the polymer molecules. The water molecules that are adsorbed first primarily remain in the free volume of the polymer. As moisture content increases, the free volume can no longer hold water molecules and additional increases in

moisture content result in a greater amount of swelling. Considering the theoretical swelling relationship, low moisture contents should cause less swelling, increases in free volume, and change in a(M) than higher moisture contents. However, the opposite behavior is observed. Kelley et al. (1987) observed the glass transition for hemicelluloses to be ca. 70°C at 6% moisture content. The reference temperature for the master curve is 60°C. A possible explanation for the observed behavior of a(M) is that below 6% moisture content a(M) is influenced by both hemicelluloses and lignin. Whereas, for moisture contents above 6%, changes in a(M) result from lignin only.

The overall master curves for E(t) and D(t) were fit to a finite series of Maxwell and Kelvin elements respectively. The parameters of the fitted equations are listed in Tables 5.3 and 5.4.

Nonlinear Viscoelasticity Model

The nonlinear viscoelasticity model presented here was used to study several loading histories. Unless noted otherwise, the material parameters used for the nonlinear strain function correspond to typical yellow poplar samples tested and are: $\rho=0.5$, $\rho_w=1.5$, $C_2=1$, $C_3=0.015$, $\mu=0.05$.

Ramp Loading

In determining the static stress-strain relationship of a material, a constant rate of strain is imposed on a specimen. The nonlinear viscoelasticity model was used to study the effect of strain rate on the linear and nonlinear stress-strain relation. Three different strain

rates were modeled for three moisture contents at $28^{o}C$. The results are presented in Figures 5.6 to 5.8.

For each moisture content, the effect of strain rate is not readily apparent in the linear region of the curve. However, large differences exist among the slope of the elastic region for different moisture contents.

Differences can be easily detected in the plateau stress and are magnified into the densification region. The strain rate effect is most pronounced for higher moisture contents. This result can be attributed to the higher relaxation rates at these moisture contents.

Nonlinear Stress Relaxation

The behavior of the nonlinear relaxation modulus ($\sigma(t)/\epsilon_o$) was tested by modeling stress relaxation experiments at $28^{o}C$ and 6% moisture content for different levels of initial strain (ϵ_o). The levels of ϵ_o used in the modeling procedure are presented in Figure 5.9.

The log-log plots of the nonlinear relaxation modulus versus time are straight parallel lines (Figure 5.10). This is consistent with behavior sited by several authors (Rosa and Fortes 1988, Meinecke and Clark 1973, Kunesh 1961, Youngs 1957). Note that the relaxation modulus decreases with increasing levels of ϵ_o corresponding to the cellular collapse region. As levels of ϵ_o enter the densification region, the relaxation modulus increases with increasing ϵ_o until it is greater than that corresponding to the linear region. The ϵ_o corresponding to the minimum in relaxation modulus is associated with the beginning of the densification region. The nonlinear strain term is equal to unity

when the nonlinear relaxation modulus is equal to the linear relaxation modulus.

Nonlinear Creep Response

The nonlinear creep response was determined experimentally and theoretically by imposing levels of constant stress (σ_o) that corresponded with strain in different regions of the material behavior. Balsa (Ochroma lagopus) cubes (20x20x20 mm) were used because little damage occurs at high strains. Using a universal servohydraulic testing machine, a constant loading rate of 0.2 MN/minute was imposed on the specimens until the desired strain level was achieved. The load was then maintained at this level and the creep strain as a function of time was recorded. The same loading history was used in modeling the response. The parameters for the nonlinear strain function corresponding to balsa were: $\rho=0.109$, $\rho_w=1.5$, $C_2=1$, $C_3=0.009$, $\mu=0$. Both the experimental and predicted results are shown in Figure 5.12 and 5.13, respectively, as normalized creep strain $((\epsilon(t)-\epsilon_o)/\epsilon_o)$. The levels of σ_o are shown in Figure 5.11.

For both the experimental and predicted results, the highest relative creep strain corresponds to the stress level associated with the yield point. The relative creep strain decreases with increasing levels of σ_o. During the densification region the relative creep strain is lower than that corresponding to the linear results. These results are supported by those found by Rosa and Fortes (1988).

Whereas the relative creep response is qualitatively consistent between the experimental and predicted results, the quantitative

results differ.   It is observed that the linear response of the balsa

differs substantially from that predicted using stress relaxation data

from yellow poplar.   Little difference has been noted among the polymer

viscoelastic response of temperate species (Kelley et al. 1987).   How-

ever, some difference is obviously present between these linear

responses.

To assess the quantitative power of the model when the linear vis-

coelastic response is known, a two parameter Kelvin element was fit to

the linear elastic response presented here for balsa.   This linear

response was then used to predict the nonlinear creep response.   The

results are presented in Figure 5.14.   Note that there is good agreement

between the experimental and predicted results for the higher plateau

and the densification region.   However, the model predictions are high

for stress levels close to the yield point.   In this region of the

stress-strain relationship, the cell walls are most sensitive to col-

lapse.   The model assumes an abrupt yield point with progressive col-

lapse of the cells.   It does not rigorously model the elastic buckling

of the cell walls under a viscoelastic deformation history.   More study

will be needed to clarify the modeling and experimental response in the

immediate region of the yield point.

CONCLUSIONS

A nonlinear viscoelasticity model for cellular materials loaded in

compression has been proposed.   The approach utilizes an empirical

extension of the Boltzmann integral in conjunction with a nonlinear

strain function to separate the linear viscoelastic response of the cell

wall material from the geometric nonlinearities of the cellular col-lapse. Modeling results are presented for ramp loading, nonlinear stress relaxation, and nonlinear creep response. The model correctly predicts the qualitative response seen for cellular materials in these loading modes. When the linear viscoelastic response of the material is known, the model accurately predicts the nonlinear creep response in the later stages of cellular collapse and densification. However, the model predicts creep strains within the region of yielding that are greater than those observed experimentally. Given the lack of exper-imental data, more study is required to access the quantitative response of the model.

The time-temperature-moisture superposition technique was success-fully used to describe the linear viscoelastic response of yellow-poplar in the radial directions. The range of moisture content and temperature conditions studied were 3-16% and 39-99°C respectively.

LITERATURE CITED

Adamson, M.J. 1980. Thermal expansion and swelling of cured epoxy resin used in graphite/epoxy composite materials. J. Mater. Sci. 15:1736-1745.

Ferry, J.D. 1980. Viscoelastic Properties of Polymers. 3rd Edition. John Wiley and Sons, New York, NY. 641 pp.

Gibson, L.J. and M.F. Ashby. 1988. Cellular Solids: Structure and Properties. Pergammon Press, New York, NY. 357 pp.

_____. and _____. 1982. The mechanics of three-dimensional cellular materials. Proc. R. Soc. Lond. A382:43-59.

Halpin, J.C. 1969. Nonlinear rubberlike viscoelasticity - a molecular approach. J. Appl. Phys. 36(10):2975-2982.

Hilyard, N.C. (ed). 1982. Mechanics of Cellular Plastics. MacMillian Press, New York, NY.

Kelley, S.S., T.G. Rials, and W.G. Glasser. 1987. Relaxation behaviour of the amorphous components of wood. J. Mater. Sci. 22:617-624.

Knauss, W.G. and I.J. Emri. 1981. Nonlinear viscoelasticity based on free volume considerations. Computers and Structures. 13:123-128.

Kunesh, R.H. 1961. The inelastic behavior of wood: a new concept for improved panel forming processes. For. Prod. J. 9:395-406.

Maksimov, R.D., E.A. Sokholov, and V.P. Mochalov. 1975. Effect of temperature and moisture on the creep of polymeric materials. Polym. Mech. 11(3):334-339.

_____., V.P. Mochalov, and E.A. Sokholov. 1976. Influence of temperature and humidity on the creep of polymeric materials. Polym. Mech. 12(6):859-864.

Meinecke, E.A. and R.C. Clark. 1973. Mechanical Properties of Polymeric Foams. Technomic, Westport, CT.

Rosa, M.E. and M.A. Fortes. 1988. Stress relaxation and creep of cork. J. Mater. Sci. 23:35-42.

Rusch, K.C. 1969. Load-compression behavior of flexible foams. J. Appl. Polym. Sci. 13:2297-2311.

Simpson, W.T. 1971. Equilibrium moisture content prediction for wood. For. Prod. J. 21(5):48-49.

Williams, M.L., R.F. Landel, and J.D. Ferry. 1955. The temperature

dependence of relaxation mechanisms in amorphous polymers and other glass-forming liquids. J. Amer. Chem. Soc. 77:3701-3706.

Wolcott, M.P., B. Kasal, F.A. Kamke, and D.A. Dillard. 1989. Modeling wood as a polymeric foam: an application to wood-based composite manufacture. Proc. Joint ASME/ASCE Mechanics Conference, July, LaJolla, CA.

Youngs, R.L. 1957. Mechanical properties of red oak related to drying. For. Prod. J. 7(10):315-324.

Table 5.1: Environmental conditions used in stress relaxation tests to construct relaxation modulus master curves.

Moisture Content (%)		Temperature Range (deg C)	
Nominal	Actual	Low	High
3	3.1	57	99
6	5.6	39	99
10	9.3	39	99
12	12.0	39	90
16	16.6	39	75

Table 5.2: Parameters for the regression equations describing the temperature shift factor (a(T)) as a function of temperature (T deg C) for different moisture contents. The equations are of the form: log a(T) = Yo - bT.

Moisture Content (%)	Temperature (C)	Yo	b
3	57-72	6.125	0.1024
3	72-99	1.647	0.0413
6	39-99	2.647	0.0432
10	39-99	5.887	0.0933
12	39-90	6.547	0.1128
16	39-75	5.770	0.0937

Table 5.3: Parameters for the Maxwell elements fit to the relaxation modulus master curve shown in Figure 5.2.

Element	E (Pa)	λ (sec)
Maxwell #1	6.287E+7	4.742E+1
2	8.530E+7	4.742E+2
3	1.054E+8	4.742E+3
4	1.280E+8	4.742E+4
5	1.141E+8	4.742E+5
6	5.165E+7	4.742E+6
7	8.729E+7	4.742E+7
8	1.244E+8	4.742E+8
9	1.070E+8	4.742E+9
10	1.150E+8	4.742E+10
11	1.052E+8	4.742E+11
12	1.189E+8	4.742E+12
13	3.160E+7	4.742E+13
14	2.028E+8	4.742E+14

Table 5.4: Parameters for the Kelvin elements fit to the creep com-
pliance master curve shown in Figure 5.3.

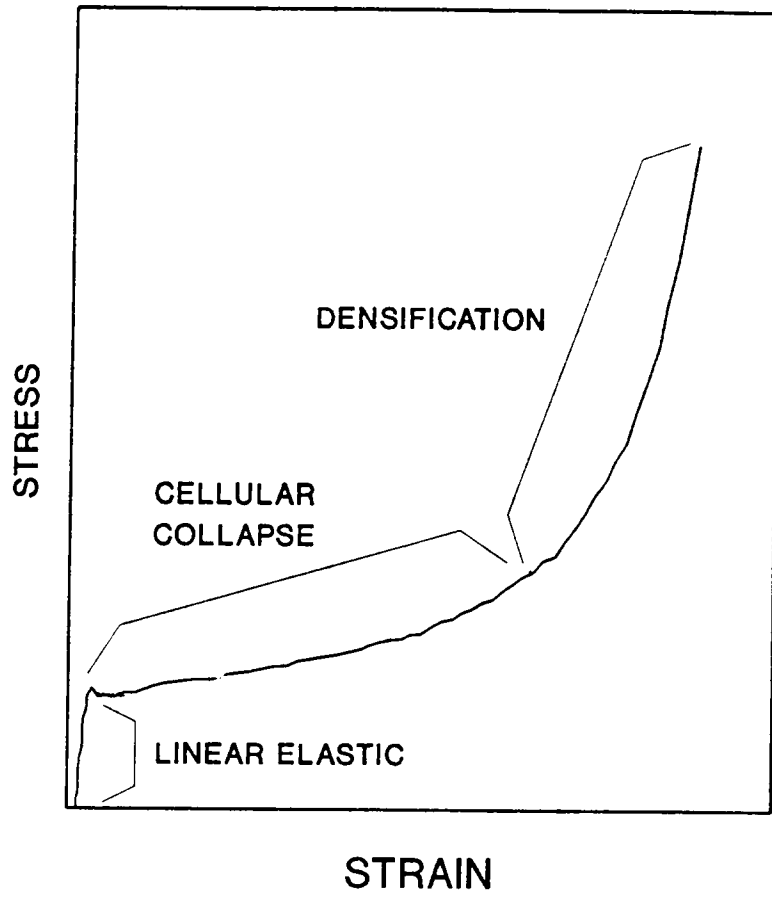| Element	E (Pa)	λ (sec)
Free Spring	1.440E+9	--------
Kelvin #1	3.245E+10	4.742E+1
2	2.194E+10	4.742E+2
3	1.416E+10	4.742E+3
4	1.169E+10	4.742E+4
5	1.115E+10	4.742E+5
6	1.227E+10	4.742E+6
7	7.143E+9	4.742E+7
8	5.506E+9	4.742E+8
9	4.177E+9	4.742E+9
10	2.523E+9	4.742E+10
11	2.069E+9	4.742E+11
12	8.221E+8	4.742E+12
13	4.909E+8	4.742E+13

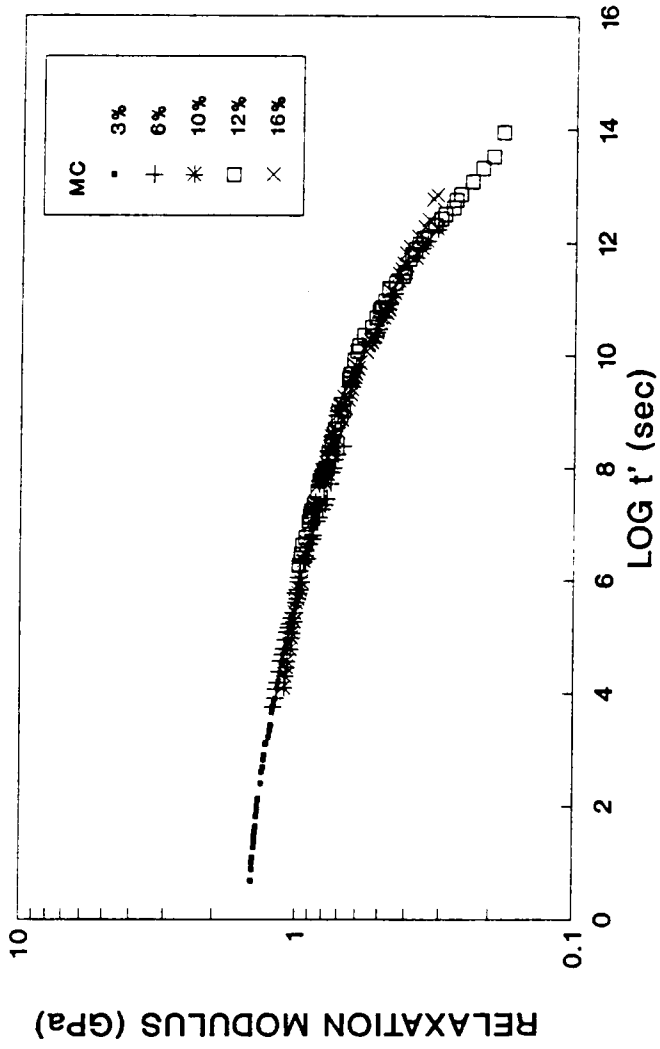Figure 5.1: Typical stress-strain diagram for a cellular material in compression.

Figure 5.2: Relaxation modulus (E(t')) plotted against reduced time (t'=t/a(T)a(M)). The master curve is shifted to a reference temperature of 60°C and a moisture content of 3%.

Figure 5.3: Creep compliance (D(t')) plotted against reduced time (t'=t/a(T)a(M)). The master curve is shifted to a reference temperature of 60°C and moisture content of 3%.

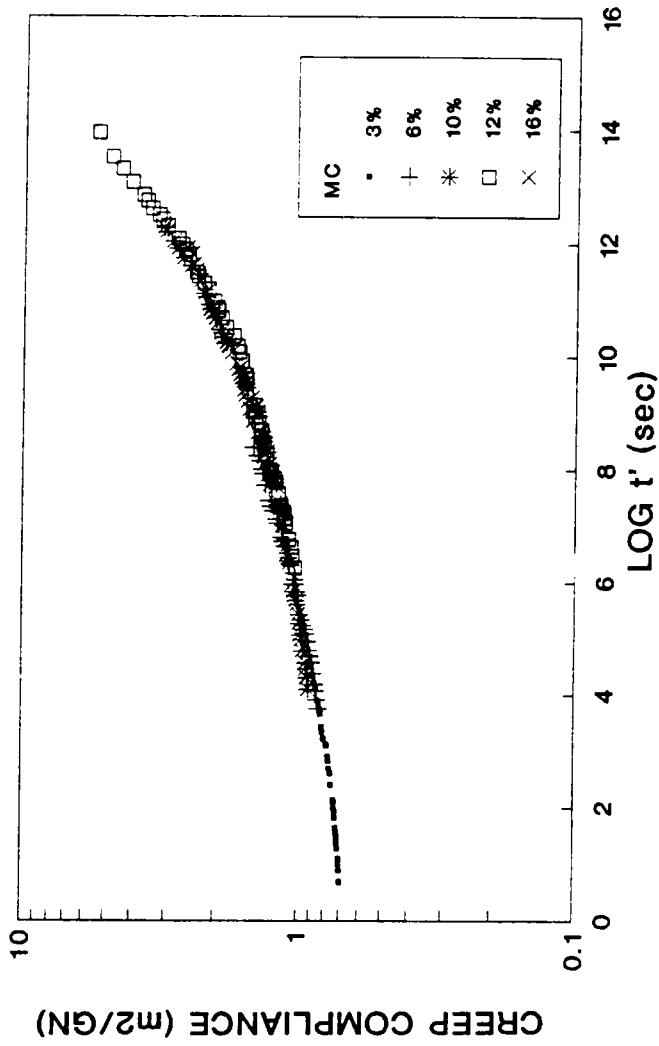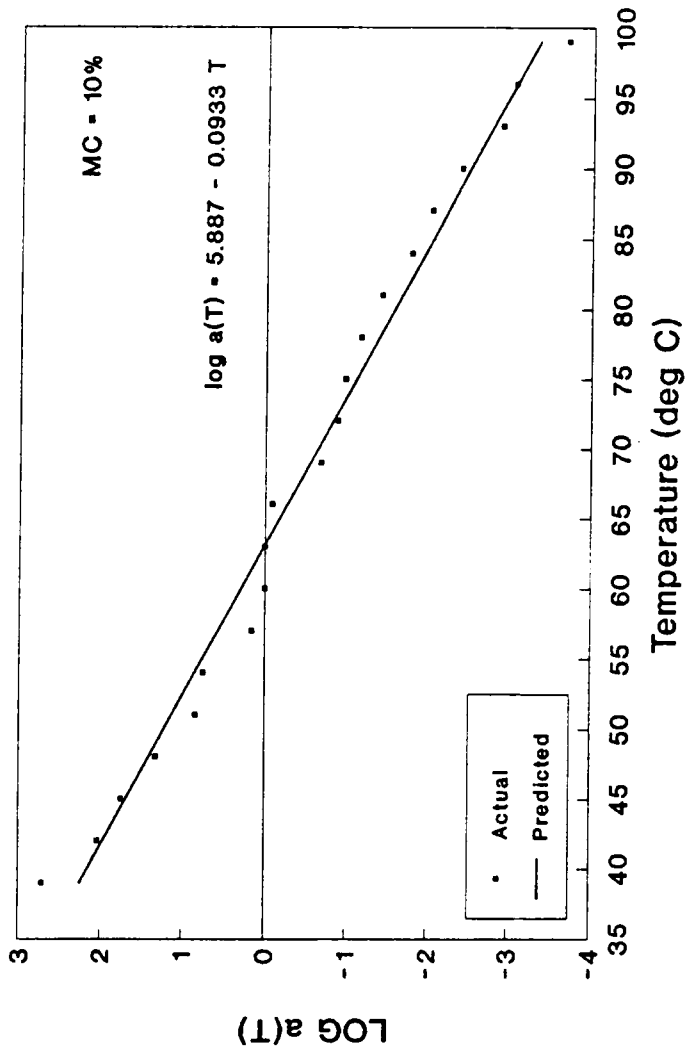Figure 5.4: Temperture shift factor (a(T)) for 10% moisture content.
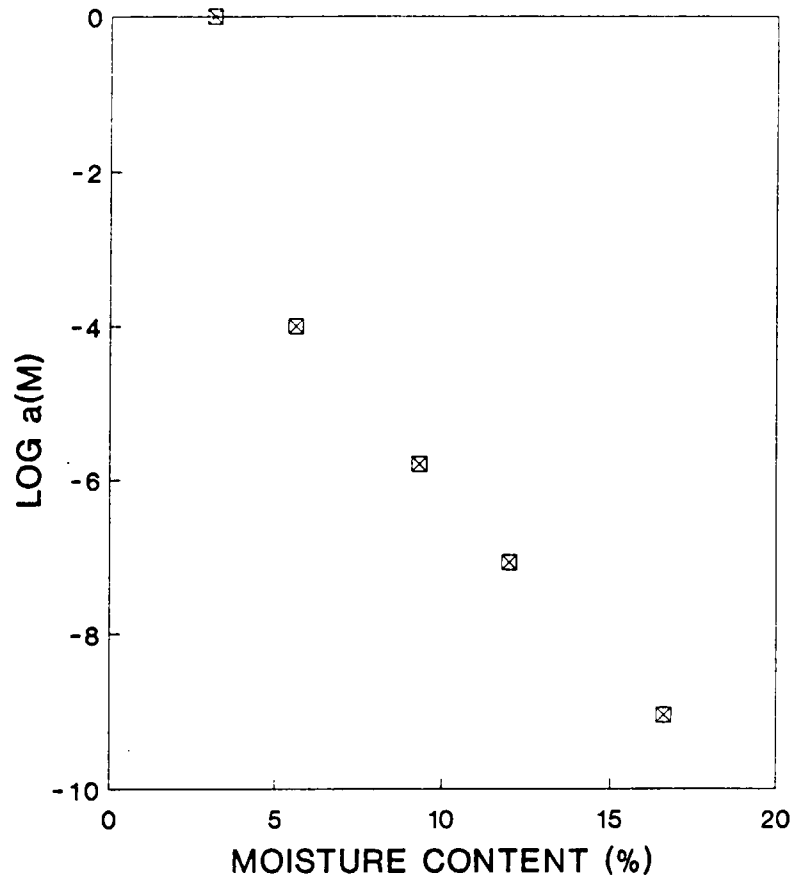
Figure 5.5: Moisture shift factor (a(M)).
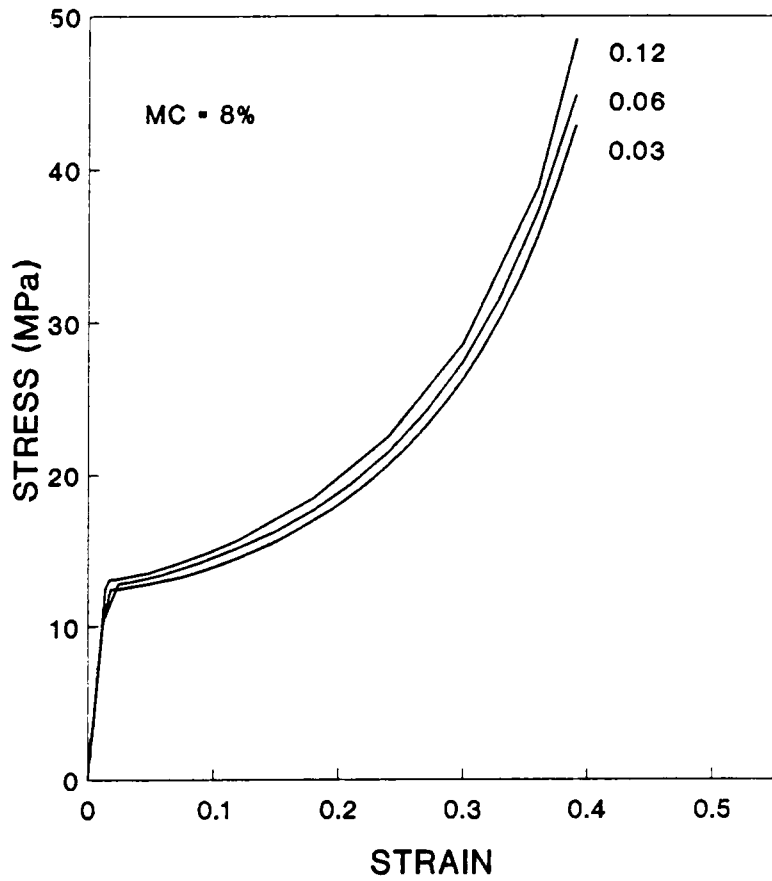
Figure 5.6: Modeling results showing the effect of strain rate on the predicted stress-strain diagram for a moisture content of 8%.
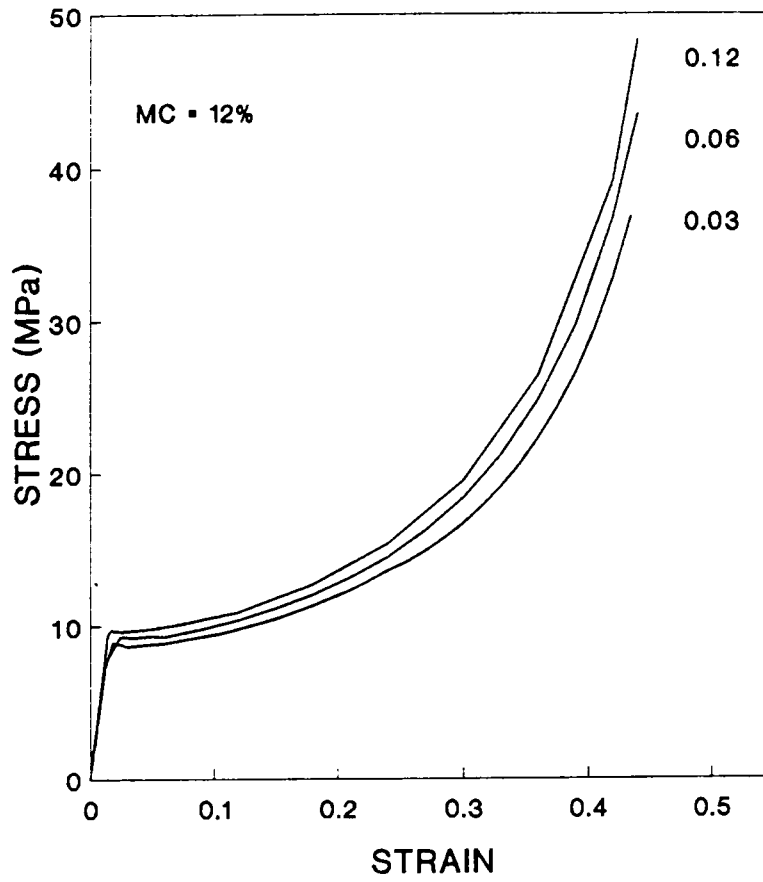
Figure 5.7: Modeling results showing the effect of strain rate on the predicted stress-strain diagram for a moisture content of 12%.
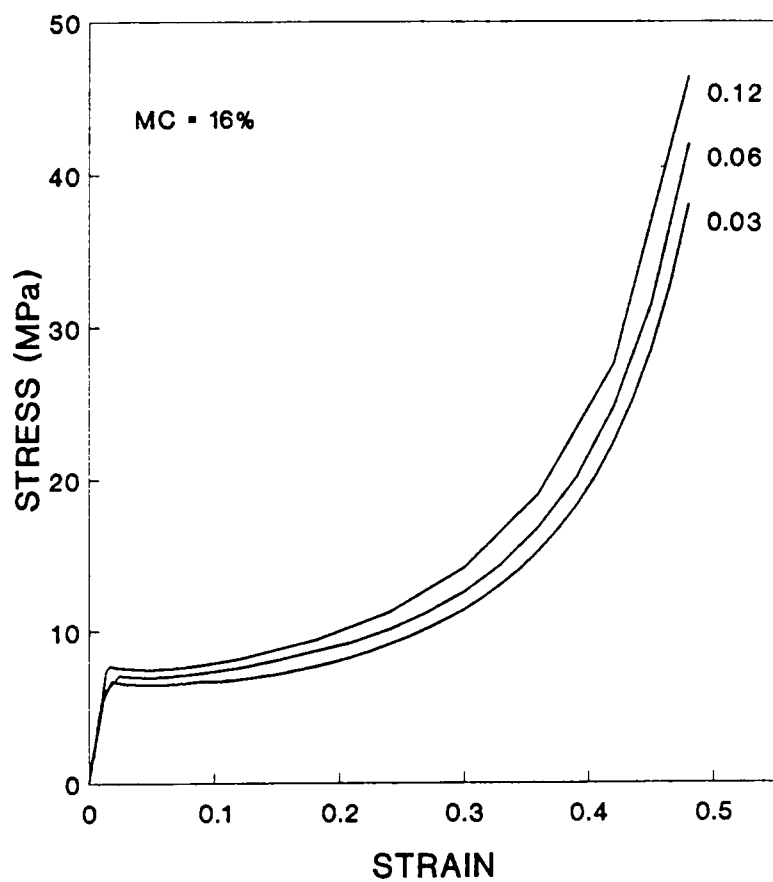
Figure 5.8: Modeling results showing the effect of strain rate on the predicted stress-strain diagram for a moisture content of 16%.
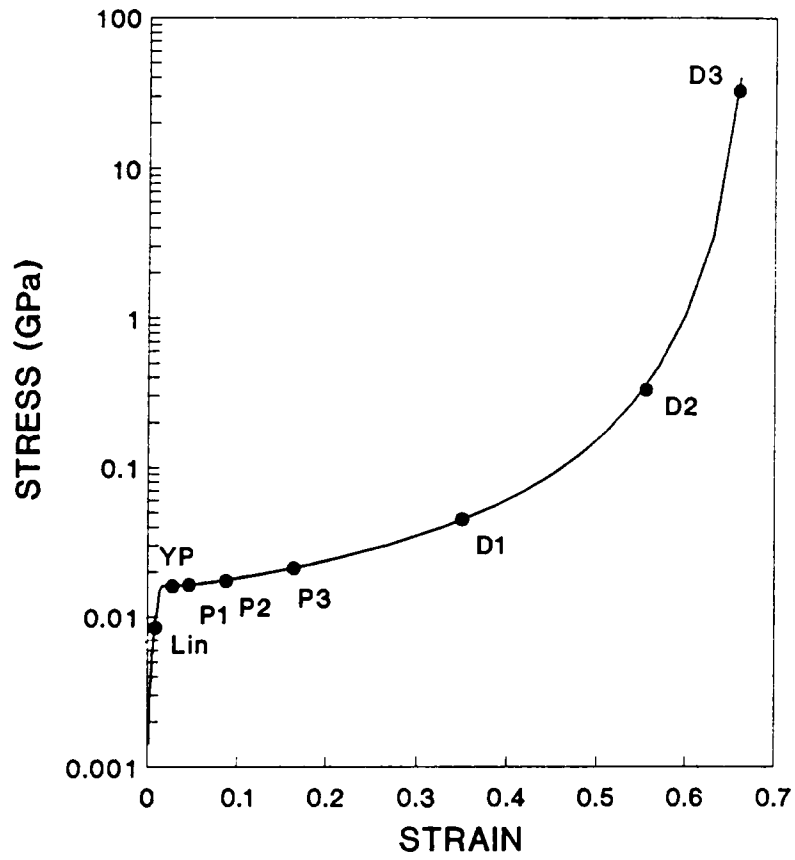
Figure 5.9: Levels of initial strain (ϵ_o) used in modeling the non-linear stress relaxation behavior.
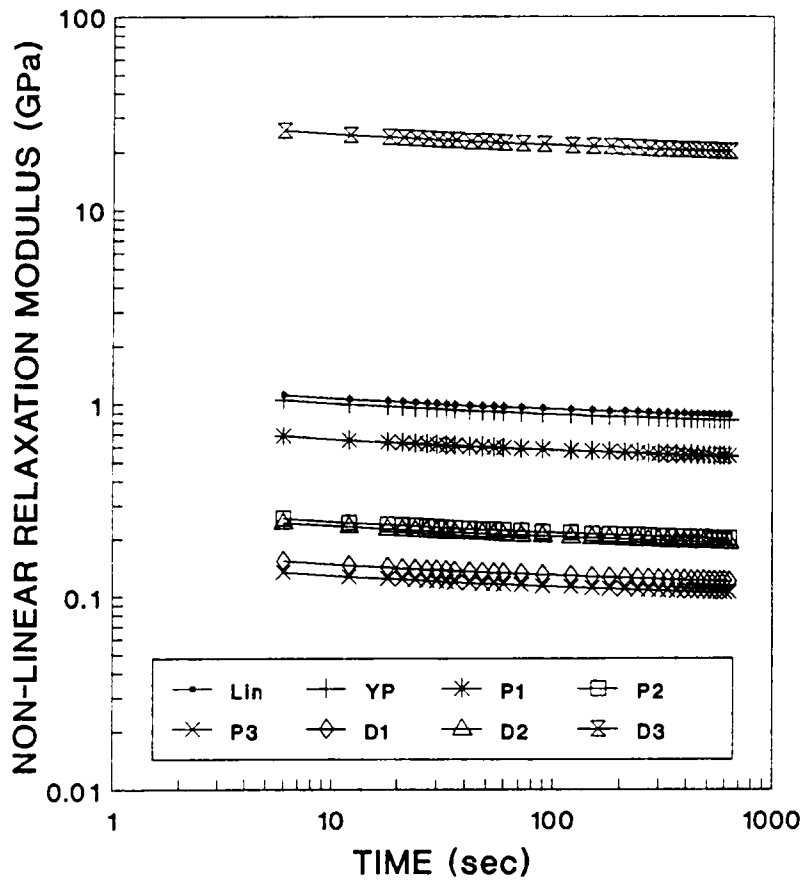
Figure 5.10: Modeling results of the non-linear stress relaxation modulus using the initial strain levels (ϵ_o) denoted in Figure 5.9.
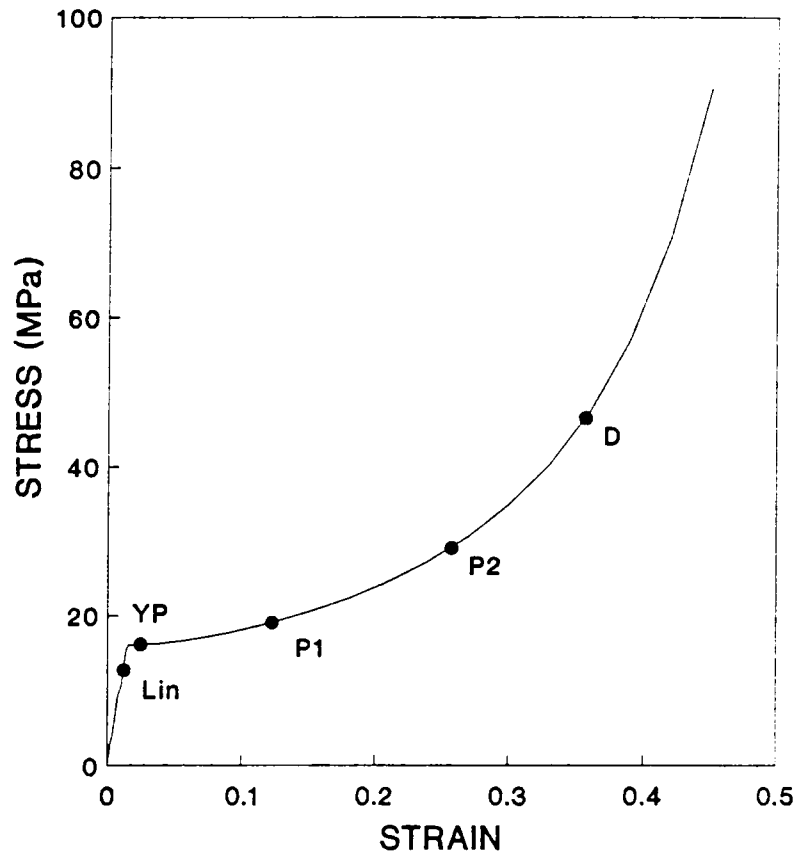
Figure 5.11: Levels of initial stress (σ_o) used in both the modeling and experimental determination of the non-linear creep behavior.
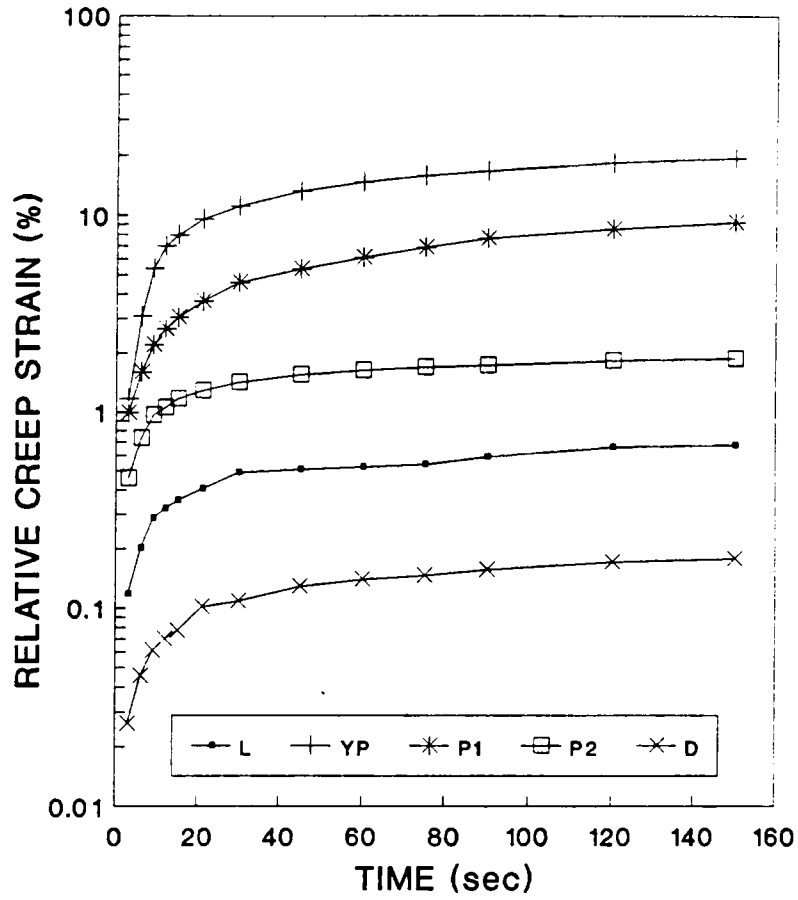
Figure 5.12: Experimental results of the non-linear creep behavior, expressed as relative creep $((\epsilon(t)-\epsilon_o)/\epsilon_o)$, of balsa in compression. The levels of initial stress (σ_o) used are displayed in Figure 5.11.
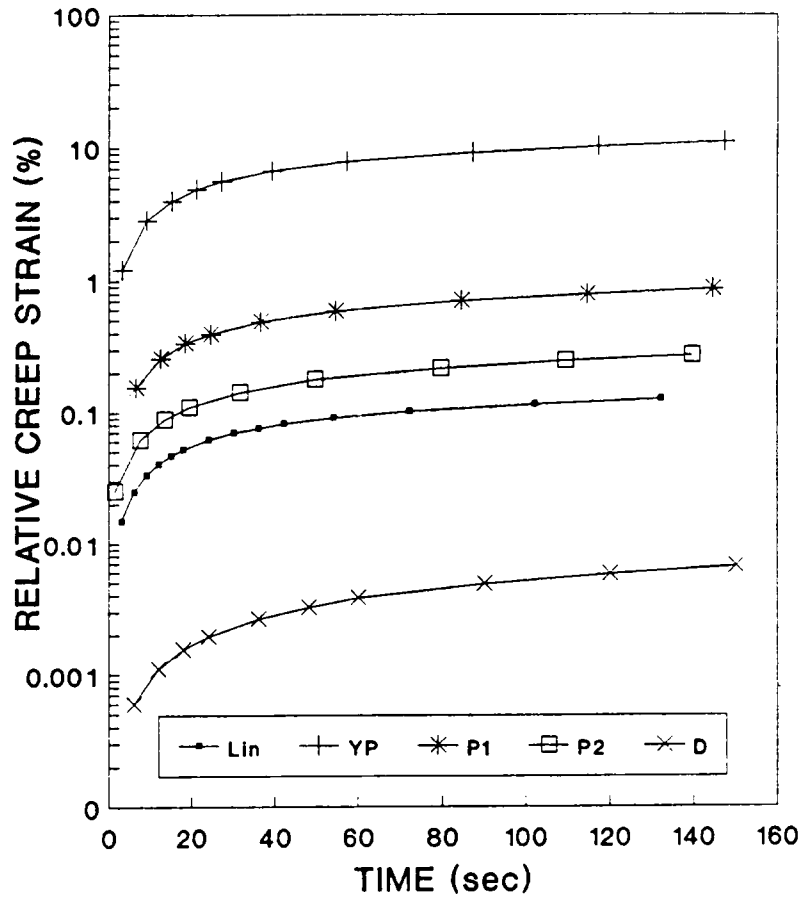
Figure 5.13: Predicted non-linear creep behavior, expressed as relative creep $((\epsilon(t) - \epsilon_o)/\epsilon_o)$, of balsa in compression. The linear creep behavior used in modeling was the creep compliance data determined from yellow-poplar and shown in Figure 5.3. The levels of initial stress (σ_o) used are displayed in Figure 5.11.
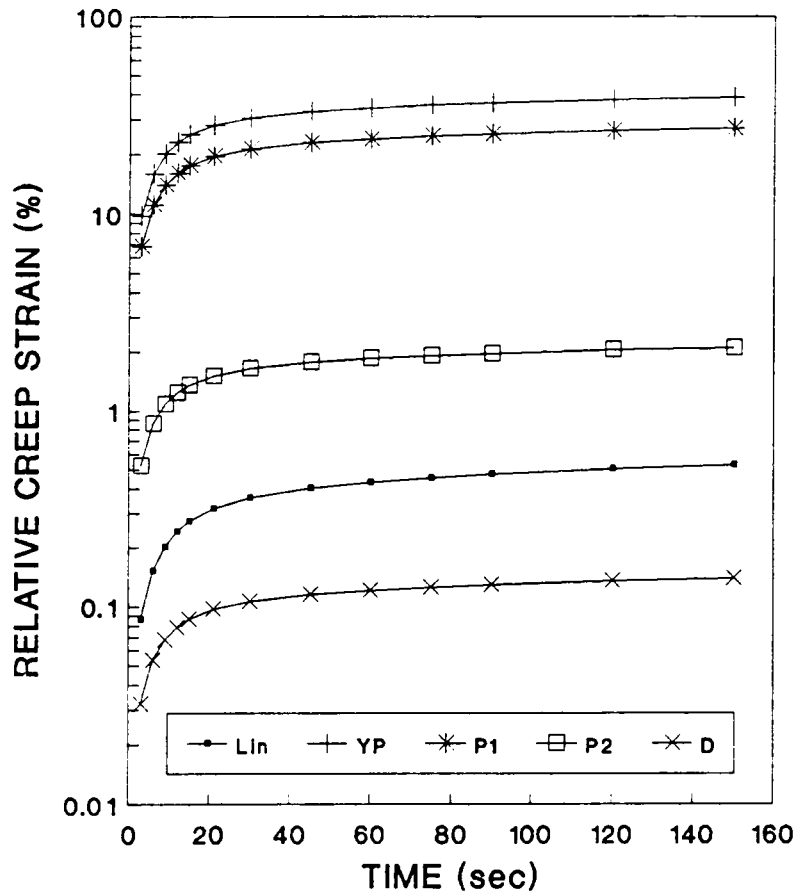
Figure 5.14: Predicted non-linear creep behavior, expressed as relative creep $((\epsilon(t)-\epsilon_o)/\epsilon_o)$, of balsa in compression. The linear creep behavior used in modeling was determined from the experimental results of balsa shown in Figure 5.12. The levels of initial stress (σ_o) used are displayed in Figure 5.11.

APPENDIX A:

TEMPERATURE SHIFT FACTORS
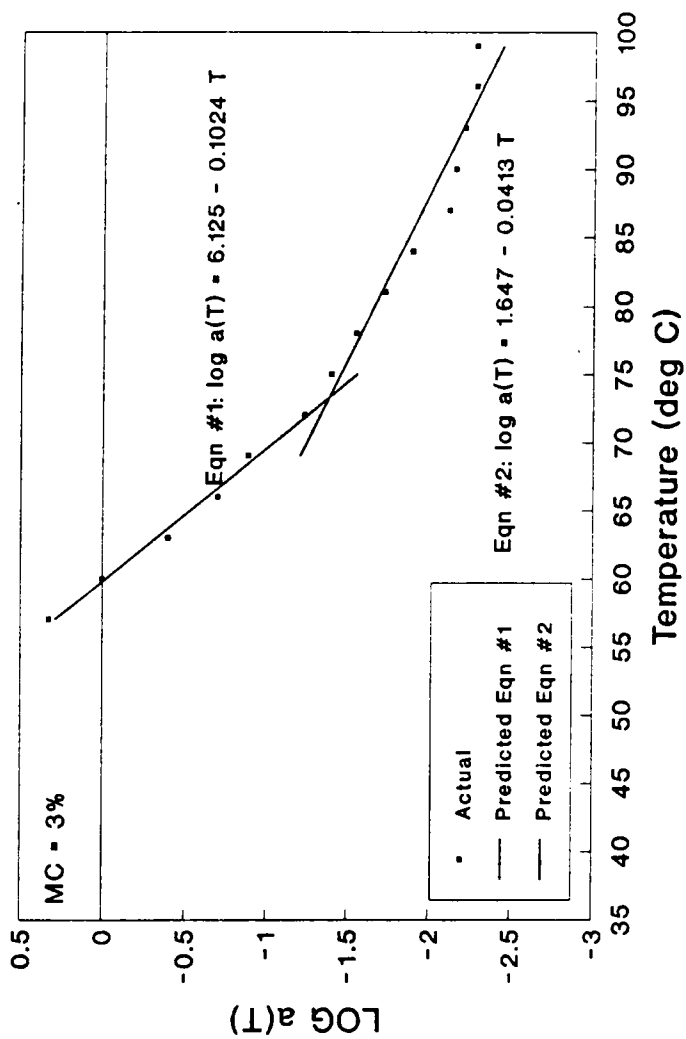
Figure A.1: Temperature shift factors (a(T)) for 3% moisture content plotted with regression equations fit to the data.
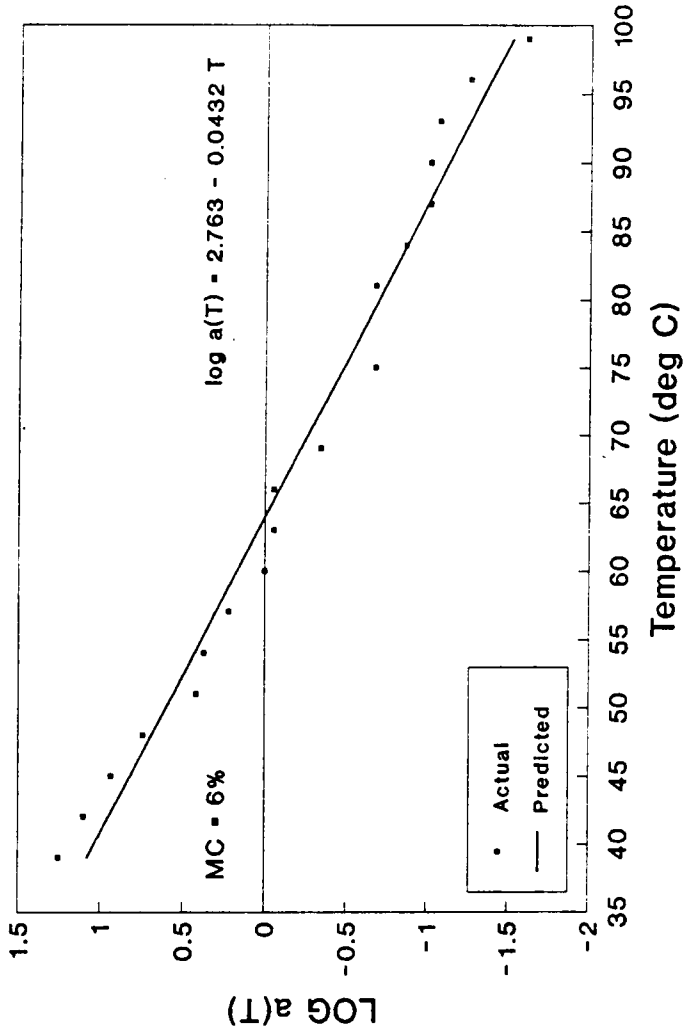
Figure A.2: Temperature shift factors (a(T)) for 6% moisture content plotted with regression equation fit to the data.
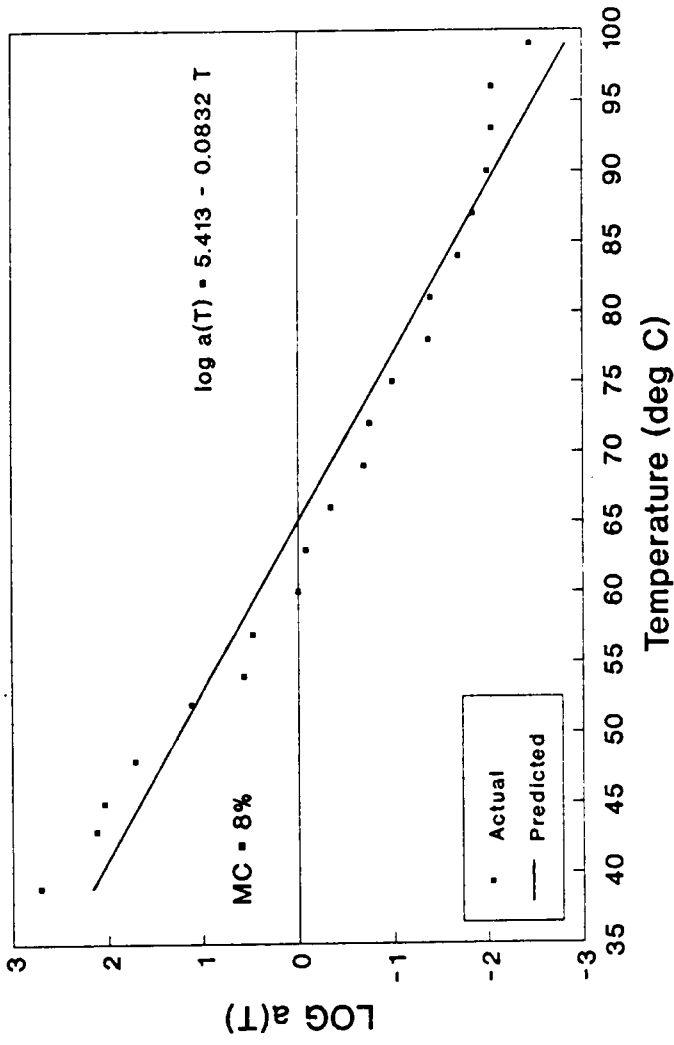
Figure A.3: Temperature shift factors (a(T)) for 8% moisture content
plotted with regression equation fit to the data.
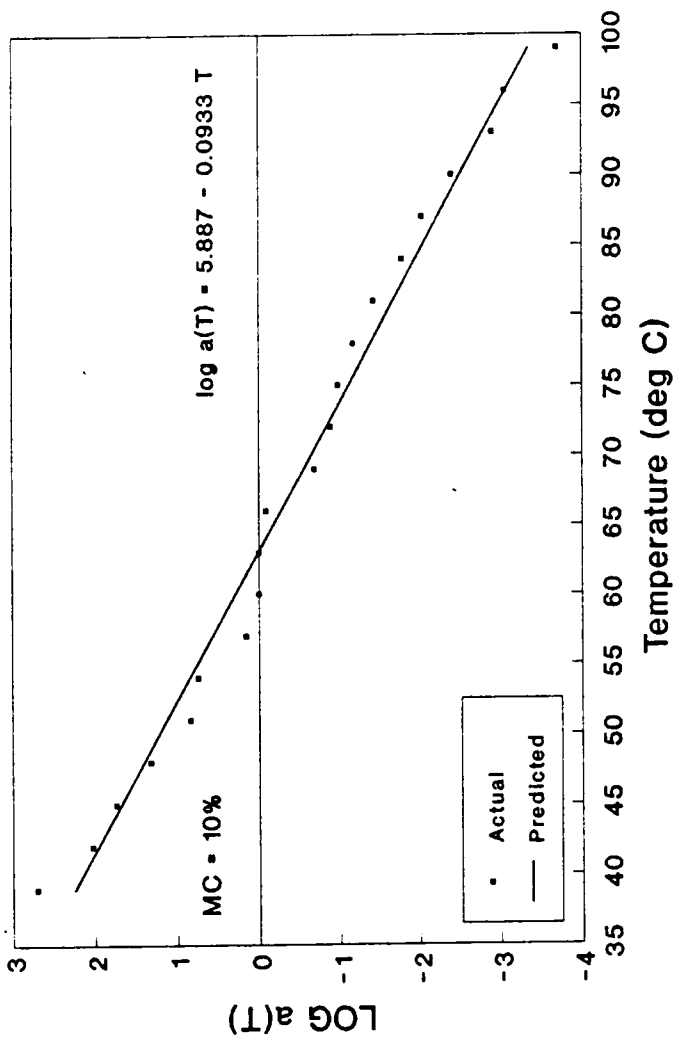
Figure A.4: Temperature shift factors (a(T)) for 10% moisture content plotted with regression equation fit to the data.
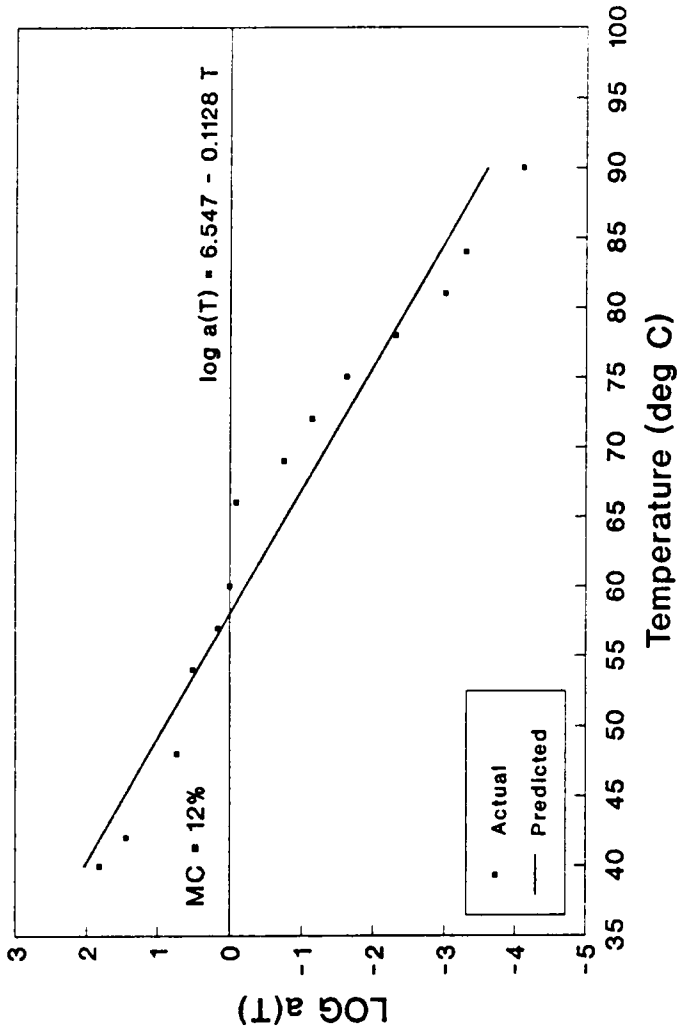
Figure A.5: Temperature shift factors (a(T)) for 12% moisture content plotted with regression equation fit to the data.
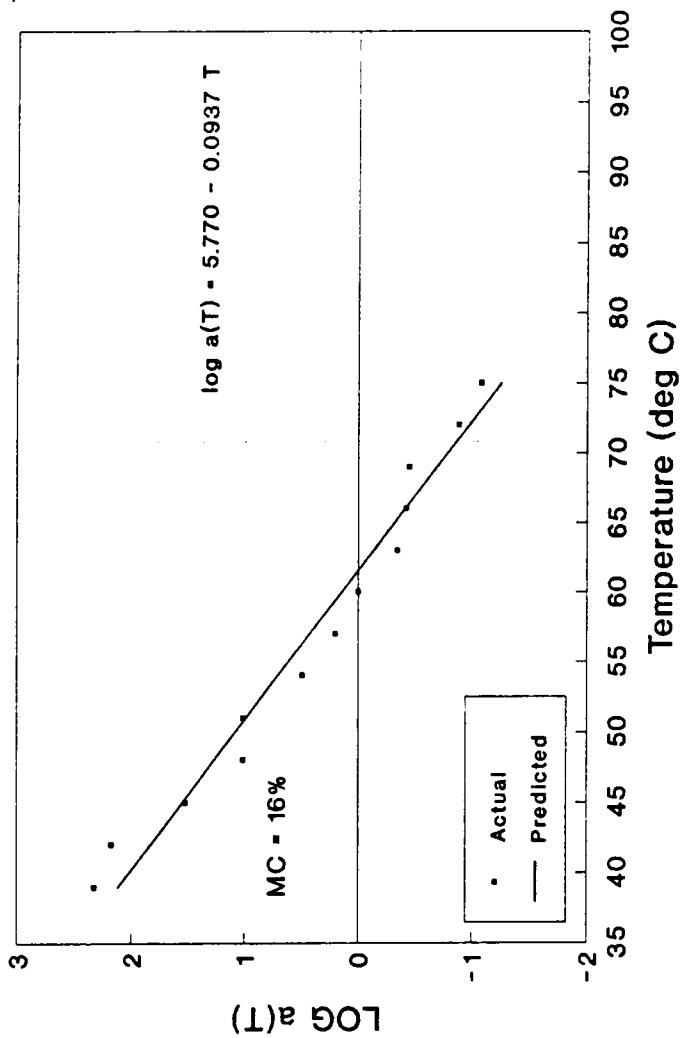
Figure A.6: Temperature shift factors (a(T)) for 16% moisture content plotted with regression equation fit to the data.

APPENDIX B:

TEMPERATURE MASTER CURVES
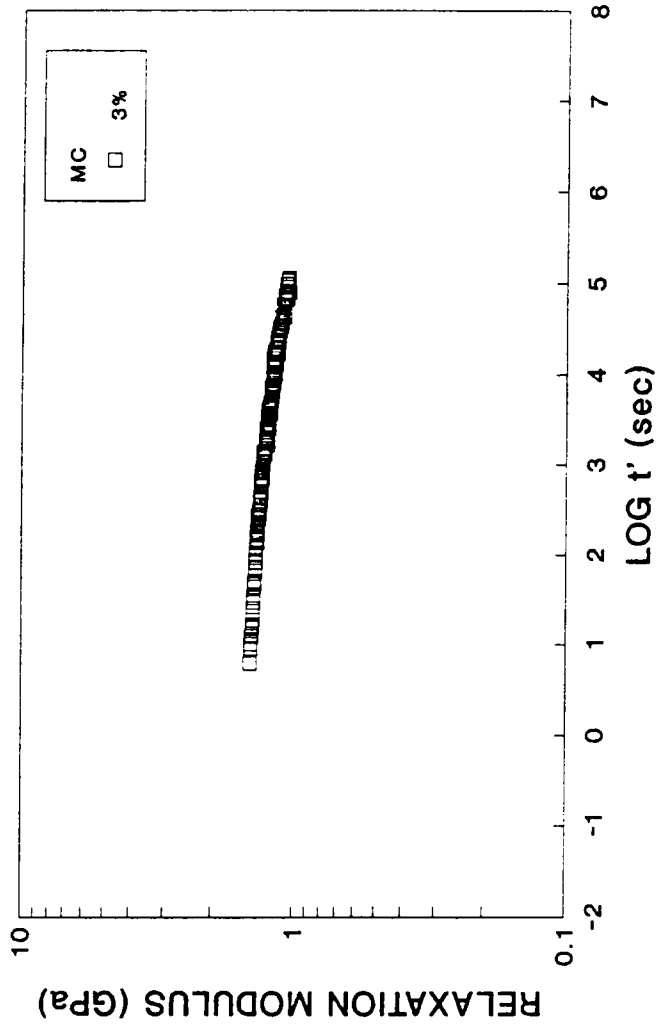
Figure B.1: Master curve of relaxation modulus (E(t)) shifted to a reference temperature of 60°C for a moisture content of 3%.
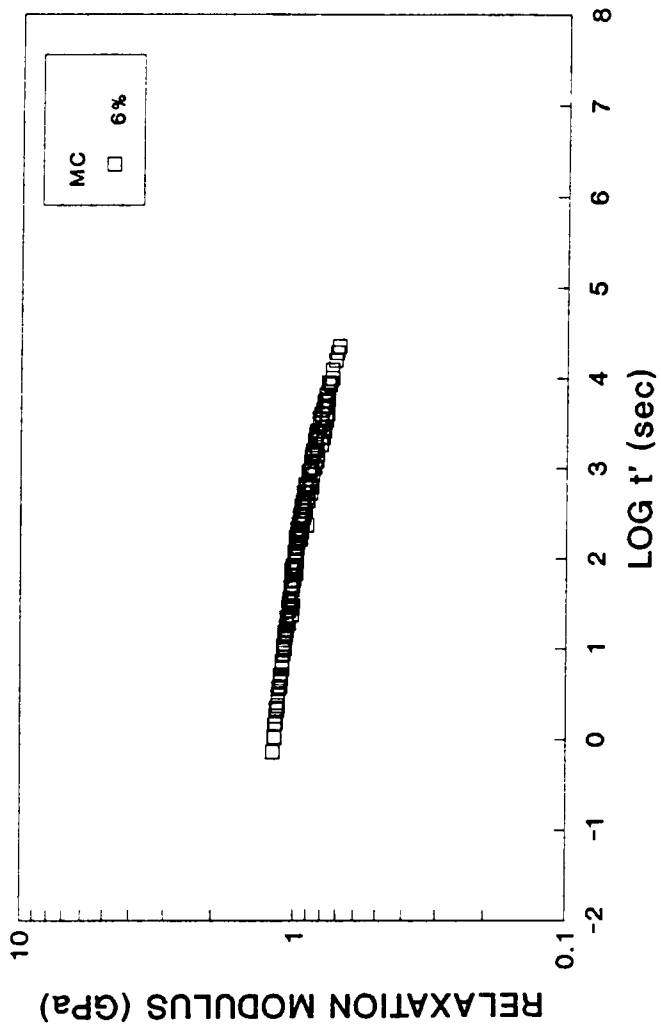
Figure B.2: Master curve of relaxation modulus (E(t)) shifted to a reference temperature of 60°C for a moisture content of 6%.
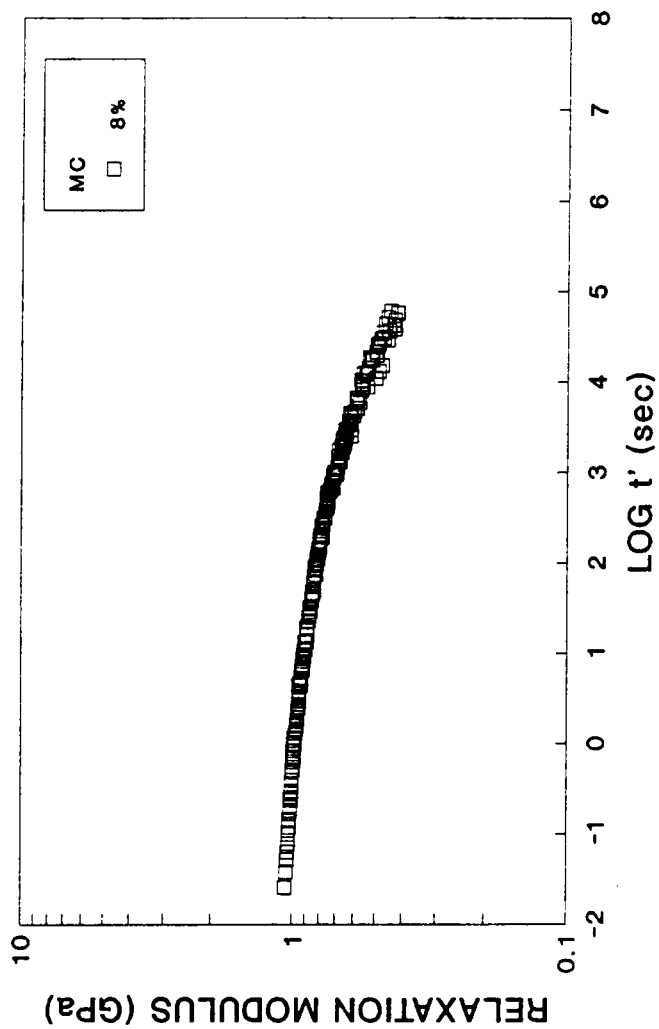
Figure B.3: Master curve of relaxation modulus (E(t)) shifted to a reference temperature of 60°C for a moisture content of 8%.
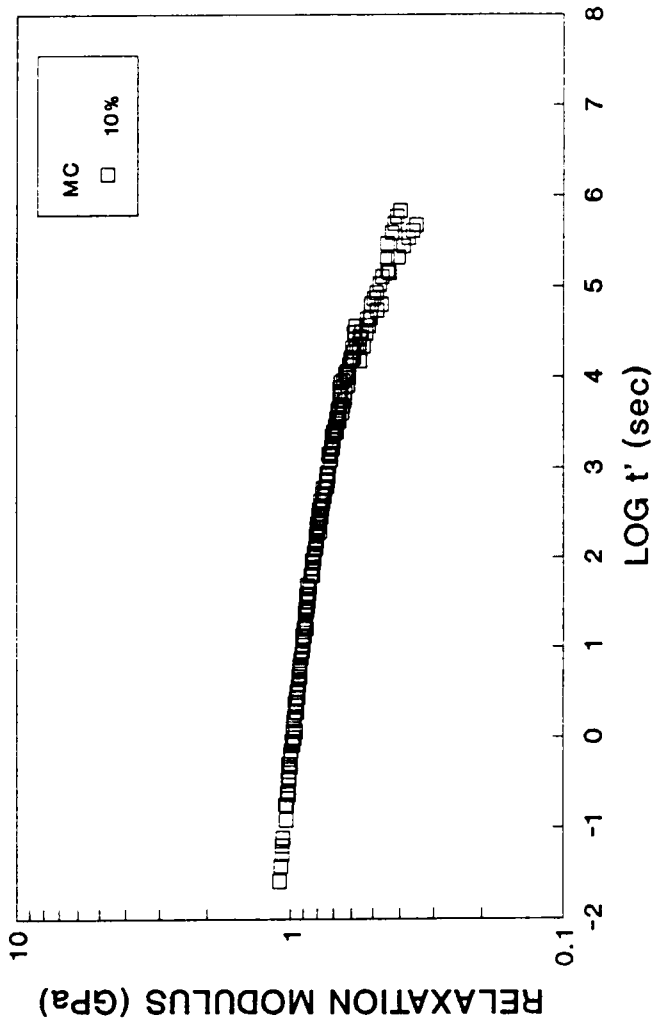
Figure B.4: Master curve of relaxation modulus (E(t)) shifted to a reference temperature of 60°C for a moisture content of 10%.
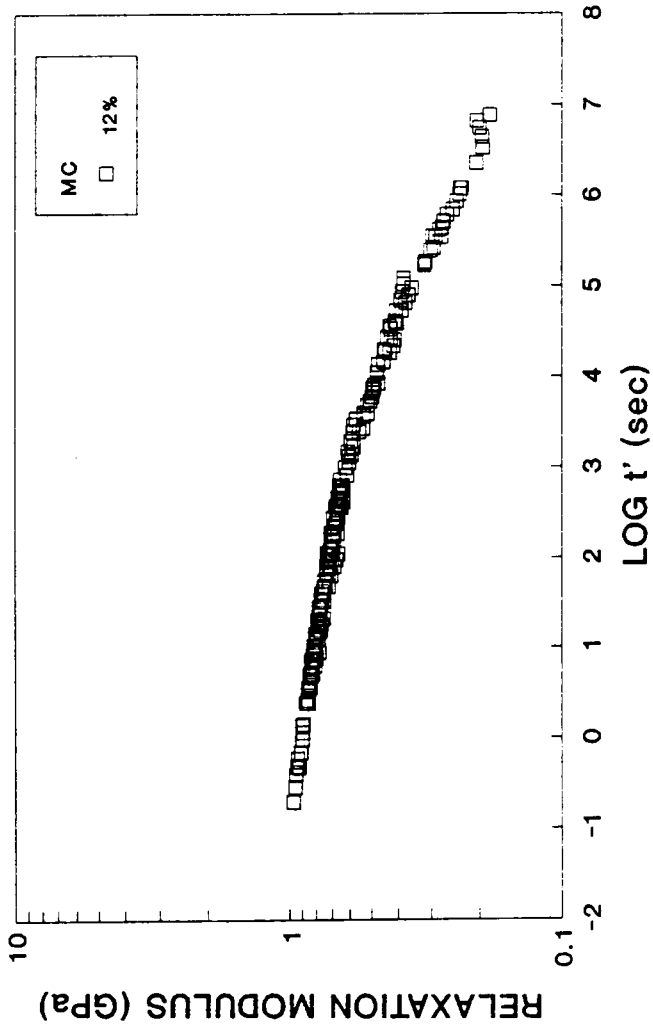
Figure B.5: Master curve of relaxation modulus (E(t)) shifted to a reference temperature of 60°C for a moisture content of 12%.

159
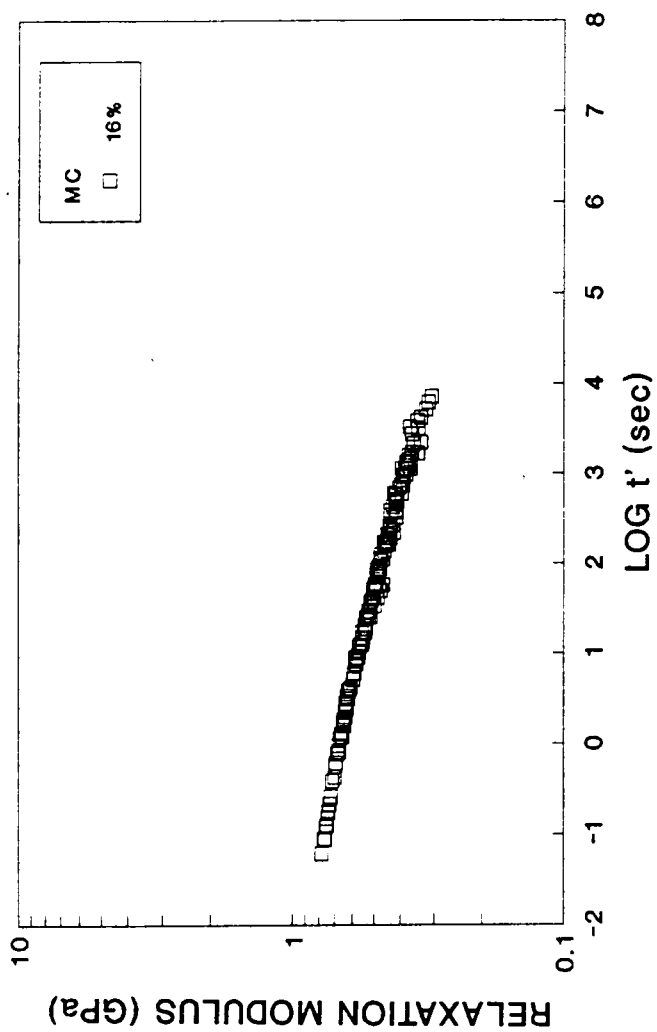
Figure B.6: Master curve of relaxation modulus (E(t)) shifted to a reference temperature of 60°C for a moisture content of 16%.

APPENDIX C:

PREDICTED TEMPERATURE AND MOISTURE CONTENT
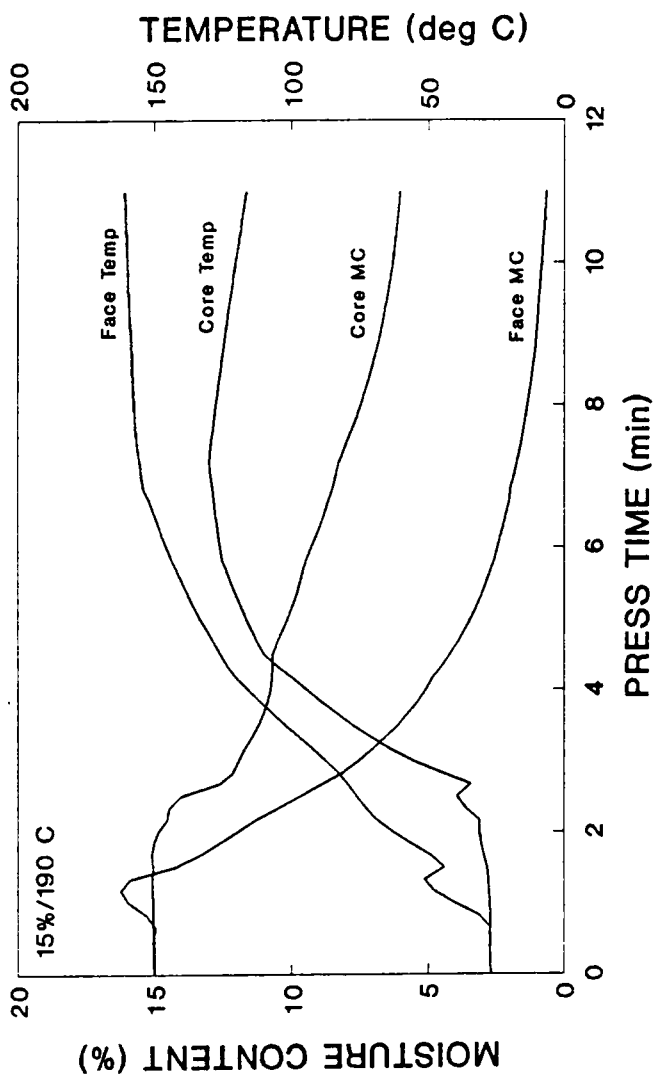
Figure C.1: Predicted average flake temperature and moisture content for panels produced with an initial mat moisture content of 15% and platen temperature of 190°C. The predictions were made with the method described in Chapter 2.
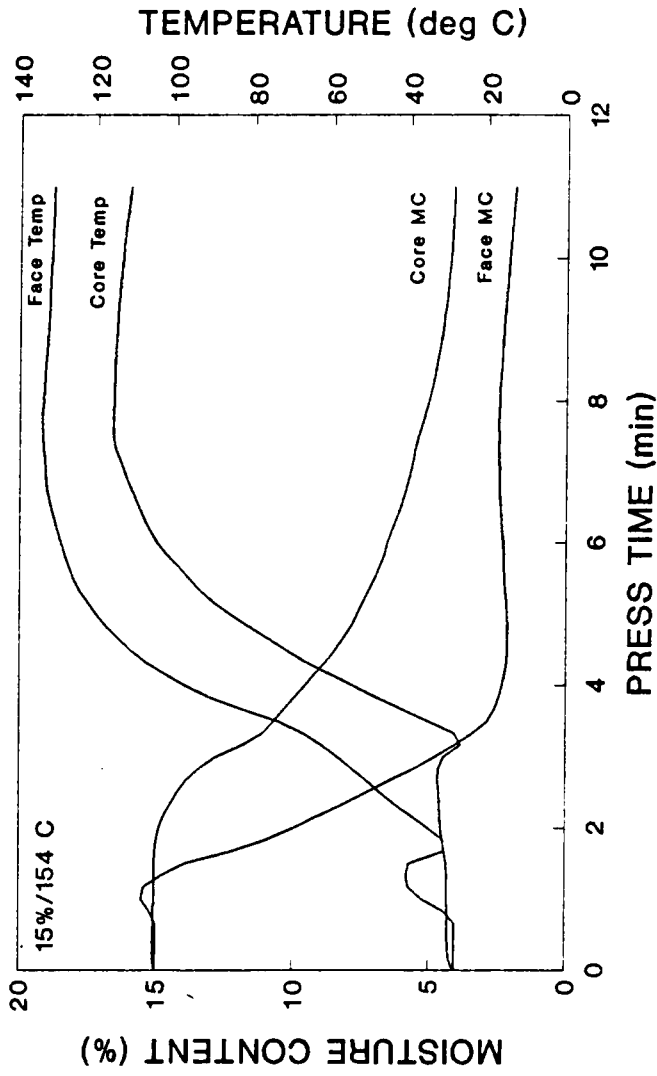
Figure C.2: Predicted average flake temperature and moisture content for panels produced with an initial mat moisture content of 15% and platen temperature of 154°C. The predictions were made with the method described in Chapter 2.
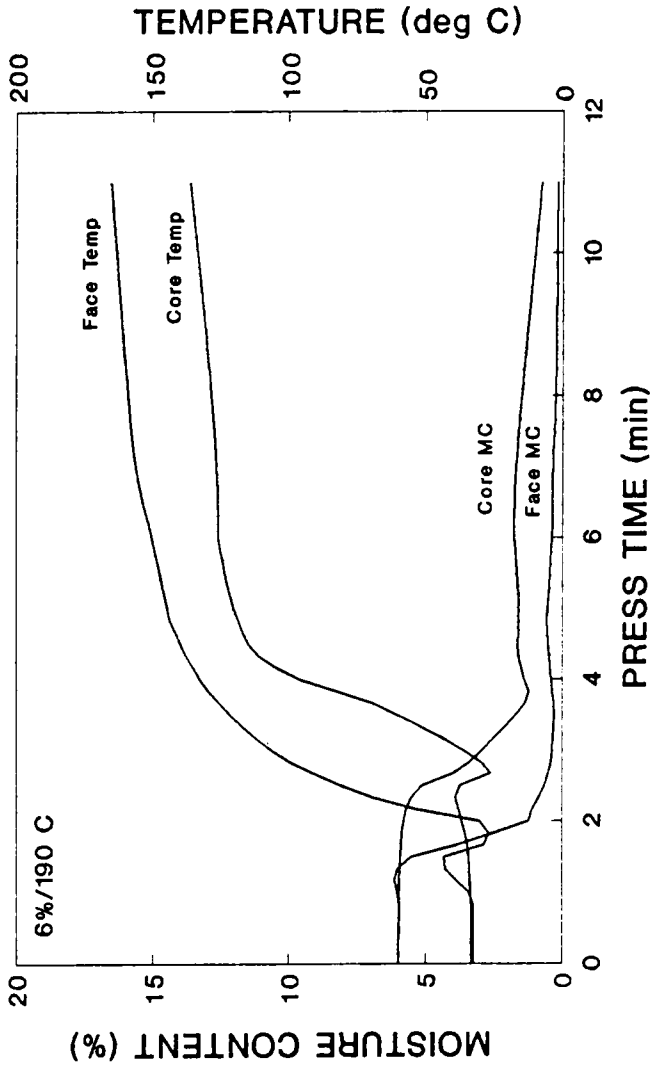
Figure C.3: Predicted average flake temperature and moisture content for panels produced with an initial mat moisture content of 6% and platen temperature of 190°C. The predictions were made with the method described in Chapter 2.

164
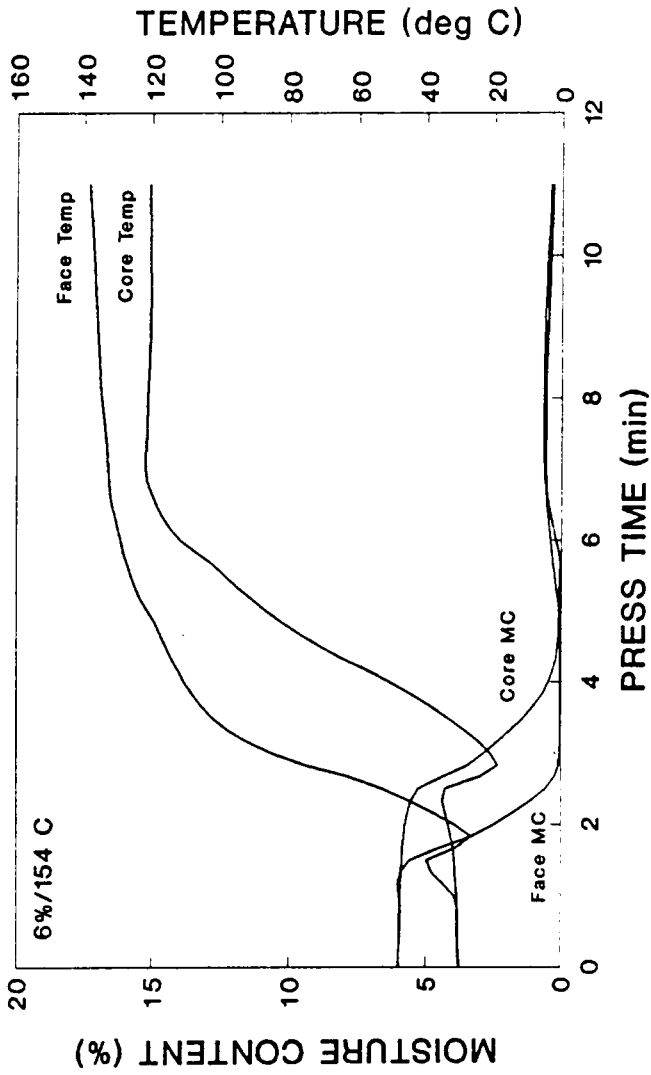
Figure C.4: Predicted average flake temperature and moisture content for panels produced with an initial mat moisture content of 6% and platen temperature of 154°C. The predictions were made with the method described in Chapter 2.

APPENDIX D:

FLAKE DEFORMATION DURING PRESS CLOSING TIME

INTRODUCTION

In Chapter 3 it was concluded that a significant portion of the density gradient must form after the press has closed. This conclusion was reached largely because little difference was noted between the face and core response when studying the relation of flake temperature to the glass transition temperature (T_g) of lignin. The non-linear viscoelasticity model presented in Chapter 5 does not incorporate recovery. However, the deformation of a flake can be modeled during the press closing time because the pressure is continually increasing with time.

METHODS

The deformation of a flake during the press closing time of the panel types presented in Chapter 2 and 3 were modeled. The environmental history was taken from the predicted flake temperature and moisture content calculated in Chapter 2 and presented in Appendix C. The stress history for each panel type was assumed to be equal to the press platen pressure on the mat. In reality, the stress in an individual flake is likely to be higher than the stress on the mat because voids exist, thereby, reducing the actual area over which the force is distributed. The actual stress and environmental histories used for modeling are given in Table C.1 to C.4. The parameters used in the non-linear strain function are as follows: $\rho=0.36$, $\mu=0.05$, $C_3=0.015$, and $C_2=0.95$.

RESULTS AND DISCUSSION

The results from modeling of the flake deformation during the press closing time of the four panel types discussed in Chapter 2 and 3

are presented in Figure C.1 and C.2. Little difference existed in the final strain between the face and core regions of the 6% moisture content panel types. However, the final strain in the face region of the 190°C/15% and 154°C/15% panel types were 34% and 11% higher than the core respectively. As can be seen in Tables C.1 and C.2, the difference in final strain for these panel types can be mainly attributed to the temperature difference. The temperature difference is greater for panels with higher initial mat moisture content resulting from the increased convective heat transfer with more available water. This analysis would indicate that for at least some panel types, the density gradient must continue to form after the press is closed.

The final strains in the face and core regions of the different panel types are analogous to the density gradients presented in Figure 3.6. When the relationship of densities and strains in the different panel types is reasonable with the exception of the 154°C/15% panel type. From the final strain results, the density gradient of this panel should be between that of the 190°C/15% and 6% moisture content panel types. This discrepancy may result from the failure to consider the recovery process. If the analysis presented here is accurate, the recovery response of the flakes after the press begins to open is critical to an accurate modeling of the density gradient formation.

Note in Tables C.3 and C.4 that the platen pressure at the end of the press closing time for the 6% moisture content panel types remains invariant for a period of time. This results from an exceeding of the maximum pressure that the press is capable of producing. Therefore, the pressure remains constant until the target thickness is reached.

Despite the different length of time required for the two panel types to reach the target thickness, the final strain in face and core are roughly equal for the panel types. The final strains are not equal for all panel types because the target platen position is overshot for both 15% moisture content panel types. The magnitude of the overshoot is greater for the 190°C/15% panel type than for the 154°C/15% panel type. This observation is consistent with the modeling results presented here.

CONCLUSIONS

The deformation of an individual flake during the press closing time has been modeled for four panel types using the non-linear vis-coelasticity model presented in Chapter 5. The environmental history used in the analysis is taken from the predicted flake moisture content and temperature presented in Appendix C and determined with the proce-dure presented in Chapter 2. From this analysis, a bulk of the density gradient must form after the press is closed for some panel types. The recovery of flake deformation also plays an important role in den-sity gradient formation as indicated from discrepancies in modeling and experimental results when recovery is not considered.

Table D.1: Environmental and stress history used for modeling the deformation of an individual flake during the press closing time of the 190°C/15% panel type. (MC = moisture content, Temp = temperature)

Time (min)	Stress (MPa)	FACE		CORE	
		MC (%)	Temp (C)	MC (%)	Temp (C)
0.00	0.00	15.00	26.81	15.00	26.78
0.17	0.24	15.01	27.12	15.03	27.03
0.33	0.26	15.01	27.17	15.03	27.04
0.50	0.26	15.00	27.21	15.04	27.04
0.67	0.30	14.99	27.23	15.04	27.04
0.83	0.72	15.31	31.28	15.05	27.13
1.00	3.32	15.93	40.25	15.06	27.34
1.17	7.95	16.23	47.73	15.07	27.58
1.33	8.02	15.89	51.23	15.07	27.84

Table D.2:   Environmental and stress history used for modeling the deformation of an individual flake during the press closing time of the 154°C/15% panel type. (MC = moisture content, Temp = temperature)

Time (min)	Stress (MPa)	FACE MC (%)	FACE Temp (C)	CORE MC (%)	CORE Temp (C)
0.00	0.00	15.00	28.25	15.00	28.52
0.17	0.21	14.99	28.26	15.09	29.78
0.33	0.24	14.99	28.27	15.08	29.92
0.50	0.24	14.98	28.28	15.07	30.01
0.67	0.28	14.98	28.29	15.06	30.06
0.83	0.74	15.19	31.08	15.05	30.10
1.00	3.59	15.51	36.77	15.04	30.13
1.17	7.95	15.41	40.19	15.03	30.16

Table D.3: Environmental and stress history used for modeling the deformation of an individual flake during the press closing time of the 190°C/6% panel type. (MC = moisture content, Temp = temperature)

Time (min)	Stress (MPa)	FACE MC (%)	FACE Temp (C)	CORE MC (%)	CORE Temp (C)
0.00	0.00	6.00	32.35	6.00	32.97
0.17	0.24	5.99	32.41	6.00	33.06
0.33	0.26	5.99	32.45	5.99	33.11
0.50	0.26	5.98	32.48	5.99	33.14
0.67	0.28	5.98	32.50	5.98	33.16
0.83	0.64	5.97	32.52	5.98	33.18
1.00	4.07	6.04	34.16	5.97	33.25
1.17	7.95	6.14	38.75	5.97	33.47
1.33	7.97	6.04	42.77	5.95	33.75
1.50	8.02	5.53	43.23	5.93	34.07
1.67	8.02	3.82	28.38	5.90	34.41

Table D.4:   Environmental and stress history used for modeling the
deformation of an individual flake during the press closing time of the
154°C/6% panel type. (MC = moisture content, Temp = temperature)

Time (min)	Stress (MPa)	FACE		CORE	
		MC (%)	Temp (C)	MC (%)	Temp (C)
0.00	0.00	6.00	30.02	6.00	30.30
0.17	0.27	5.99	30.26	5.99	30.53
0.33	0.27	5.97	30.40	5.98	30.63
0.50	0.27	5.96	30.49	5.97	30.70
0.67	0.33	5.94	30.56	5.96	30.75
0.83	1.31	5.93	30.62	5.95	30.79
1.00	6.55	5.96	31.81	5.94	30.87
1.17	8.01	6.01	35.15	5.93	31.07
1.33	8.01	5.92	38.28	5.91	31.33
1.50	8.01	5.60	39.77	5.89	31.62
1.67	8.01	4.51	31.31	5.85	31.93
1.83	8.01	3.31	26.75	5.82	32.60
2.00	8.01	2.50	31.47	5.76	33.44
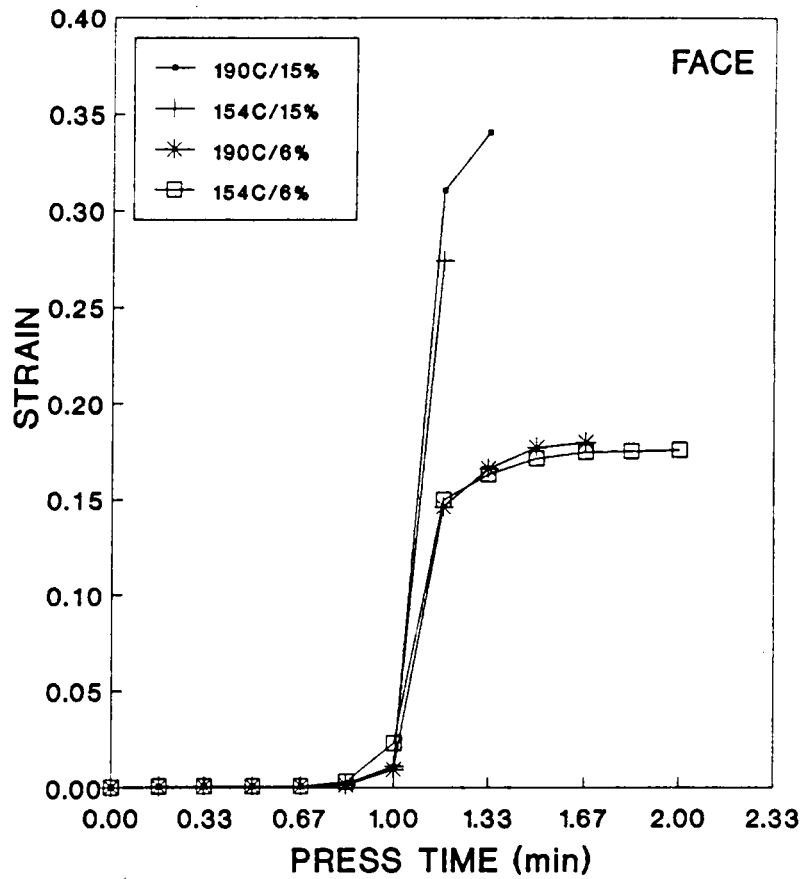
Figure D.1: Predicted strain in an individual flake in the face region of a panel during press closing time. Environmental and stress histories used for the modeling procedure are given in Table C.1 to C.4.
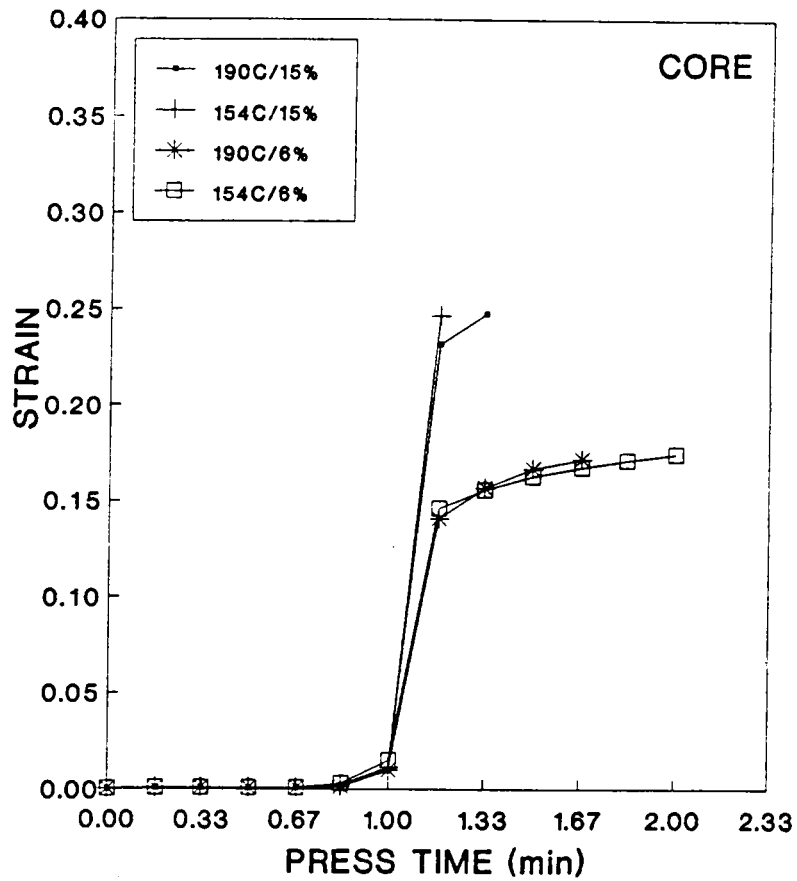
Figure D.2: Predicted strain in an individual flake in the core region of a panel during press closing time. Environmental and stress histories used for the modeling procedure are given in Table C.1 to C.4.

APPENDIX E:

NONLINEAR VISCOELASTICITY MODEL

```
'===================================================================
'                 Model for VE behavior of polymeric foams
'===================================================================
REM $DYNAMIC
DIM i, j, k, sr, cr, numpt, nchng, mcls, nt AS INTEGER
DIM tme(numpt), strn(numpt), strs(numpt), temp(numpt), mc(numpt) AS DOUBLE
DIM rdtme(numpt), lredtme(numpt) AS DOUBLE
DIM msf(2, 6), invatm(numpt), yo(2, 6), bi(2, 6) AS DOUBLE
DIM slpam, slpat, atlo, athi, am, at, delmc AS DOUBLE
DIM mu, c3, c2, rho, rrho, Ew, e, rrhoep AS DOUBLE
DIM tmst, a, b, c, z AS DOUBLE
DIM o(2, numpt), ep(nelmt, numpt), d(nelmt), lam(nelmt) AS DOUBLE
DIM tmei, tmej, h, slpsig, deltme, fsep, kep(nelmt), msig(nelmt) AS DOUBLE
DIM strsj, strni, strnj, slpstrn AS DOUBLE
DIM lep, lsig, plep, nonlin AS DOUBLE


CLS
'===================================================================
'                       Input Front End
'===================================================================
GOSUB SrKey        ' Choose between Stress Relax and Creep
'GOSUB FoamKey     ' Input data for the foam modeling
GOSUB HistKey      ' Input history data (time,stress/strain,temp,mc)
'GOSUB TransForm   ' Transforms real time into reduced time vector
'GOSUB VEKey       ' Input info for Kelvin or Maxwell Elements
GOSUB trialVE

IF sr THEN         ' Solve linear ve problem using 1st order approx
    GOSUB srSolution       'for stress relaxation
  'GOSUB srNLin            'solve the non-linear solution from lin sol and foam
END IF

'GOSUB OuttPut     ' Output data to a file

END

'===================================================================
'                        SUB SrKey
'               selects stress relaxation or creep mode
'===================================================================
SrKey: '

   CLS
   KEY 1, "STRESS RELAX": KEY(1) ON: ON KEY(1) GOSUB Srelax
   KEY 4, "CREEP": KEY(4) ON: ON KEY(4) GOSUB Creep
   KEY LIST

   DO: LOOP UNTIL sr OR cr

RETURN

'===================================================================
'                        SUB  Srelax
'                   sets mode to stress relaxation
'===================================================================
Srelax: '
        CLS
        KEY(1) OFF: KEY(4) OFF
        KEY 1, "": KEY 4, ""
        sr = 1
```

```
          cr = 0
          PRINT "Stress Relaxation mode has been chosen."
          SLEEP 2
RETURN


'=====================================================================
'                              SUB Creep
'                          sets mode to creep
'=====================================================================
Creep: '
          CLS
          KEY(1) OFF: KEY(4) OFF
          KEY 1, "": KEY 4, ""
          sr = 0
          cr = 1
          PRINT "Creep mode has been chosen."
          SLEEP 2
RETURN


'=====================================================================
'                             Sub FoamKey
'                       inputs data for foam models
'=====================================================================
FoamKey: '

  mu = .05
  c3 = .015
  c2 = .1
  rho = .5

Disp: CLS
  PRINT "The default values for the foam parameters are:"
  PRINT
  PRINT "1.        density = "; rho
  PRINT "2.      exp ratio = "; mu
  PRINT "3.           c3 = "; c3
  PRINT "4.           c2 = "; c2
  PRINT


  INPUT "OK ? (y/n)", ans$
  IF ans$ = "y" OR ans$ = "Y" THEN GOTO Back

  INPUT "Input variable to change (1,2,3,4)", nchng
  IF nchng = 1 THEN INPUT "Density = ?", rho
  IF nchng = 2 THEN INPUT "Exp Ratio = ?", mu
  IF nchng = 3 THEN INPUT "c3 = ?", c3
  IF nchng = 4 THEN INPUT "c2 = ?", c2
  GOTO Disp

Back: RETURN


'=====================================================================
'                             Sub HistKey
'                    reads input file for all history data
'=====================================================================
HistKey: '
```

```
CLS
PRINT "An input file must be specified."
PRINT
PRINT
PRINT "The file must contain the following data in matrix form."
PRINT "------------------------------------------------------------"
PRINT
PRINT "Number of Points"
IF cr THEN PRINT "Time (min), Stress (Pa), Temperature (C), Moisture Content (
IF sr THEN PRINT "Time (min), Strain, Temperature (C), Moisture Content (%)"
PRINT " obs(1)"
PRINT " obs(2)"
PRINT " obs(3)"
PRINT "   ."
PRINT "   ."
PRINT "   ."
PRINT
PRINT
PRINT "Begin the file with    Time = 0."
PRINT "Data can be seperated by either spaces or a comma."

' LINE INPUT "Drive ?", dr$
'FILES dr$
' LINE INPUT "Filename ?", fli$
· dr$ = "a:": fli$ = "trialin.dat"
OPEN dr$ + fli$ FOR INPUT AS #1
INPUT #1, numpt

' Redimension arrays now that have value for numpt
REDIM tme(numpt), strn(numpt), strs(numpt), temp(numpt), mc(numpt) AS DOUBLE
REDIM msf(2, 6), invatm(numpt), yo(2, 6), bi(2, 6) AS DOUBLE
REDIM rdtme(numpt), lredtme(numpt) AS DOUBLE
FOR i = 1 TO numpt
    IF sr THEN INPUT #1, tme(i), strn(i), temp(i), mc(i)
    IF cr THEN INPUT #1, tme(i), strs(i), temp(i), mc(i)
    strn(i) = strn(i) / 10
    IF strn(i) > 1 THEN errn = 2
    tme(i) = tme(i) * 60              'convert time from min to sec
    rdtme(i) = tme(i)
    'temp(i) = temp(i) + 3 * i: mc(i) = 9.3
    'RINT tme(i), strs(i), temp(i), mc(i)
NEXT i

'SLEEP 10
CLS
PRINT "History data has been retrieved."
SLEEP 2
IF errn THEN
    PRINT "Strain data is too large!"
    PRINT "Program halted."
    STOP
END IF

RETURN


'================================================================
'                          Sub srSolution
'              time based solution for linear creep response
'================================================================
```

```
srSolution: CLS
          PRINT "Solving Linear VE Equations"
          PRINT

      '------------------------instantaneous solution--------------------
      strnj = strn(1)
      FOR i = 1 TO nelmt    'all the maxwell elements
          sig(i, 1) = strnj * e(i)
          msig(i) = sig(i, 1)
      NEXT i
      PRINT USING "##.####^^^^"; sig(1, 1) + sig(2, 1) + sig(3, 1)

      '-----------------------time solution------------------------------
      tmei = 0                            'last time
      tmej = 0                            'next time
      FOR j = 2 TO numpt                  'for each real time step
          h = (10 ^ INT(LOG(rdtme(j)) / LOG(10))) / 10'10 time steps per decade
          FOR z = rdtme(j - 1) + h TO rdtme(j) STEP h
              nt = 1
              GOSUB srSolve
          NEXT z

          IF tmej < rdtme(j) THEN
              nt = 0            'go solve last time because above iteration
              GOSUB srSolve     ' does not come out even
          END IF


          FOR i = 1 TO nelmt         'collect stress in each element at end of real t
              sig(i, j) = msig(i)
          NEXT i
          PRINT USING "##.####^^^^"; sig(1, j) + sig(2, j) + sig(3, j)

      NEXT j

   RETURN

'======================================================================
'                         Sub srSolve
'        solves for the linear creep response using 1st order approx
'======================================================================
srSolve: '

          '------------------time--------------------
          tmei = tmej                 'update last time
          IF nt THEN
              tmej = z       'update next time
          ELSE
              tmej = rdtme(j)
          END IF

          '---------------interpolate strain----------
          strni = strnj
          IF nt THEN
              slpstrn = (strn(j) - strn(j - 1)) / (rdtme(j) - rdtme(j - 1))'slope o
              deltme = tmej - rdtme(j - 1) 'time jump for interpolation
              strnj = strn(j - 1) + slpstrn * deltme 'interpolated stress for tmej
          ELSE
              strnj = strn(j)
          END IF
```

```basic
            '-------------maxwell elements----------------
            FOR k = 1 TO nelmt          'do for each element in prony series
                msig(k) = (lam(k) / (lam(k) + h)) * (e(k) * (strnj - strni) + msi

            NEXT k
            ' PRINT USING "##.####^^^^"; msig(1); msig(2); msig(3)
            'SLEEP 1
     RETURN

'=====================================================================
'                            Sub srNLin
'       solves for the non-linear creep response from linear and foam
'=====================================================================
srNLin: CLS
        PRINT "Linear Solution is Complete!"
        PRINT
        PRINT "Solving Non-Linear Equations"

        FOR i = 1 TO numpt

            lep = strn(i)
            o(1, i) = tme(i)
            o(2, i) = lep
            FOR j = 1 TO nelmt
                lsig = lsig + sig(j, i)       'total linear stress
            NEXT j
            IF lep > c3 / c2 THEN
                plep = lep - c3 / c2
                rrhoep = rrho * (1 - (1 - 2 * mu / 3) * plep - mu * plep ^ 2) ^ -
                nonlin = ((c3 / c2) / lep) * ((1 - rrho ^ (1 / 3)) / (1 - rrhoep
            ELSE
                nonlin = 1#
            END IF

            o(3, i) = lsig * nonlin

        NEXT i

RETURN




'=====================================================================
'                            Sub OuttPut
'             output non-linear results to an ASCII file
'=====================================================================
OuttPut: CLS
        PRINT "Non-linear solution is complete!"
        PRINT
        INPUT "Drive for output file?", dr$
        FILES dr$
        PRINT
        INPUT "Output Filename?", flo$
        OPEN dr$ + flo$ FOR OUTPUT AS #2
        FOR i = 1 TO numpt
            PRINT #1, USING "##.####^^^^  ##.####^^^^"; o(1, i); o(2, i)
        NEXT i
        CLS
        PRINT "Analysis is complete."
```

```
    RETURN

trialVE: '
        CLS
        nelmt = 3
          REDIM kep(nelmt), ep(nelmt, numpt), d(nelmt), lam(nelmt) AS DOUBLE
          REDIM msig(nelmt) AS DOUBLE
          'REDIM sig(nelmt, numpt) AS DOUBLE
          'REDIM e(nelmt) AS DOUBLE
        e(1) = 44: lam(1) = 10
        e(2) = 444: lam(2) = 100
        e(3) = 4444: lam(3) = 1000

    RETURN
```

The vita has been removed from
the scanned document